UNIVERSITY OF GENOVA

PHD PROGRAM IN BIOENGINEERING AND ROBOTICS

The interplay between movement and perception: how interaction can influence sensorimotor performance and neuromotor recovery

by

Giulia Sedda

Thesis submitted for the degree of *Doctor of Philosophy* (XXII cycle)

April 2020

Prof. Silvio P. Sabatini	Supervisor
Prof. Vittorio Sanguineti	Supervisor
Prof. Giorgio Cannata	Head of the PhD program

Thesis Jury:

Prof. Peter J. Bex, *Northeastern University, Boston*	External examiner
Prof. Robert Volcic, *New York University Abu Dhabi*	External examiner
Prof. Roberto Raiteri, *University of Genoa*	Internal examiner

Dibris

Department of Informatics, Bioengineering, Robotics and Systems Engineering

Declaration

I hereby declare that except where specific reference is made to the work of others, the contents of this dissertation are original and have not been submitted in whole or in part for consideration for any other degree or qualification in this, or any other university. This dissertation is my own work and contains nothing which is the outcome of work done in collaboration with others, except as specified in the text and Acknowledgements. This dissertation contains fewer than 60,000 words including appendices, bibliography, footnotes, tables and equations and has fewer than 100 figures.

Giulia Sedda
May 2020

Abstract

Movement and perception interact continuously in daily activities. Motor output changes the outside world and affect perceptual representations. Similarly, perception has consequences on movement. Nevertheless, how movement and perception influence each other and share information is still an open question.

Mappings from movement to perceptual outcome and vice versa change continuously throughout life. For example, a cerebrovascular accident (stroke) elicits in the nervous system a complex series of reorganization processes at various levels and with different temporal scales. Functional recovery after a stroke seems to be mediated by use-dependent reorganization of the preserved neural circuitry.

The goal of this thesis is to discuss how interaction with the environment can influence the progress of both sensorimotor performance and neuromotor recovery. I investigate how individuals develop an implicit knowledge of the ways motor outputs regularly correlate with changes in sensory inputs, by interacting with the environment and experiencing the perceptual consequences of self-generated movements. Further, I applied this paradigm to model the exercise-based neurorehabilitation in stroke survivors, which aims at gradually improving both perceptual and motor performance through repeated exercise.

The scientific findings of this thesis indicate that motor learning resolve visual perceptual uncertainty and contributes to persistent changes in visual and somatosensory perception. Moreover, computational neurorehabilitation may help to identify the underlying mechanisms of both motor and perceptual recovery, and may lead to more personalized therapies.

Table of contents

List of figures

List of tables

Chapter 1

Overview

This thesis addresses the interplay between movement and perception, which constantly occurs in daily activities. The way perception influences movements through sensory perturbations is well documented, for example in contexts such as adaptation to force fields or to visuomotor rotation induced by prisms; on the contrary, the mechanisms by which movements affect perception are less known, for example by guiding a persistent improvement of the perceptual discrimination and/or detection capabilities following motor practice with a perceptive stimulus.

Neural mappings from movement to perceptual outcome and vice versa are not fixed, but continuously adapt throughout life. Adaptation follows the course of the individual's life, including unexpected events that can change it profoundly. For example, motor or sensory impairment can cancel existing mappings and create new ones to compensate for lost skills. Similar to motor and perceptual skill learning, exercise-based neurorehabilitation aims at gradually improving both perceptual and motor performance through repeated exercise.

In this thesis, I specifically address the idea that continuous experience of the perceptual consequences caused by self-generated movements can induce both sensorimotor learning (see Part I, Chapters 2, 3, 4, 5) and neuromotor recovery (see Part II, Chapters 6, 7, 8).

Chapter 2 describes the state of the art related to the movement-perception interplay. I review the main studies on how perception and movement influence each other, the use of ambiguous stimuli and the contribute of cognitive (explicit) strategies.

In Chapter 3, I illustrate the design attributes of ambiguous moving stimuli, with particular emphasis on the *aperture problem* with a 'plaid' pattern, which is composed by a pair of overlapped drifting gratings. By adjusting the relative difference of contrast of the two gratings, they appear either sliding one over the other or cohere into a single moving pattern.

The plaid pattern is the visual stimulus adopted in the studies presented in the next two chapters.

Chapter 4 shows that active interaction with the plaid stimulus alters the subsequent perception of its motion, reducing perceptual uncertainty. An active group and two control groups performed the same perceptual test before and after a training. During training, only the active group performed self-generated movements to interact with the stimulus. I found that the perceptual threshold for the direction of stimulus motion changed significantly following training only in the active group. In addition, I found that the motion direction was strongly correlated with direction of movement measured during the active training, consistent with the idea that perceptual change is tied to motor learning.

Under a Bayesian framework, a model of the experiment was developed and used to fit the pre- and post-training data of the perceptual test. Results suggest that observers who control the stimulus movement improve their internal model of plaid geometry. Moreover, model simulations correctly predict the visual bias induced by the plaid and reproduce some important experimental evidences of the previous literature.

Chapter 5 describes a companion experiment, in which active interaction with a plaid stimulus induces both visual and somatosensory changes. Four groups of participants performed a visual or proprioceptive judgement test before and after the same training, in which they interact with the stimulus through self-generated movement. Results show that the active interaction between the observer and the stimulus can induce both visual and somatosensory changes, which can be interpreted as a perceptual skill learning.

Chapters 6 reviews the main studies related to computational models of motor learning, including models of sensorimotor adaptation, skill learning and recovery. Recently, computational models have been applied to the rehabilitation field, providing quantitative predictions on neuromotor recovery process.

In Chapter 7, I use the dynamical systems framework to model the trial-by-trial dynamics of exercise-induced recovery from stroke. The model explicitly addresses the extent to which training in one direction affects performance of subsequent movements in other directions (spatial generalization).

In Chapter 8, I present a computational model of recovery from unilateral spatial neglect (USN) through exercise. Neglect is often observed in right-hemisphere stroke patients. The model reproduces the main observations of prism adaptation experiments and was fitted to data from a rehabilitation trial based on a novel VR-based rehabilitation approach, involving reaching movements within an adaptive environment.

Taken together, all these findings indicate that visual perceptual ambiguity is resolved by motor learning with self-produced movements, which contributes to persistent changes in visual and somatosensory perception. Moreover, computational models may have a strong impact on neuromotor rehabilitation: they may help identifying the underlying mechanisms of both motor and perceptual recovery, and may lead to patient-specific strategies of therapy.

Part I

Mechanisms of sensorimotor learning through interaction with the environment

Chapter 2

State of the Art

2.1 Introduction

The interplay between movement and perception is a top-flight element of daily life.

Movement influences perception by changing the outside world, and has a direct impact on perceptual representations. For example, moving a mouse on a table changes the position of virtual objects on the screen; likewise, head motion alters spatial relations to surrounding objects and, hence, which of their properties are visually perceived (Aytekin et al., 2014). Either active or passive self-produced movements can generate useful sources of perceptual information (Gibson, 1979, 2002): for instance, moving the hand over an object's surface enables to feel its shape, temperature, and texture.

Similarly, perception has consequences on movement: for example, while holding objects with different size and configuration, both the arm movements and the grip shape of the hand will be different (Gibson, 1979). Likewise, the presence of an obstacle in a path leads the runner to change their own trajectory or to jump the obstacle.

This idea that movement affects perception and vice versa developed quite recently. In the second half of the 20^{th} century, classical computationalist cognitivism represented the dominant doctrine in cognitive sciences. As regards visual perception, the most important theoretical contribution within the cognitive theory was that of D. Marr (see Marr and Ullman (1981)). He suggested that the perceptual visual input is the retinal image, which is the set of projections of the points that form the visible surface of a static object in a given time instant, whereas the cognitive output is a linguistic-symbolic representation of the perceived object shape. For Marr, the visual system takes detailed snapshots of the external environment through the object representations, without any reference to movement.

Marr's theory was a reaction to the ecological theory of J. J. Gibson (Gibson, 1979), which developed in the same years. The Gibsonian theory is based on three assumptions: 1. perception is a direct collection of information and does not require mental representations based on inferential processes; 2. perception is used to guide the action and not for collecting information not relevant to movement; 3. given the first two premises, the environment must offer sufficient information to lead the action. In this regard, the concept of *affordance* is fundamental: it is the set of potential uses that an object offers to individuals. The extracted information does not concern only psychophysical variables, such as direction, brightness, spatial frequency, wavelength or duration, but also higher-order relational characteristics functional to movement, which are invariant under deformations generated by eye, head, torso and whole body movements. For Gibson the stimulus is not the single static retinal image, but the optical flow itself, that is the dynamic configuration of luminous points that radiate the retina.

Afterwards, movement-based accounts of perception developed diversely. It has been suggested that movement and perception share the same common representations and control each other bidirectionally. This is the central idea of both the *common coding* (Prinz, 1997) and the *event coding* (Hommel et al., 2001; Müsseler, 1999) theories, which speculate that the planned movements in the early stages of motor control are represented in the same format as the perceived events in the final stages of perception. These theories and their subsequent modifications (Schütz-Bosbach and Prinz, 2007b; Zwickel et al., 2007) do not explicitly deal with the mechanisms of the available reciprocal information between the motor and sensory system. They make no assumptions or predictions about where shared representations should occur in the processing hierarchy.

In the early nineties the idea that experience and cognition are a product of the individual exploratory activity took hold. This concept has been called *enaction*, a word that was introduced into the cognitive sciences by Varela et al. (1991): according to the *enactivist* theory, cognitive structures in general and perception in particular emerge from recurrent sensorimotor patterns between perception and movement. Thus, cognition would emerge from our sensorimotor activity (Varela et al., 1991). J. J. Gibson is recognized as the precursor of the enactivism.

Sensorimotor enactivism (SE) is a particular conceptual framework that specifically investigates visual perception. It suggests the idea that visual perception is a form of action. The first motivation of this proposal lies in the lack of recognition of the action contribution to vision by classical computational theories, and the inability of these theories to explain how computational processes can generate a conscious visual experience. According to SE,

the visual system is not a passive recipient of sensory inputs coming from the environment, because vision is an activity through which the individual collect information from the environment by constantly moving eyes, head and body, and this information is related to the task to be fulfilled (Findlay and Gilchrist, 2003). SE moves away from the idea that vision is functionally dedicated, fully or in part, to driving the action (as it was for Gibson) (Noë, 2004, 2010). The first SE proposal comes from O'Regan and Noë (2001), who suggest the idea that perception and perceptually-guided action depend on the capability to anticipate the sensory effects of bodily movements. This implies that perception requires to collect the so-called *sensorimotor contingency*, i.e. experiencing the visual and somatosensory consequences of self-generated movements (O'Regan and Noë, 2001). Knowing this set of rules, the individual has an implicit knowledge of the ways motor outputs regularly correlate with changes in sensory inputs. This acquaintance derives from exploratory ability and not from a propositional knowledge.

The concept of sensorimotor contingencies can also take on a different meaning from the one just mentioned. Noë (2004) proposes another definition, starting from the distinction between two levels of perceptual content, which can be defined as *factual* or *perspective*. Factual matter is in relation to the way things really are, whereas the perspective matter is determined by the way things appear according to movement. In this new proposal, the perceptual experience consists of a series of *expectations* concerning how the perspective perception is in relation to the control of the intentional movements - oriented to the action - that our body allows. The sensorimotor contingencies would now be the individual ability to perceive the way object appearance changes in relation to the movement with respect to the object.

Similarly, the possibility of experiencing the real presence of hidden aspects of a certain object, such as the back of an apple, is due to the sensorimotor aspect of perception, that is the ability to anticipate the perceptual variations given by bodily movements with respect to the object, which is revealed as the individual moves. In line with this view, perceptual experience is a process of feature extraction resulting from a practical skill concerning the ways the body can be used to create perceptually guided actions (Noë and O'Regan, 2002). For instance, Held and Hein (1963) tested this idea in their famous work on kittens in the kitten carousel. Each kitten underwent the same visual stimulation, but only one kitten received the stimulation caused by self-generated movements. Results show that only the active kitten subsequently displayed normal visually guided behaviour.

According to the proposal that sensory modalities depend on sensorimotor contingencies, there is evidence that each perceptual modality is linked to a specific system of sensorimotor

invariance. For example, the visual-tactile replacement apparatus (VTRA) made by P. Bach-y-Rita allows us to capture images by a digital video camera worn by a person and to transform them into a skin stimulation code (Bach-y Rita, 1972; Bach-y Rita and Kercel, 2003). In this way the visual stimulus is transformed into a tactile stimulus and can be perceived as such. Bach-y Rita et al. (1969) shows that, after an initial period of adaptation, blind subjects from birth are able to orient themselves in space and recognize objects on the basis of the tactile impulses provided by the VTRA. According to SE, this result is not achieved with static subjects, but only through repeated dynamic interaction with the environment. In fact, participants must be able to move the video camera connected to the VTRA and to explore the surrounding space, thus becoming familiar with the regularities in the variation of tactile stimuli that the movement involves (sensorimotor regularity). Surprisingly, some particularly experienced subjects claim that they no longer perceive the stimulus in tactile, but visual format (O'Regan, 2011).

However, the SE theory has also undergone many criticisms, because it has not always provided a solid theoretical framework based on empirical evidence. For instance, several studies proposed a knowledge description of sensorimotor contingencies in modern neuroscientific terms, but they had to use neurocomputational models that cannot keep the idea of a perception that does not use computations or propositional-inferential representations (Chalupa and Werner, 2004; Miikkulainen et al., 2006; Seth, 2015). In fact, currently there are several models that manage to better explain the functional complexity of the human visual brain in general and the *act of seeing* in particular, but they are computational models that describe both the cortical activity and the processes necessary for viewing through representations based on algorithmic implementations (DiCarlo et al., 2012). In addition, it seems that things are much more complex also as regards the structural and functional organization of sensory modalities (Bertelson and De Gelder, 2004; Macpherson, 2015; O'Callaghan, 2008; Spence and Driver, 2004) on which, however, there is still no well-defined theory.

Furthermore, mappings from movement to perceptual outcome and vice versa are not fixed (Kaas, 1991): they can be very different, sometimes even in conflict, and especially in continuous adaptation throughout life. For example, motor or sensory impairment can cancel existing mappings and create new ones to compensate for lost skills (Xerri, 2012). In the end, how sensory and motor systems share information and influence each other is still poor understood.

2.2 Influence of perception on movement

The way perception affects movement has been well documented in literature. It is also known that vision often dominates among all sensory modalities, even when visual information is not task-relevant (Colavita, 1974; Posner et al., 1976; Sinnett et al., 2007).

The influence from perception to movement has been particularly investigated in terms of both the observational learning (Hecht et al., 2001; McCullagh et al., 1989; Vogt, 1995, 1996), which is the ability to reproduce movements by watching other people's performance on a long time scale, and the visuomotor coupling, which refers to the concurrent effects of visual perception on movement in object-oriented performance (Brass et al., 2001; Vogt, 2002).

In the framework of observational learning, for instance Vogt (1996) investigated if the movement representation necessary for motor control is already formed during model observation. This hypothesis was supported by several brain imaging studies which showed that most of the cortical and subcortical structures involved in motor performance are also activated during motor imagery (Decety and Ingvar, 1990; Jeannerod, 1994). Accordingly, the authors hypothesized that motor imagery should not only affect global performance measures such as accuracy, speed or error rate (Heuer, 1989), but also more fine aspects of motor output such as the temporal coherence across trials, which normally results after longer periods of physical practice. This hypothesis was tested in a study where subjects learned to reproduce a sequence of cyclical arm movements (Vogt, 1995). Subjects were tested in one of the following four conditions: (1) visual imagery, in which they were asked to imagine the motion displayed on the screen, (2) motor imagery, in which they were asked to imagine performing the movement, (3) physical rehearsal, in which they rehearsed the movement physically, or (4) counting backwards from a two-digit number in steps of three in order to block mental rehearsal and thus measure the performance/memory decay. Results showed that mental rehearsal and physical practice led to similar improvements in temporal consistency, supporting the idea that these two different approaches share features of temporal patterning of motor performance (Vogt, 1995). This suggested that watching a movement pattern is not just visual processing, but may involve an internal representation of either external or self-generated movements (Jeannerod, 1994). These and further behavioural findings (Shiffrar and Freyd, 1993; Viviani and Stucchi, 1992) were supported by several neurophysiological studies that documented the involvement of motor cortical areas in movement perception, such as studies of *mirror neurons* (Di Pellegrino et al., 1992; Gallese and Goldman, 1998; Rizzolatti et al., 1996).

In the context of visuomotor coupling in object-guided performance, for example Vogt (2002) found that during a reaching task the adaptive responses to changes of a target's position were equally fast as responses to changes of the hand position of a person while reaching for a target. Since response to shifts of object position are known to be processed in the dorsal cortical pathway (Jeannerod et al., 1995; Jeannerod and Jeannerod, 1997), the comparable short latencies for model-guided response suggest that the same pathway may be shared.

In addition, several studies showed that visual motor-related properties of graspable objects such as size, shape and orientation can prime movement (Craighero et al., 1996; Domalain et al., 2008; Gibson, 1977; Tucker and Ellis, 1998). For instance, in the study of Craighero et al. (1996) subjects were seated in front of a screen and were required to grasp, as fast as possible, a bar inserted inside a rectangular hole. The bar orientation was randomly changed trial by trial. At the beginning of each movement subjects were informed about the incoming bar orientation. Before or after the go-signal, a picture was displayed, representing a rectangle with the same (congruent) or different (incongruent) orientation of the bar, or a circle (neutral orientation). Results showed that the presentation of a visual prime, whose orientation was congruent with the required grip movement, improved the reaction time (i.e. the time between the go-signal and the releasing of the initial position) for that movement only when visual information was given before the go-signal. No difference was found between incongruent and neutral trials. These results showed that movement could be primed by visual stimuli. In contrast, visuomotor priming did not occur after the internal onset of a movement, as shown by the fact that priming was absent before the go-signal. The visuomotor priming was supported by studies on the organization of the cortical grasping circuit in primates (Jeannerod et al., 1995; Sakata et al., 1995; Taira et al., 1990).

2.3 Influence of movement on perception

There is a remarkable literature supporting the idea that motor learning is involved in neural plasticity in both motor and sensory systems. In particular, the majority of the evidence relates to changes to the somatosensory system (Henriques and Cressman, 2012; Ostry and Gribble, 2016), in which training-related changes to movement and motor cortex are accompanied by somatosensory plasticity, presumably as a result of the repeated pairing of somatic input and movement. Similarly, learning-related changes in auditory function have been reported in the context of speech motor learning (Lametti et al., 2012; Nasir and Ostry, 2009).

In contrast, there is substantially less work on the effects of motor learning on visual function and none suggesting persistent effects which reflect visual perceptual learning.

Motor priming of visual motion perception was presented preliminarily by Ishimura (1995); Ishimura and Shimojo (1994). They showed that the movement direction of the individual hand can bias the concurrent perceived motion direction of several ambiguous motion displays, such as the Ternus display, the barber pole stripe, and both square-wave and sinusoidal gratings. This fascinating phenomenon is called *action capture*, and demonstrates that movement can affect simultaneous visual motion perception. Other online changes to visual perception which accompany movement was reported (Müsseler, 1999; Schütz-Bosbach and Prinz, 2007a), based on the idea that movement is controlled by the anticipation of its intended effects.

More recently, both movement execution (Beets et al., 2010b; Zwickel et al., 2007) and movement planning (Wohlschläger, 2000) were found to shape the visual perception of a moving stimulus. Movement could bias perceptual sensitivity toward visual occurrences that either share features with the simultaneous motor performance (Wohlschläger, 2000) or that deviate from the expected sensory consequences of movements (Zwickel et al., 2007). For instance, Wohlschläger (2000) found that movement could prime perceptual sensitivity toward visual events when they shared at least one motion feature with concurrent movement, condition which is called *assimilation effect*, as for instance when movement and percept participate to the same motion direction or spatial dimension. When this common dimension is given, movement planning is sufficient for motion priming. In an analogous way, Zwickel et al. (2007) investigated the online influence of self-produced movement on motion perception, see Figure 2.1. Participants were asked to control an independent stimulus motion by hand movements in a specific direction. The direction of the stimulus motion changed unpredictably and was either congruent or not with the concurrent movement. Participants' task was to detect the deviation as soon as it occurred. The authors found that self-produced movement can bias perceptual sensitivity toward visual instances diverted from the expected sensory consequences, condition which is called *contrast effect*.

Similarly, in the oculomotor system the direct and simultaneous influence of a movement on corresponding perceptual representations has been much studied. For example, smooth pursuit eye movements can induce a deformed perception of the image speed (Freeman et al., 2010; Souman et al., 2006).

On the other hand, a small number of studies have examined the effects of motor learning on vision. For example, in Brown et al. (2007) participants had to intercept a moving stimulus after having learned to compensate a force field in a given direction. Authors found that

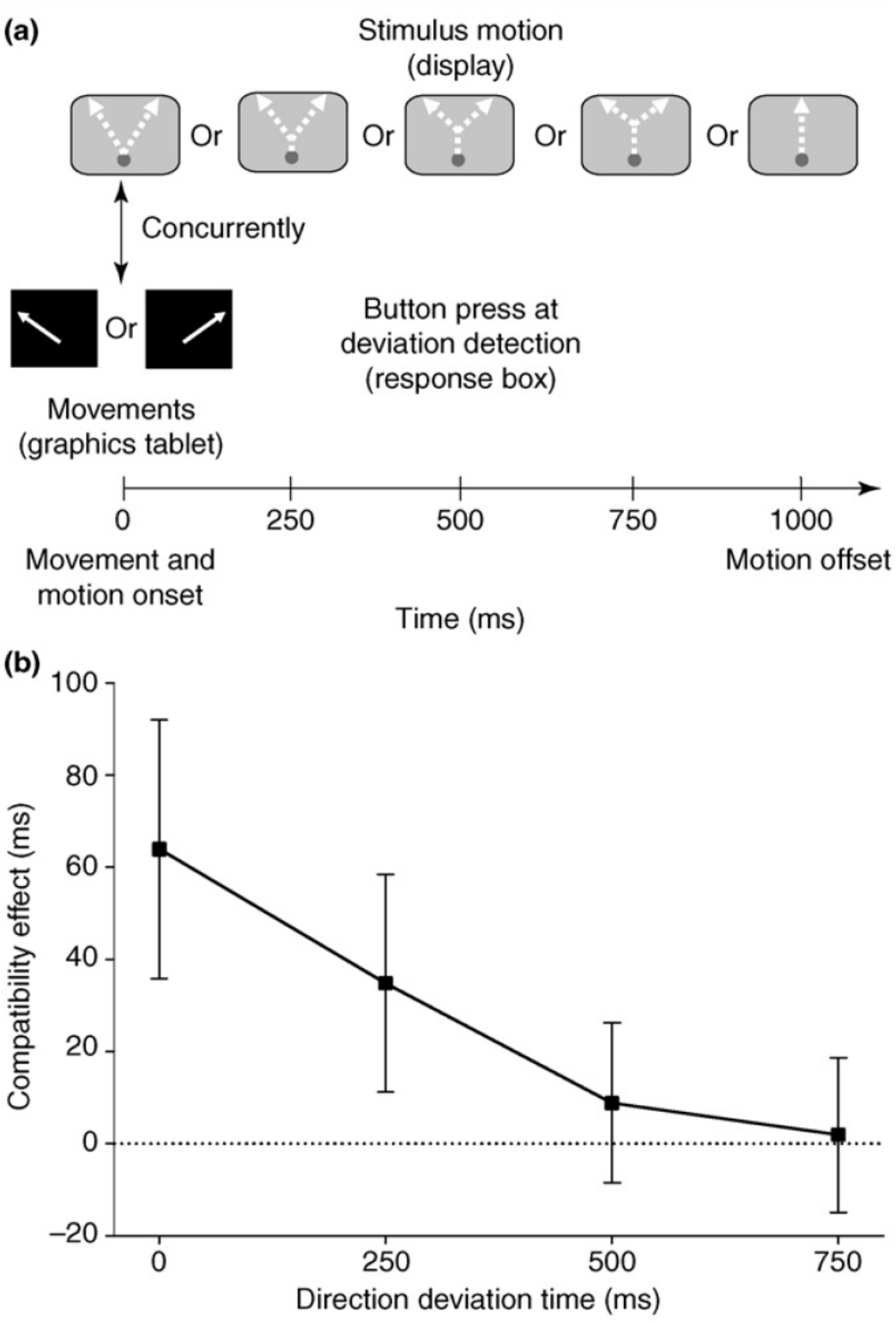

Figure 2.1 Participants performed vertical hand movements that deviated 45 deg to the left or right. They were asked to give a speeded response as soon as they notice the motion deviation from its initial direction. The deviation occurred with equal probability to the left or right of vertical after 0, 250, 500, or 750 ms, or not at all. From Zwickel et al. (2007).

movement initiation toward the moving object differed depending on the direction of the learned force field, indicating that expectations regarding visual motion are changed as a result of learning. Likewise, in Beets et al. (2010a) participants were trained to make movements that violated to different degrees the 2/3 power law (Lacquaniti et al., 1983). Results showed that there were improvements in visual discrimination of movements that corresponded to those which they experienced during training. These studies indicate that motor learning can induce a bias in visual perception.

Similarly, several works investigated how practising a movement can improve visual discrimination of the same movement (Beets et al., 2010b; Hecht et al., 2001; Zwickel et al., 2007) and lead to an increased neural activity of the cortical motor areas when that movement is observed (Calvo-Merino et al., 2005; Engel et al., 2008; Reithler et al., 2007).

2.4 The role of ambiguous stimuli

In order to isolate the direct effects of movement and perception from the effects due to changes in the external world, several studies mentioned above used ambiguous visual stimuli (Beets et al., 2010b; Mitsumatsu, 2009; Wohlschläger, 2000). The idea is that in the presence of ambiguous perceptual evidence, where two or more equally justified percepts are possible, movement manipulation can polarize the visual perception towards an interpretation more consistent with the concurrently performed motion. More specifically, movement is assumed to generate a model of the expected perceptual consequences of the same movement (Wolpert and Miall, 1996), and ambiguity is resolved by the perceptual interpretation that corresponds most to the model.

For instance, Beets et al. (2010b) found that the perceptual interpretation of an ambiguous (bistable) rotating object converged to a single percept when the participant reported their perceived rotation only with a congruent hand movement, see Figure 2.2. Participants were asked to match the velocity of their hand movement with that of a rotating cylinder-shaped cluster of dots, by either pressing a key on a keybord or moving the handle of a manipulandum. The rotating cylinder-shaped stimulus could be seen as moving clockwise or counterclockwise. Authors investigated four conditions: the effects of movement type (instructed vs. percept-dependent movements) and congruency (movement and perceived motion in coherent vs. opposite direction). Stimulus presentation was always independent of participants' movement. Results showed that the percept stability was affected by congruency only in percept-related movements, in which congruent movements stabilized the percept, whereas incoherent movements did not.

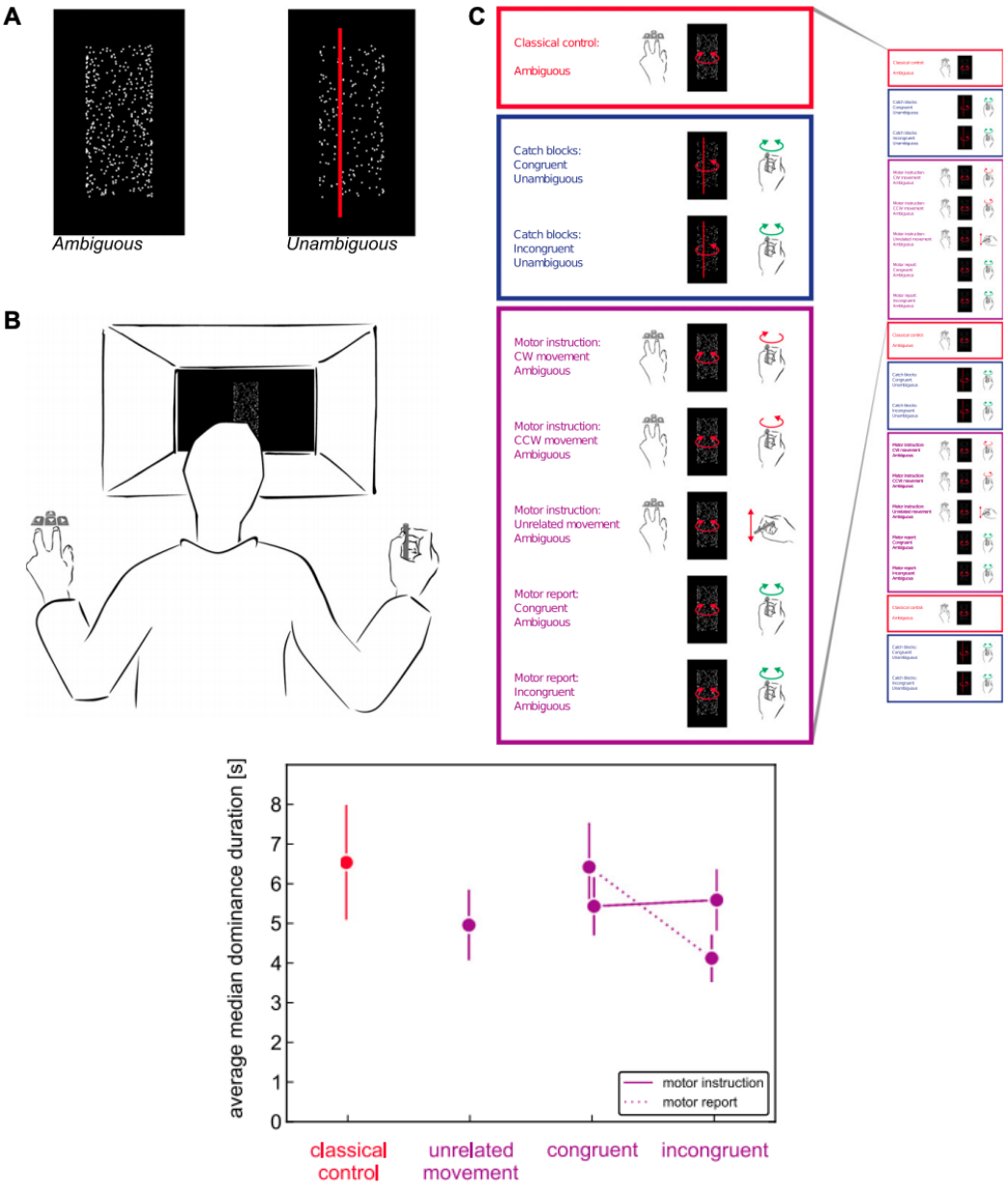

Figure 2.2 (A) Visual stimuli which observers viewed through a tunnel. The ambiguous stimulus could be interpreted as a cylinder rotating clockwise or counterclockwise. (B) Experimental setup. Participants sat in front of a tunnel through which the visual stimuli were presented, in order to occlude the self-produced movements. Left hand wa sused to press one of the arrow keys, whereas the right hand was used for rotating the turntable, or to make movements along the vertical plane of the right side of the tunnel (not shown). (C) Experimental conditions. The green arrow above the right hand indicates that the manipulandum handle was used to indicate the perceived rotation direction of the cylinder, otherwise the arrow keys were used. The block order is illustrated on the right. From Beets et al. (2010b).

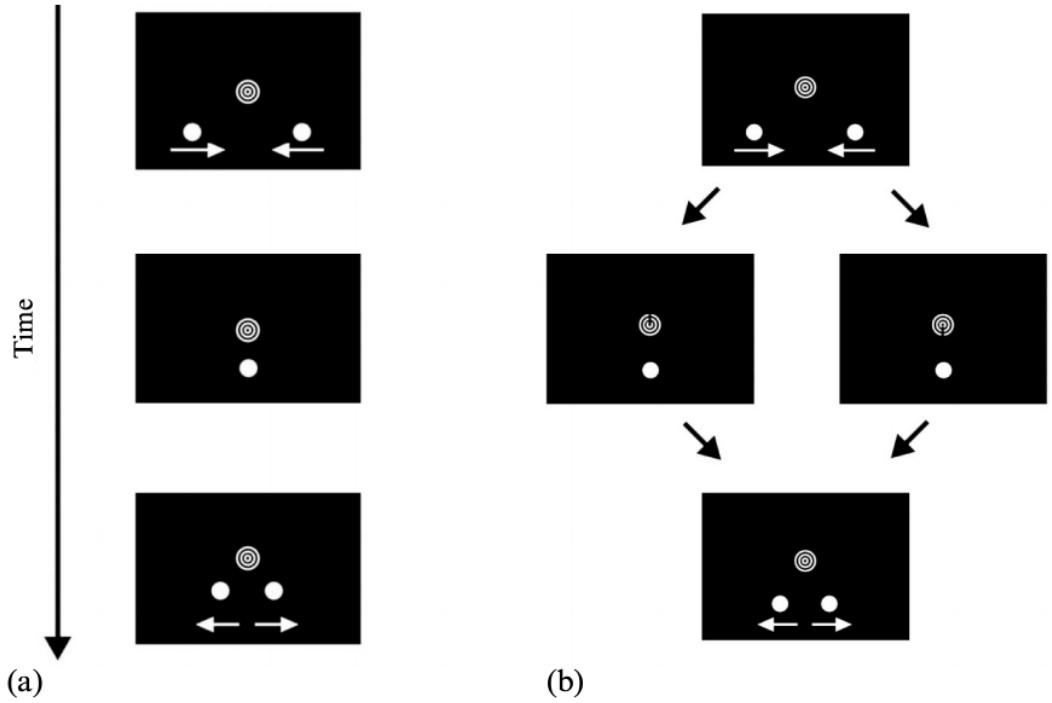

Figure 2.3 Schematic illustration of the visual stimuli: (a) two disks move horizontally toward and then pass each other, the central ring serving as a fixation figure; (b) upon superposition, a small gap is presented on the upper or lower side of the ring. From Mitsumatsu (2009).

Similarly, in Mitsumatsu (2009) participants controlled the movement of two disks on the screen through a mouse, see Figure 2.3. The disks were initially separated and then moved horizontally toward each other. The ambiguity was represented by the fact that disks could be seen as passing over each other or bounce off each other. Results showed that the direction of the simultaneous hand movement polarized the perception of the two disks moving on each other; however, this biased perception was not observed when movement direction and perceived direction were unrelated. Subsequent experiments revealed that this effect could not be attributed to the level of participants' attention, and the hand movement to control the stimulus motion was critical to the occurrence of biased perceptual representation.

These results on ambiguous stimuli provide evidence that the motion control and the motion perception can be coupled bidirectionally, even if movement has no consequences in the external world, so that the stimulus does not change, but its perception changes. The ambiguity level can be changed by manipulating some features of the stimulus. For example, in the stimuli used in the studies mentioned above (Beets et al., 2010b; Mitsumatsu, 2009) the ambiguity can be removed if the two disks or the dots have different color or shape.

Comparable results were found with binocular rivalry (Maruya et al., 2007) or unambiguous stimuli with high perceptual uncertainty (Keetels and Stekelenburg, 2014). These studies describe the *congruence effect*, in which a correspondence between movement and perception (for example rotation in the same direction) led to an increase in perceptual stability, compared to the case of an inconsistent relationship (rotation in opposite directions).

2.5 The role of a cognitive (explicit) strategy

In works on human motor learning, there is extensive evidence that explicit, cognitive factors contribute to learning (Krakauer and Mazzoni, 2011; Taylor and Ivry, 2013). Indeed cases where intentional cognitive factors do not contribute are probably the exception. Among the exceptions would be the adaptation observed with gradual introduction of perturbations, use-dependent learning that arises from repetition of movements and the gradual improvement observed over the course of learning (implicit learning) even in the presence of more rapid and presumably cognitively mediated changes in performance (explicit learning). Whether or not the perceptual changes that accompany learning are resistant to cognitive influences merits further consideration.

In the context of the visual motion processing, explicit expectations can shape the visual perception of a moving stimulus (Veto et al., 2018b). It seems possible that shared motor representations may occur at multiple levels, some of which are under cognitive control. Several studies suggest cognitive involvement when movement can bias visual perception in presence of ambiguous visual stimuli (Beets et al., 2010b; Wohlschläger, 2000). For instance, in Veto et al. (2018b) participants were exposed to the same ambiguous stimulus as in (Beets et al., 2010b), and learned one of two possible mechanical models that linked movement with perception (gear or belt), see Figure 2.4. Authors tested if the suggested internal model could bias the effect of movement on perception. Participants used a visual representation of a manipulandum handle in order to report the percept, and were instructed that the ambiguous cylinder and the handle were either coupled through a belt or through gears (Figure 2.4a). This resulted in four conditions: the internal model (gear or belt) and the correspondence between the perceived rotation of the cylinder and the rotation of the handle (congruent or incongruent). Results showed that handle motion in the same direction as perceived movement stabilized perception, replicating the well-known *congruence effect* (Beets et al., 2010b). Thus the interplay between the internal model and coherency factors suggested that the internal representation on how movement was coupled with its observable effects significantly affected the visual percept. In the other case, when movement was in

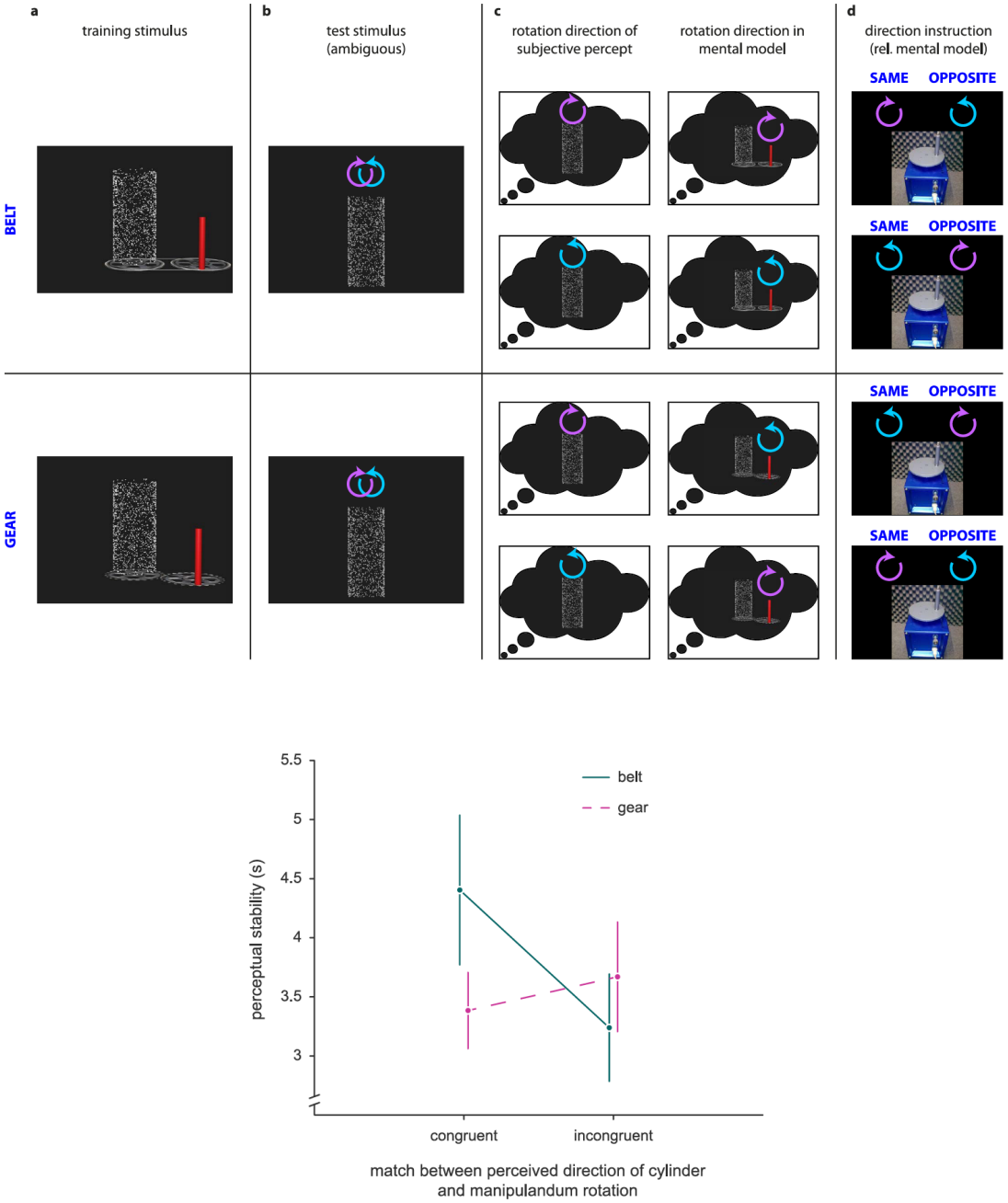

Figure 2.4 Stimuli, percept, and task. (a) First, participants learned the mechanical model ("belt" or "gear" layout), by controlling the displayed motion with the manipulandum handle. Then, a block of unambiguous motion followed, where participants had to report the rotation of the red lever attached to the wheel, in accordance with the subsequent experimental block ("same direction instruction" or "opposite direction instruction"). Then, the red lever disappeared and the mechanics was covered by a virtual desk, while the task remained unchanged. (b) All test blocks showed the same, ambiguous, motion cylinder. (c) Two possible perceptual interpretations of the test stimulus (clockwise and counterclockwise). (d) Instruction (manipulandum rotation in the same or opposite direction as that of the red lever in the mental model). Note that in the "belt" condition, the same/opposite direction instruction leads to congruency/incongruency between perceived and performed rotation, while this relationship is reversed in the "gear" condition. From Veto et al. (2018b).

the opposite direction to that of the perceived motion, no congruence effect was detected. This suggested that the influence of the previously learned mechanical model counteracted the congruency bias. Therefore, the explicit knowledge is one of the possible sources of the effect, and not the only one.

Differently, other studies investigated conscious and unconscious effects of movement-related visual stimulus and demonstrated that the effects of movement on perception can take place independently of awareness (Maruya et al., 2007; Veto et al., 2018a).

In summary, the currently available experimental works show divergent evidence both in the processing hierarchy and where the shared representations occur.

Chapter 3

Design attributes of ambiguous moving stimuli

3.1 Introduction

The visual system can be thought of as an organized machinery for gaining information about the surrounding world. Clearly, this information must be detailed and accurate in order to be useful.

When observing a natural scene, this appears generally very complex, since it consists of multiple objects, some of which can be static and others in motion, lying in the background or in the foreground. In addition, objects at different distances can have overlapped projections upon the two-dimensional retinal image. Due to this overlap, in the retinal image new features are formed, such as corners and edges, which are not directly attributable to any object. In order to define the constituent objects of the scene, the visual system decomposes such images: this perceptual processing is called *image segmentation* (Movshon et al., 1985; Rodman and Albright, 1989; Stoner and Albright, 1992). In the absence of segmentation, for each spatial location of the retinal image there can be a single value for each of the scene attributes, such as for example color, depth, light intensity, or movement. On the contrary, image segmentation allows a multi-valued representation of one or more scene attributes on each image position (Stoner and Albright, 1996).

Usually, the visual system is able to uniquely distinguish the objects that compose the scene. This occurs by combining the multiple cues present in the natural scene, which normally allow us to disambiguate its interpretation (Nakayama, 1985). Nevertheless, in some particular cases the composing elements of the visual scene can give rise to multiple perceptions, all equally likely. A typical example is the illusion of the Necker cube (Necker,

1832), which can be perceived in two perspectives oriented in different directions, as shown in Figure 3.1. The Necker cube is designed so that the front and the rear faces are of equal

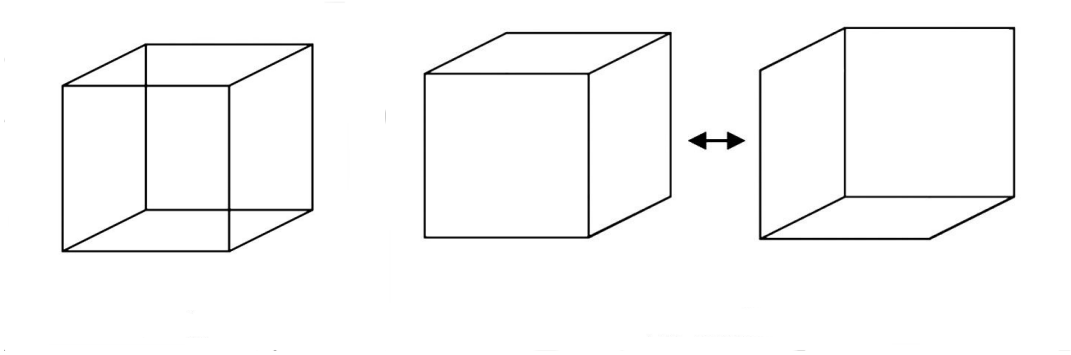

Figure 3.1 On the right, the Necker cube. On the left, its possible representations.

size. This situation produces a retinal image that the brain can interpret in two ways, which correspond to a projection of the cube seen from different positions. Faced with the problem of where the cube is located, the brain oscillates between the two perceptions.

3.2 The aperture problem

In the domain of motion processing, a well-known example of visual ambiguity is the *aperture problem* (Adelson and Movshon, 1982; Fennema and Thompson, 1979). This problem is often presented using a grating, which is a stimulus consisting of bright and dark bars that alternate periodically, thus resulting in a square-wave spatial pattern with a specific orientation. Two other parameters characterize a grating: 1) the contrast that relates to the magnitude of the intensity difference between the lightest part of the luminance distribution and the darkest part; and 2) the spatial frequency that is defined as the number of grating cycles per degree of vision angle.

When a grating moves behind a circular aperture, only the motion orthogonal to its orientation (i.e., perpendicular to the bars) can be perceived, whereas the motion parallel to the bars is not visible because it causes no change in the stimulus luminance; see Figure 3.2. Thus, grating's motion results ambiguous, because there are infinite possible motions with different directions and speeds that appear identical (Adelson and Movshon, 1982). As shown in Figure 3.2, the vector drawn in the *velocity space* displays the grating's motion in the direction indicated by the vector's angle at a speed given by its length. The dashed line represents the ensemble of velocities compatible with the grating's motion. This line is

parallel to the grating's bars and orthogonal to the velocity vector (Adelson and Movshon, 1982; Fennema and Thompson, 1979).

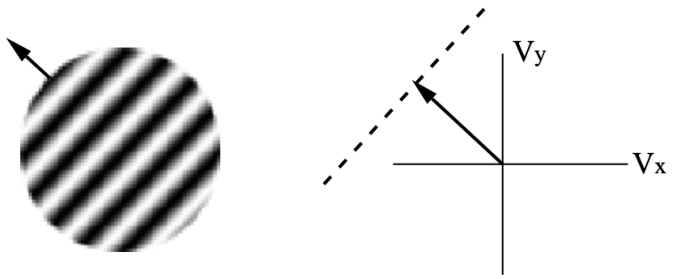

Figure 3.2 The velocity-space representation of a single grating stimulus moving behind a circular aperture. The dashed line indicates the locus of velocities compatible with the motion of the grating.

3.2.1 The size of the aperture

The sensors of the visual system are the cells located in the retina: they work on a very small portion of the visual field, called *receptive field*, and respond to extremely small variations in light intensity. The receptive field of a cell can be thought of as an aperture through which the cell responds to a stimulus in the visual scene.

The outputs of the retina cells with nearby and partially overlapping receptive fields are subsequently combined in order to provide a consistent representation of the visual world. The visual cortex has a dense and hierarchical organization into numerous areas, each of which contains a separate representation of the retinal image. The flow of visual information from the retina to higher order districts is processed by cells with larger and more complex receptive fields. As receptive field sizes increase, the likelihood of an aperture problem decreases; see Pack (2001) for a review.

In monkey and humans, visual motion information is analysed through a series of stages beginning in the *primary visual cortex* (V1). Receptive fields in V1 are very small, with size typically below a degree of visual angle in the foveal and parafoveal areas. V1 neurons project to many visual regions dedicated to extracting specific elemental information about the visual scene (Adelson and Bergen, 1991); however, the area that is most specialized for analysing motion is the *middle temporal area* (MT or V5) (Pack and Born, 2001). MT neurons have larger receptive fields than V1 neurons, about 10 times larger in diameter, ranging from less than 3 deg in fovea up to 30 deg in the far periphery (Albright and Desimone, 1987). The

size of the receptive field also increases more with increasing eccentricity in MT than in V1 (Albright, 1984; Gattass and Gross, 1981).

Both V1 (Hubel and Wiesel, 1968) and MT (Zeki, 1974) contain *velocity-tuned* neurons, which respond best to motion in a particular direction and with a particular speed, and weakly or not at all to motion in the opposite direction or with different speed. Most MT neurons are velocity-tuned, compared with approximately a quarter in V1.

3.2.2 Global and local velocities

If we consider rigidly translating objects, the velocity measured at specific locations on the object (known as *local* or *component* velocity) should correspond to the velocity of the whole object (which is termed *global* or *pattern* velocity). Nevertheless, it depends on whether we are talking about the *true* velocity of the sampled location or the velocity that the visual system perceives. This discrepancy between local and global velocities is the aperture problem (Bradley and Goyal, 2008).

Movshon et al. (1985) investigated the aperture problem in monkeys and found that it occurs for motion-sensitive V1 neurons but not for a portion of MT neurons: given a complex moving pattern, motion-sensitive V1 neurons encode local components' motion, whereas $\sim$25% of MT neurons encode the motion of the complex pattern. They found that $\sim$25% of MT cells were pattern selective, $\sim$40% were component selective, and the rest were unclassified.

Albright (1984) also distinguished two classes of MT neurons (type I and type II) based on their direction and orientation preferences: $\sim$61% of MT neurons had an orientation preference perpendicular to their preferred direction of motion (type I, similar to V1 neurons), while $\sim$29% had an orientation preference parallel to their preferred direction (type II). In addition, type I neurons were found to correspond to component-motion neurons, and type II neurons to pattern-motion neurons (Albright et al., 1986). Nevertheless, the way motion information is processed in the visual path, and in particular in areas V1 and MT, is still an open issue.

3.3 The plaid stimulus

If two drifting one-dimensional gratings are superimposed, they form a moving two-dimensional *plaid* pattern. When the plaid stimulus moves behind a circular aperture, the two composing gratings can be perceived to move as a single pattern (condition named *coherent motion*), or

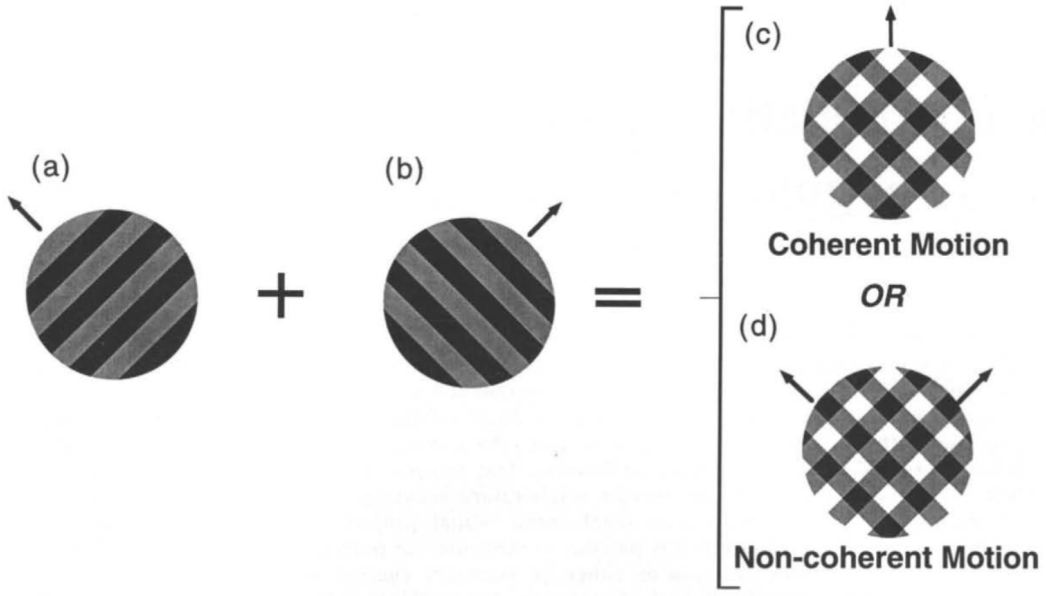

Figure 3.3 A moving plaid stimulus is composed by two superimposed drifting gratings (a, b). The resultant percept can be either a coherent pattern motion (c), or the transparent motion of the two gratings sliding past one another (d). From Stoner and Albright (1996).

to move independently (condition named *non-coherent or transparent motion*) (Adelson and Movshon, 1982; Wallach, 1935), as shown in Figure 3.3.

Most explanations on how the coherent pattern motion is estimated are based on one of three rules (Adelson and Movshon, 1982): *intersection of constraints* (IOC), *vector average* (VA), or *feature tracking* (FT). The IOC rule is a geometric construction also known as the *velocity-space* solution. As each grating has a locus of possible motions, the velocity vector of the resulting coherent plaid points to the intersection of both constraint lines (see Figure 3.4, circle) (Adelson and Movshon, 1982). The VA solution corresponds to the average of the normal velocities of the two composing gratings. Graphically, this is represented in velocity space by the point located halfway between the two normal velocities (see Figure 3.4, square). A FT solution for intensity patterns corresponds to the velocity of some of their features. In plaid stimuli, for example, it can be the locations of maximum luminance at the grating intersections (Ferrera and Wilson, 1990; Mingolla et al., 1992). It is worth to noting that for plaid patterns both the FT and IOC solutions correspond to the true pattern motion.

Which of the three solutions best describes human perception is still an open question: the probability of identifying the coherent plaid motion strongly depends on both the observer's perceptual ability and the stimulus attributes, of which the most relevant include luminance (Stoner et al., 1990), contrast (Champion et al., 2007; Stone et al., 1990; Thompson, 1982),

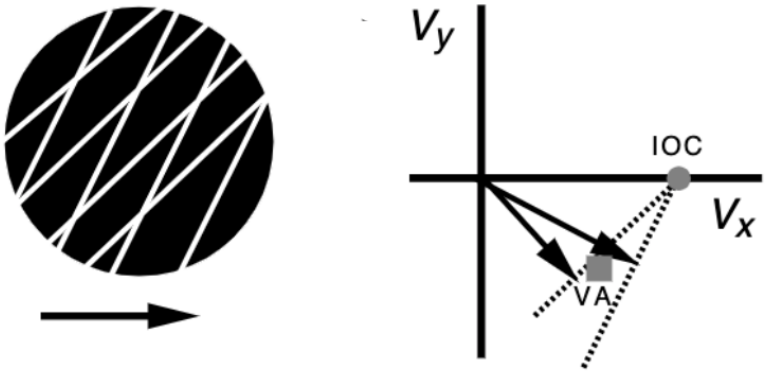

Figure 3.4 On the left, a moving plaid pattern. On the right, velocity space representation. IOC solution (grey circle) is the intersection point of the constraint (dashed) lines of both gratings. VA solution (grey square) is the average of the two normal velocities. From Weiss et al. (2002)

gratings' direction and speed (Burke and Wenderoth, 1993; Ferrera and Wilson, 1990; Hupé and Rubin, 2004; Kim and Wilson, 1993; Welch and Bowne, 1990), exposure duration and eccentricity with respect the retinal image (Yo and Wilson, 1992b).

3.3.1 Luminance configuration

Luminance configuration (LC) is one of the most effective and well-documented attribute in modulating the perceptual segmentation in static images (Beck et al., 1984; Metelli, 1974). More recently, this property has been measured also in moving plaid patterns (Movshon et al., 1985; Rodman and Albright, 1989; Stoner and Albright, 1992; Stoner et al., 1990).

Stoner et al. (1990) investigated the effect of surface segmentation in motion coherency by manipulating LC, in order to control perceptual transparency in moving plaid patterns, as shown in Figure 3.5. Plaid can be seen as the combination of drifting occlusive surfaces (i.e. *transparent motion*), in which a proximal surface (foreground) overlaps a distal surface (background) in the formation of the retinal image, or as a single moving pattern (i.e. *coherent motion*). Depending on the physical properties of the occlusive surfaces, there are *transparent surfaces*, which partially attenuate light reflected off of the surfaces they occlude, or *opaque surfaces*, which provide complete attenuation. LC can be consistent or not with the superimposition of such surfaces, as shown in Figure 3.6. Authors found that the probability of reporting transparent motion increases as the LC is adjusted to arouse a percept of superimposed surfaces. Together with other studies (Adelson and Movshon, 1982; Kooi et al., 1992; Shimojo et al., 1989; Trueswell and Hayhoe, 1993; Vallortigara and Bressan,

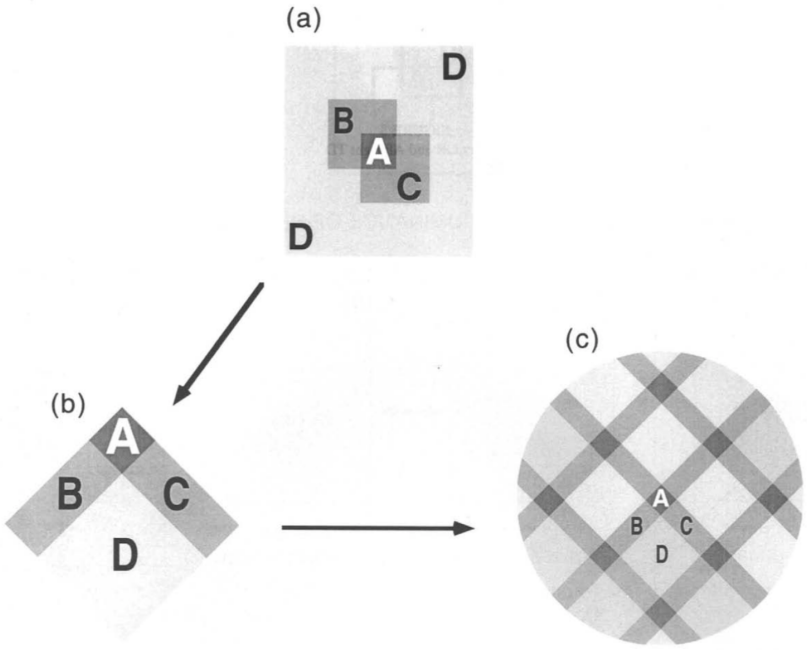

Figure 3.5 Transparency manipulation in plaid stimuli. Each plaid (c) can be seen as composed of four distinct repeating subregions (a, b), identified as A, B, C, and D. Region D is normally viewed as background, regions B and C as overlapping surfaces, and region A as their intersection. From Stoner et al. (1990).

1991), these results suggest that the depth ordering of segmentation cues is used to elicit the integration of visual motion signals (Albright and Stoner, 1995; Stoner and Albright, 1996).

Many studies on perceptual transparency showed that this effect is most likely when the contrast of the background observed through the transparent foreground surface is less than or equal to the contrast of the background observed directly (Beck et al., 1984; Metelli, 1974); see Figure 3.6. This stems from the fact that luminance contrast within a background surface is normally attenuated when viewed through an occlusive foreground surface. It follows that the transparent percept is elicited by a given LC only if the observer decodes some portions of the image as foreground and other regions as background. This means that motion coherency should also be dependent upon foreground/background (or *context*) interpretation (Albright and Stoner, 1995; Stoner and Albright, 1996).

It is worth noting that there are many image features that influence context interpretation, and they has to be in accordance in order to elicit a percept of transparency. Qian et al. (1994) proposed that locally unbalanced motion signals in different directions are perceptually transparent.

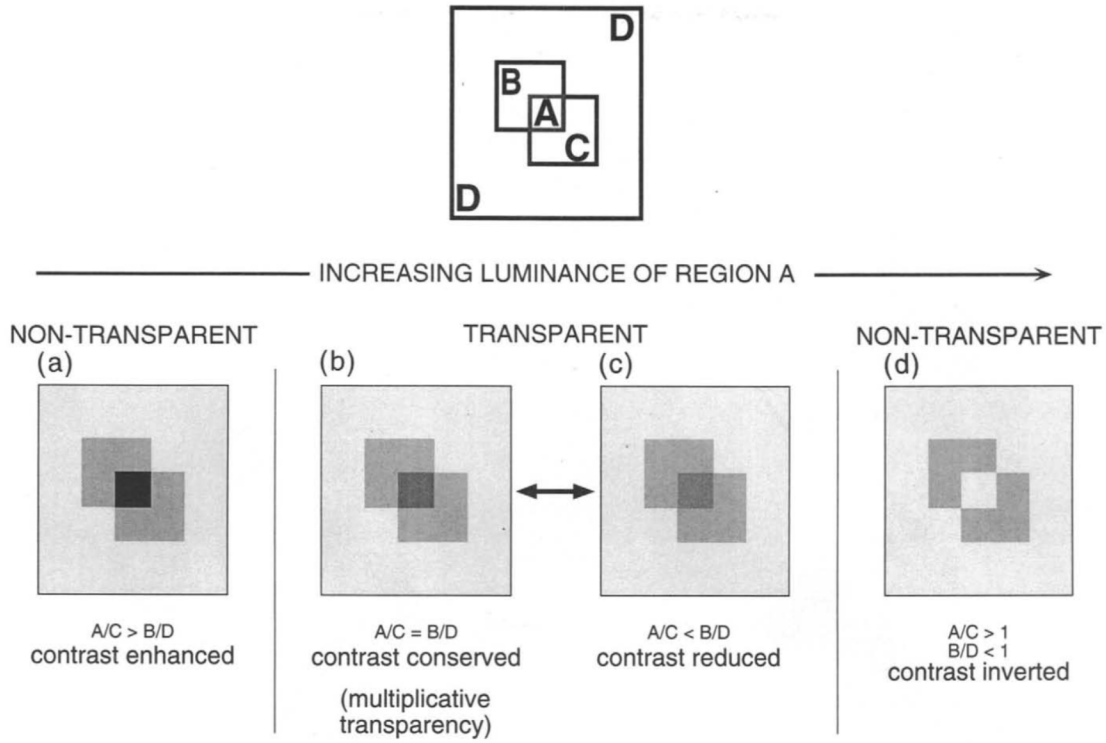

Figure 3.6 Luminance ratios within the pattern must follow the luminance rules governing perceptual transparency in order to convey a sense of depth ordering. Each pattern can be seen as composed of four distinct repeating subregions: region D is normally viewed as background, regions B and C as overlapping surfaces, and region A as their intersection. Perceptual transparency is most likely if the contrast ratio A/C is conserved (b) or reduced (c) relative to the contrast ratio B/D, but perceptual transparency is not likely if the contrast ratio A/C is enhanced (a) or inverted (d). From Stoner et al. (1990).

Albright and Stoner (1995) confirmed that perceptual coherency for both static and moving plaids depends upon agreement between attributes related to LC and context interpretation. Furthermore, they found that the same plaid stimulus can induce either coherent or transparent perception, and this is highly correlated with foreground/background interpretation. The critical role of context assignments supports authors' idea that the motion system has access to neural processes of image segmentation, which integrate the information needed for the image formation from natural scenes.

Several studies investigated the effect of LC manipulation in terms of their spectrum of Fourier components (Noest and Van Den Berg, 1993; Plummer and Ramachandran, 1993; Stoner and Albright, 1992; Trueswell and Hayhoe, 1993). This has been a controversial aspect, because LC manipulation alters the spectrum of Fourier components associated with the moving plaid. In particular, if a plaid stimulus undergoes a LC adjustment eliciting a percept of overlapped surfaces, its Fourier components move in the coherent pattern direction (Stoner et al., 1990; Victor and Conte, 1992). These observations led to an opposite prediction for the results of Stoner et al. (1990): coherent motion should be more likely for transparent plaids. However, it can be shown that Fourier components moving in the pattern direction are minimized whit transparent plaid stimuli by considering that in an early stage of neuronal processing the image intensity undergoes a roughly logarithmic compression (MacLeod, 1978; Macleod et al., 1992). With this clarification the psychophysical results of Stoner et al. (1990) are in agreement with the predictions of a mechanism based upon the spectrum of Fourier components.

3.3.2 Gratings' contrast

The dependence of the perceived speed of single gratings on contrast had been demonstrated widely (Adelson and Movshon, 1982; Champion et al., 2007; Stone et al., 1990; Thompson, 1982; Thompson et al., 2006; Yo and Wilson, 1992b).

Thompson (1982) found that a reduction in contrast induces a decrease in perceived speed for slow moving gratings, but the perceived speed increases for faster moving gratings.

Adelson and Movshon (1982) found that gratings' contrast affect also the perception of coherent motion in plaid stimuli. During their experiments, participants were shown a superimposed pair of sinusoidal gratings that could each be varied in orientation, direction and speed of motion, contrast and spatial frequency. After a small period of exposure ($\sim$1.5 s), they were asked to report if the pattern appeared 'coherent' or 'incoherent'. Gratings had the same contrast, spatial frequency and speed, and moved at an angle of 135 deg to one

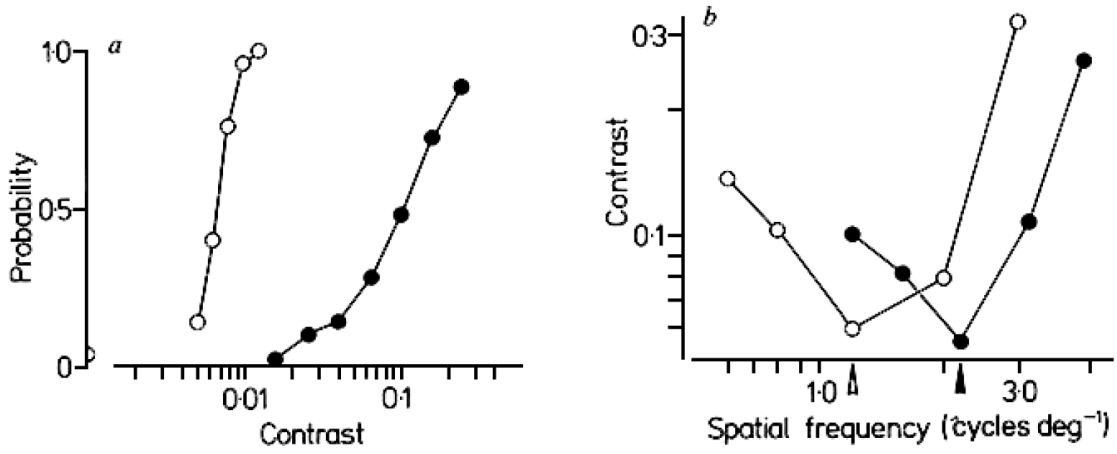

Figure 3.7 a) The influence of contrast on the probability of detection (open symbols) and coherence (filled) of two superimposed sinusoidal gratings. b) The combined influence of both spatial frequency and contrast on coherence. From Adelson and Movshon (1982).

another. In a first experiment the contrast of one grating was fixed at 0.3, while the other was varied. Figure 3.7a shows the probability of detecting low-contrast grating when the other has a high-contrast (open circles), and the probability of a coherent percept (filled circles). Both probabilities rise as the contrast increases, but coherence is favoured by the contrast values that allow us to observe both gratings distinctly.

Adelson and Movshon (1982) investigated also the combined effect of gratings' contrast with their relative spatial frequency on coherence. They used a staircase procedure in which both the contrast and the spatial frequency of the first grating were fixed, while both the contrast and spatial frequency of the other grating were varied until the observer was able to perceive the coherent motion on half of the trials. In two different experiments the spatial frequency of the first grating was fixed at 1.2 cycles/deg (filled circles) and 2.2 cycles/deg respectively, and both have a fixed contrast of 0.3. Results show that coherence increases as the spatial frequency of the two gratings become similar, as shown in Figure 3.7b.

Subsequently, Stone et al. (1990) measured systematically the effect of the relative contrast of two gratings on the perceived direction of plaid motion. They found that, when the composing gratings of a plaid have different contrasts, the perceived direction of the coherent pattern is not predicted by the IOC rule, but there is a bias in the direction of the higher-contrast grating. During the experiment, participants were presented with a moving plaid stimulus composed of a pair of sinusoidal gratings seen through a two-dimensional Gaussian window. Gratings had the same spatial frequency (1.6 cycles/deg) and were oriented symmetrically at ± 60 deg from the vertical axis. Participants were asked to report if the pattern moved to the right or left of subjective vertical. Authors called *perceived vertical* the

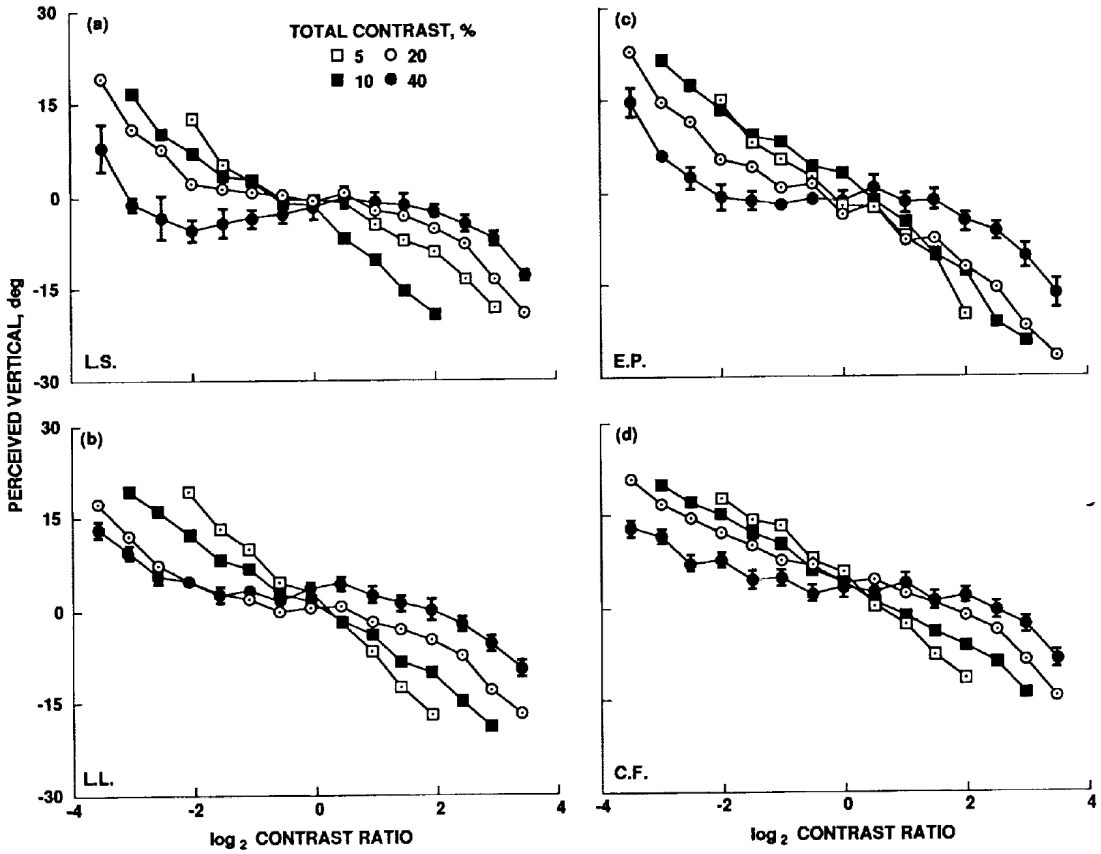

Figure 3.8 Perceived vertical represented as a function of $log_2(contrastratio)$ at total contrast of 5, 10, 20, and 40% for four participants. Error bars indicate standard deviations. Leftward biases have positive values. From Stone et al. (1990).

direction for which participants chose left or right with equal probability, and define it as the difference in degrees with respect to the true vertical. The true plaid direction was changed by varying the speed ratio of the two gratings, while the plaid speed was kept constant at 2 deg/s. The contrast ratio of the two gratings was varied, whereas the total contrast of the plaid was kept constant at 5, 10, 20 or 40%.

Results of Stone et al. (1990) show that when the gratings' contrast ratio is equal to 1 there is no bias in the average perceived vertical, which indicates that there is no systematic bias. On the contrary, as the contrast ratio is different from 1, the perceived vertical is biased toward the motion direction of the higher-contrast grating, as displayed in Figure 3.8. Authors suggest also that perceived plaid motion is computed by the IOC rule of the perceived speed of the component gratings rather than their true speeds.

More recently, Champion et al. (2007) revised and extended the study of Stone et al. (1990). Authors tested the effect of contrast on the perceived direction of a moving plaid by

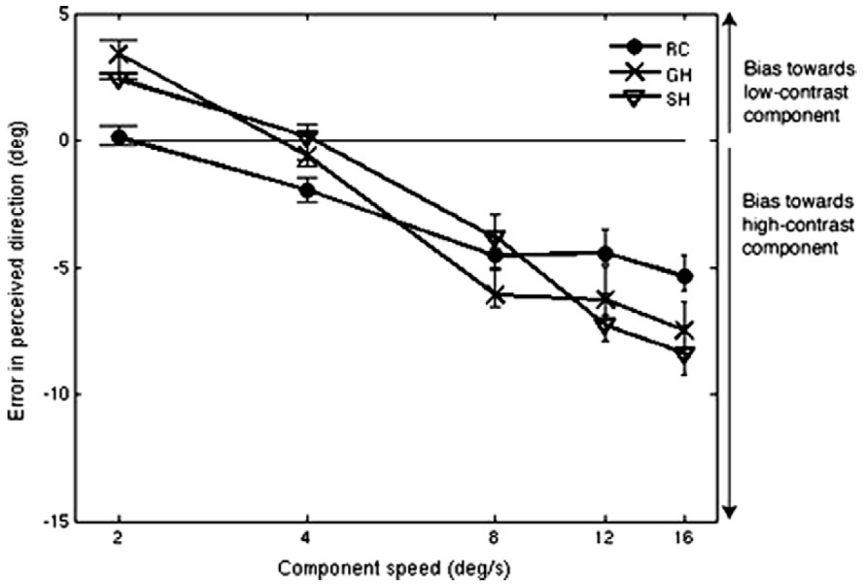

Figure 3.9 Errors in perceived plaid direction as a function of component speed, for three subjects. The solid horizontal line at zero represents the prediction of the IOC model. Error bars represent 95% confidence intervals. From Champion et al. (2007).

testing a wider range of component speeds than used previously (from 2 to 16 deg/s). Results displayed in Figures 3.8, 3.9 show that the perceived direction of moving plaid with equal physical component speed and unequal component contrast is biased towards the direction of the higher-contrast component at faster speeds, but towards either the high-contrast or the low-contrast grating at the slowest speeds (i.e. under ~ 4 deg/s). These results suggest that the IOC rule applied to either physical or perceived component speed is not able to predict the perceived speed changes across a wide range of contrasts.

3.3.3 Type I vs Type II plaids

An important feature of the IOC rule is that all pairs of components lying along the circle indicated in Figure 3.10 result in the same plaid vector. Therefore, composing gratings of various orientations and drift rates can construct different plaid patterns, which share the same plaid speed and direction as long as the direction and speed of each component is constrained by the following relation:

$$v_p = v_c / \cos\theta \tag{3.1}$$

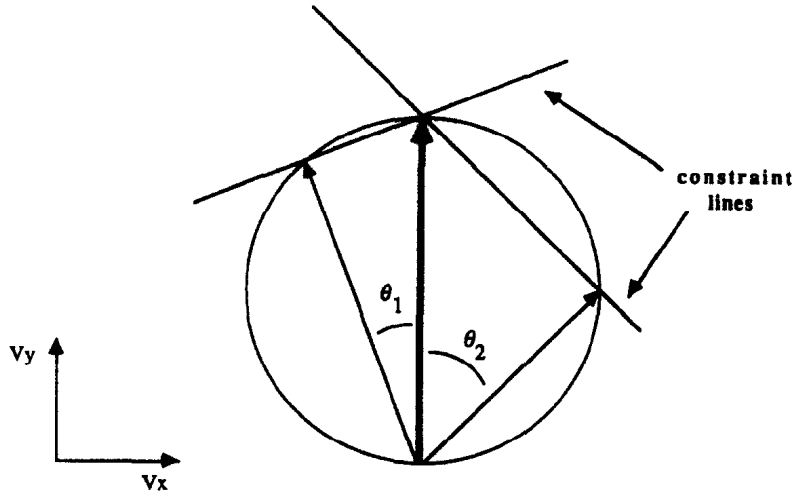

Figure 3.10 Representation of IOC rule in velocity space. Thin arrows displays the motion of the two component gratings, whereas the thick one indicates the motion of the resultant two-dimensional pattern. θ_1 and θ_2 show the directions of the components relative to the resultant. From Ferrera and Wilson (1990).

where v_p is the plaid speed, v_c is the component speed, and θ is the difference between the plaid and the component's directions.

Ferrera and Wilson (1987) classified plaid stimuli in three types of patterns displayed in Figure 3.11, called *type I symmetric plaid*, *type I asymmetric plaid*, and *type II plaid*, and measured their perceived direction. Authors originally distinguished between type I and type II plaids on the basis of their deeply different effects as masks. The task required detection on a test component moving in the direction of the superimposed masking plaid predicted by the IOC rule. Results showed that threshold changes for type I patterns were independent of the angle between the two masking gratings over a wide range, whereas for type II patterns threshold changes were determined by the mask component whose motion direction was closest to the IOC resultant.

One of the main differences between type I and type II patterns is from their geometrical arrangement, so that the resultant of type I plaids, both symmetric or asymmetric, lies between the directions of the two composing gratings (VA prediction correspond to IOC prediction), whereas for type II patterns the resultant is outside the two components and agrees with the IOC solution (VA and IOC predictions are different). Therefore, type II plaids provide a more rigorous test of the IOC rule, whereas in type I plaids these solutions can be mistaken (Cropper et al., 1996; Ferrera and Wilson, 1990).

Ferrera and Wilson (1990) found that the perceived direction of type I plaids corresponds to the IOC solution, whereas for type II patterns it is significantly biased toward the average

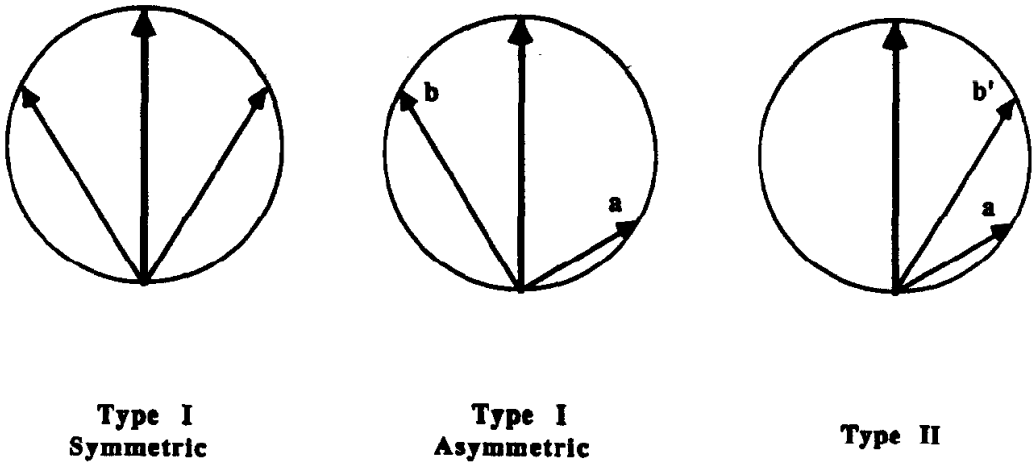

Figure 3.11 Velocity-space diagrams different types of plaid stimuli: type I symmetric, type I asymmetric, and type II. All three plaid types have the same intersection-of-constraints resultant (thick arrows), despite having different pairs of components (thin arrows). From Ferrera and Wilson (1990).

direction of the two component gratings by about 7.5 deg. All perceptual differences between type I and type II patterns suggested that the underlying neural circuitry for analysing them is different (Ferrera and Wilson, 1987, 1990).

3.3.4 Motion direction of component gratings

Kim and Wilson (1993) studied the dependence of moving plaids on the amplitude of the angle between the component gratings. Authors found that the coherent motion is more likely perceived for angles of less than ± 45 deg, whereas for angles of ± 45 deg or greater the components were perceived to slide transparently. The results were confirmed when the ratio of component contrasts or speeds was changed over a factor of 2 and the spatial frequency ratio was varied up to 9:1.

As reported previously, the perceived direction of a type II plaid does not correspond to a pure VA or a pure IOC mechanism. Burke and Wenderoth (1993) investigated the dependence of perceived direction of type II plaids on the angle between the components gratings, and found that it gradually shifts from the VA to the IOC solution as the angle between the components increases.

3.3.5 Motion direction of plaid stimulus

Visual system shows a greater sensitivity to horizontal and vertical stimuli than to oblique ones, and this evidence is known as the *oblique effect* (Appelle, 1972). Subsequent studies related this result to orientation-selective V1 neurons (Furmanski and Engel, 2000; Mansfield, 1974).

Hupé and Rubin (2004) studied this paradigm in type I moving plaids and demonstrated that the direction of plaid motion can influence the relative strength of coherent percept. Figure 3.12 shows the relative cumulative time spent perceiving coherency, $C/[C+T]$, in both cardinal and oblique directions for each participant. On the top, it can be observed that plaids moving in cardinal directions cohere about 25% more than plaids moving in oblique directions. On the bottom, the polar representation highlights that there is also a difference between the two cardinal directions: the coherent motion percept is more likely when plaids move in horizontal than in vertical direction.

Figure 3.13 displays the natural log of the time between stimulus onset and the first report of transparency, Ln(RTtransp), in each of the eight directions tested for all participants: it can be seen that plaids moving in cardinal directions show longer response times to report transparency (RTtransp).

3.3.6 Exposure duration of moving plaids

Several studies investigated the effect of exposure duration on perceived direction of moving plaids (Bowns, 1996; Yo and Wilson, 1992a,b).

Yo and Wilson (1992b) used type II patterns constructed with component gratings having the same spatial frequency and contrast. They found that perceived direction is biased toward the VA direction at short durations (< 90 ms) and moves to the IOC solution after a certain delay. This delay depends on contrast: for instance, at 5% of contrast, the perceived direction after 1 s of stimulus exposure remained biased by more than 20 deg.

Afterwards, Yo and Wilson (1992a) confirmed that the motion direction of symmetric type I plaids is accurately perceived at all exposure durations, whereas for type II patterns it appears to move in the VA direction for durations below about 60 ms.

More recently, Hupé and Rubin (2003) found that perception of moving plaids is bi-stable over time: at stimulus onset they can be perceived as moving coherently or transparently, but a sustained stimulus presentation yields a continuous alternation between coherent and transparent percepts over time.

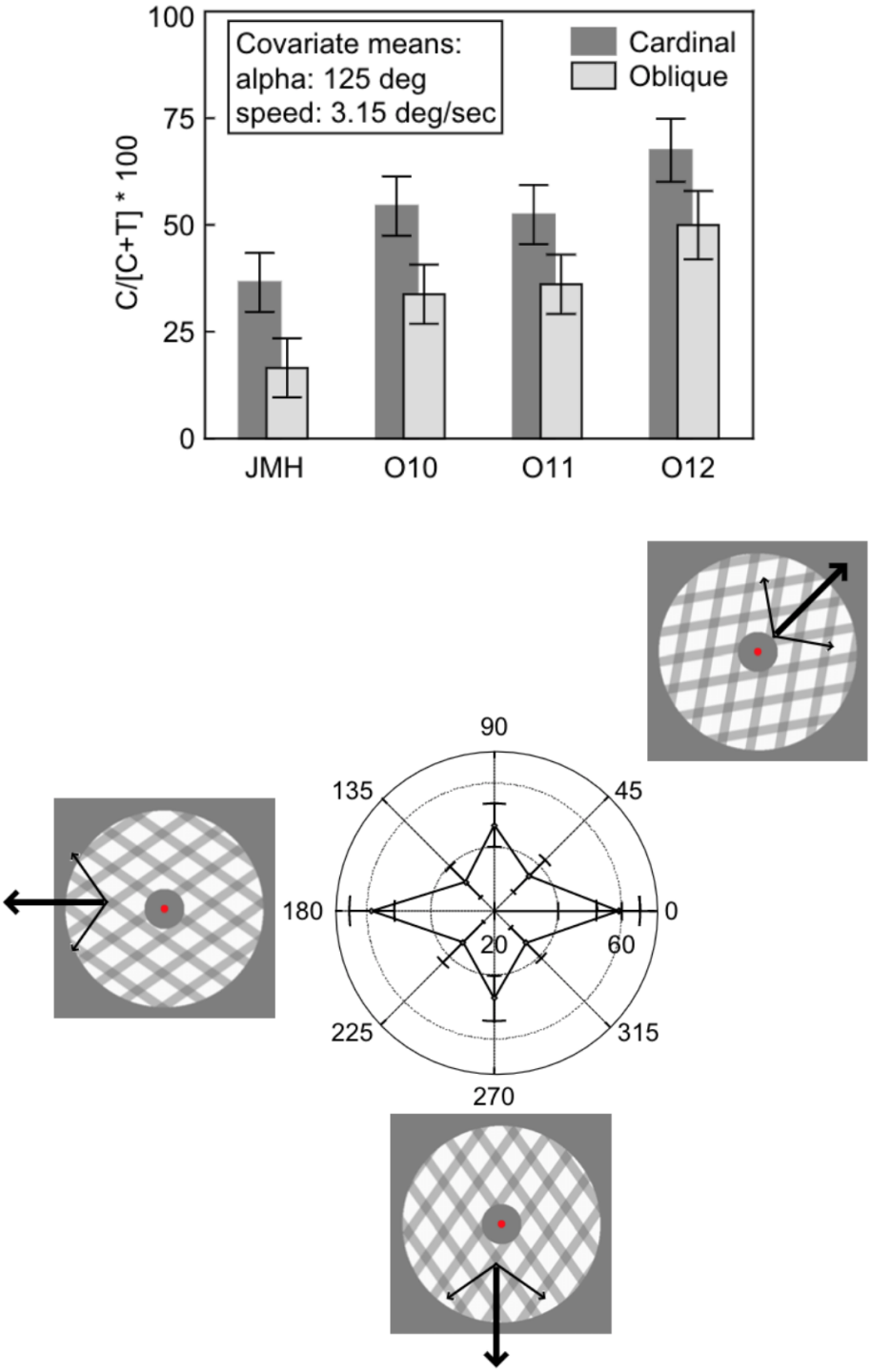

Figure 3.12 On the top, the probability of perceiving the coherent percept for both cardinal and oblique directions for each participant. On the bottom, polar plot of the effect of the plaid global direction on the probability of coherency, as measured by $C/[C+T]\cdot 100$. Icons depict examples of plaids. Arrows indicates directions of both plaid (thick arrow) and gratings (thin arrows). From (Hupé and Rubin, 2004)

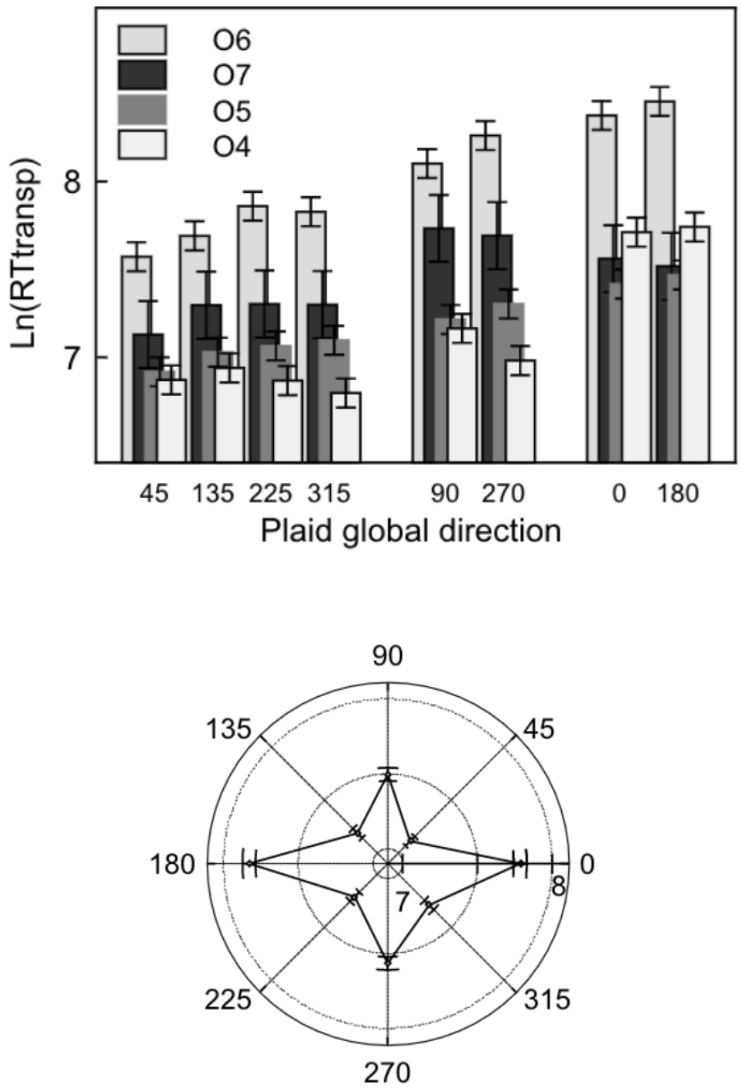

Figure 3.13 On the top, average response times to see transparency for the tight directions of motion and for each participant. On the bottom, polar plot of the effect of the plaid global direction on $Ln(RTtransp)$. From Hupé and Rubin (2004)

3.3.7 Perceived speed of moving plaids

Velocity of moving plaids involves speed as well as direction. Several studies investigated how plaid speed is perceived, and its dependence on other stimulus parameters, for example gratings' contrast.

Ferrera and Wilson (1991) compared perceived plaid speed to that of a single cosine grating. This study showed that perceived speed for both type I and type II plaids was determined by the spatial frequency of the moving intersections, and not by the spatial frequency of the single composing gratings. Moreover, type I and type II patterns show identical speed processing, but significantly different direction processing. These evidences suggest that the final stage of speed and direction computations occur in parallel (Bergen and Wilson, 1985; Wilson et al., 1992).

The effect of contrast on speed perception was first reported by Thompson (1982), who demonstrated that lower-contrast stimuli appear to move slower than higher-contrast stimuli at slow speeds. However, as speed increases this effect reduces and at high speeds can even reverse, so that low-contrast stimuli seem to move faster than high-contrast stimuli. In contrast, Stocker and Simoncelli (2006) found that there is no evidence for a reversal effect for speeds up to 12 deg/s, such that the lower-contrast stimulus was perceived to be slower than the higher contrast stimulus.

Stone and Thompson (1992) investigated speed perception in type I moving plaids and found that the influence of gratings' contrast on perceived component speeds is largely independent of the absolute contrast level, and appears to follow a quasilinear function of log contrast ratio.

In addition, results from Bowns (1996) on type II patterns show that when speeds of the two component gratings are similar, the perceived direction of plaid motion is consistent with the VA solution, whereas it moves to the IOC solution when speeds are dissimilar. Moreover, the bias of perceived plaid direction decreased with increasing plaid speed (Stocker and Simoncelli 2006).

3.3.8 Eccentricity of the visual field

Several studies investigated the dependence of the perceived direction of moving plaids on the eccentricity of the visual field.

Ferrera and Wilson (1990) measured direction-discrimination thresholds in foveal visual conditions. Results show that thresholds averaged about 1.0 deg for type I plaids and about 5.0 deg for type II plaids.

Yo and Wilson (1992a,b) measured the perceived direction of type I and type II patterns whit an increased eccentricity of the visual field (15 deg). They found no effect in the perceived direction of type I plaids, whereas for type II patterns the perceived direction was considerably biased away from the IOC to the VA solution (about 25 deg in all visual field quadrants). This indicates that type II plaids can not be properly processed in the visual periphery.

3.4 Conclusion

Plaid stimuli are excellent candidates as ambiguous patterns and, as highlighted in the previous paragraphs, in the literature many studies have investigated how their visual perception can be modified by modulating the parameters of the stimulus.

Yet, is it possible to modify this perception if the observer actively control the stimulus? Let's imagine that the plaid motion is generated and controlled directly by the observer's hand moving on a plane. This will allow her/him to experience the sensorimotor contingencies that bind the movement of the hand to the sensory consequences it produces. How does the observer's perception of the stimulus change? Furthermore, is this change temporary, or is it possible to learn in a more persistent way some invariant characteristic of the stimulus, such as its geometric construction?

To answer these questions, I hypothesized that it was possible to control this perception by interacting directly with the stimuli. To do this, I selected the stimulus parameters for which perception is more uncertain and far from the coherent motion percept. This situation of uncertainty, as demonstrated in other studies (Bejjanki et al., 2011; Briscoe and Grush, 2020; Maiello et al., 2018), can facilitate the integration of heterogeneous information, derived from different sensory systems.

Firstly, I chose type II plaids in order to have a better discriminability between the direction of the coherent motion of the global pattern (IOC solution) and the direction of the transparent motion of the gratings (VA solution), because with type II plaids the IOC and VA solutions do not coincide. To increase this distinction, I chose a very large angular difference between the two solutions (about 60 deg), and a small angular difference between the gratings directions (about 10 deg). Moreover, I adopted the oblique directions and a low speed (equal to 5 deg/s), in order to facilitate the perceptual bi-stability of the pattern between coherent and transparent motion.

Gratings have been designed to have the same contrast and the same spatial frequency, whose values are in line with the choices made by the studies found in the literature; values

of spatial frequency are at the limits of the range for which the (human) contrast sensitivity is highest on average (Robson, 1966). The diameter of the circular aperture is also in line with the values found in the literature.

In the next two chapters more details are provided on which parameters are manipulated during each experimental study.

Chapter 4

Motor training disambiguates perception of complex visual stimuli [1]

4.1 Introduction

Movement and perception influence one another. This interplay begins during development when acquiring sensorimotor skills and persists throughout life, and depends on active interaction with the environment (Held and Hein, 1963). The influence of movement on perception has been documented in situations in which motor adaptation or motor skill learning affects subsequent perceptual tasks. Situations such as force field (Mattar et al., 2012; Ostry et al., 2010; Vahdat et al., 2011), visuomotor (Cressman and Henriques, 2009; Volcic et al., 2013) and prism adaptation (Beckett, 1980; Harris, 1963), maze tracing (Mirdamadi and Block, 2020) and goal directed movement (Cuppone et al., 2018) each show that perceptual changes occur in conjunction with learning. Similarly, perceptual learning has been shown to affect movement. Changes in movement are observed following perceptual training in both upper-limb movement (Henriques and Cressman, 2012; Ostry and Gribble, 2016) and speech (Lametti et al., 2012; Nasir and Ostry, 2009). However, the majority of this work has focused on the somatosensory system and its relation to movement. By comparison, the role of sensorimotor learning in establishing the relationship between movement and vision has been less explored (Beets et al., 2010b; Brown et al., 2007). This lack of understanding maybe attributable to the use of scenarios involving reduced visual displays, in which possible changes to visual perception are limited.

[1] *A manuscript with material from this chapter has been submitted as Sedda, G., Ostry, D. J., Sanguineti, V., and Sabatini S. P. (2020). Motor training disambiguates perception of complex visual stimuli.*

Vision is inherently ambiguous, as for example when we look at objects with shadows or in different lighting. With development, through movements and our interactions with the environment, we learn to combine different cues and contextual information to solve this ambiguity. As an experimental model for this process, properly impoverished and fragmented stimuli can be used to make visual perception more difficult.

In the present study, I use a moving stimulus, known as a plaid, which when seen through an aperture is inherently ambiguous (Adelson and Movshon, 1982; Fennema and Thompson, 1979; Wallach, 1935). A plaid is a complex pattern composed of two superimposed drifting gratings that move in different directions, separated by a defined angle. By varying either features of the individual gratings (spatial frequency, drifting speed, contrast, depth, luminance) or plaid properties (drifting speed, presentation time), it is possible to modulate the stimulus perceptual ambiguity (Hupé and Rubin, 2004; Kim and Wilson, 1993; Stoner and Albright, 1992). The stimulus can be perceived either as a coherent moving pattern in a single direction, or as two overlapping gratings, which slide over each other in different directions (a situation referred to as transparent motion) (Stoner et al., 1990). As a general rule, the perception of coherent motion in a single direction is promoted when the plaid stimulus is balanced, i.e. the properties of the two composing gratings are similar (e.g. in spatial frequency, contrast, or luminance).

Here I show that movement affects the way we make sense of complex visual information. We use plaid stimuli in which the direction of plaid motion is tied to direction of movement. We find that perceptual uncertainty associated with moving plaids is reduced when participants directly control plaid movements. Simulation of the perceptual data using a Bayesian generative model of plaid perception suggests that movement training promotes the fine-tuning of the internal representation of plaid geometry.

4.2 Materials and Methods

4.2.1 Subjects

A total of 30 subjects (11 male and 19 female, 18–30 years old) participated in this study. All participants had normal or corrected-to-normal vision and reported no history of neurological disorder. They were naïve to the purpose of the study and received written and verbal instructions before the start of the experiment. Each participant was randomly assigned to one of three groups (10 participants per each group). The research conforms to the ethical standards laid down in the 1964 Declaration of Helsinki that protects research participants

and was approved by the Ethical Committee of the Dept of Informatics, Bioengineering, Robotics and Systems Engineering, University of Genoa. Each subject signed a consent form conforming to these guidelines.

4.2.2 Apparatus

Visual stimuli were presented on a 19-inch LCD monitor (Samsung B2430L) at 1920×1080 pixels, and refreshed at 60 Hz. In a dimly lit room, participants were seated in front of the screen at about 57 cm of distance, so that the visual angle of the whole display was 60 deg; see Figure 4.1A. In one part of the experiment (see below) participants grasped the puck of a digitizing tablet (CalComp, Inc, 3200-series DrawingSlate II, Model 32120) to actively drive the motion of the visual stimulus using planar movements. The digitizer had a 305 mm$\times$457 mm workspace, and a 125 Hz sampling rate. The center point of the screen was mapped onto the center of the digitizing tablet, with a 1:1 scale factor, see Figure 4.1C.

4.2.3 Stimuli

We presented a plaid stimulus composed of two square-wave gratings through a circular aperture, about 13 deg in diameter, on a black background, as shown in Figure 4.1A. The luminance of the black background outside the aperture was 0 cd/m^2. The two gratings had normal directions θ_1 and θ_2. The plaid moved at speed $v = 5$ deg/s in the direction $\theta = 45$ deg (from the lower left corner of the screen to the upper right corner). $\Delta\theta_1 = \theta_1 - \theta =$ -60 deg and $\Delta\theta_2 = \theta_2 - \theta =$ -75.5 deg define the relative directions of the individual gratings with respect to the direction of the plaid. With this geometric arrangement the ratio between the two gratings speeds is $\cos\Delta\theta_1 / \cos\Delta\theta_2$. In particular, stimuli were designed as plaids, whose direction fell outside the range of the directions of the two component gratings (type II plaid, see Ferrera and Wilson (1990)). In particular, we chose gratings directions that were relatively close to one another, and far away from the direction of the whole plaid pattern. Because of this geometric arrangement the plaid motion direction was distinct from that of the gratings (Cropper et al., 1996), and the directions of gratings were sufficiently close to one another to be interchangeable with their average. Each grating was composed of dark (55-65 cd/m^2) and light (115-125 cd/m^2) stripes, and a spatial frequency of 0.6 cycle/ deg. Stimulus was presented in transparency (Stone et al., 1990; Stoner and Albright, 1992; Stoner et al., 1990), and the perceptual uncertainty was modulated by varying the contrast level of

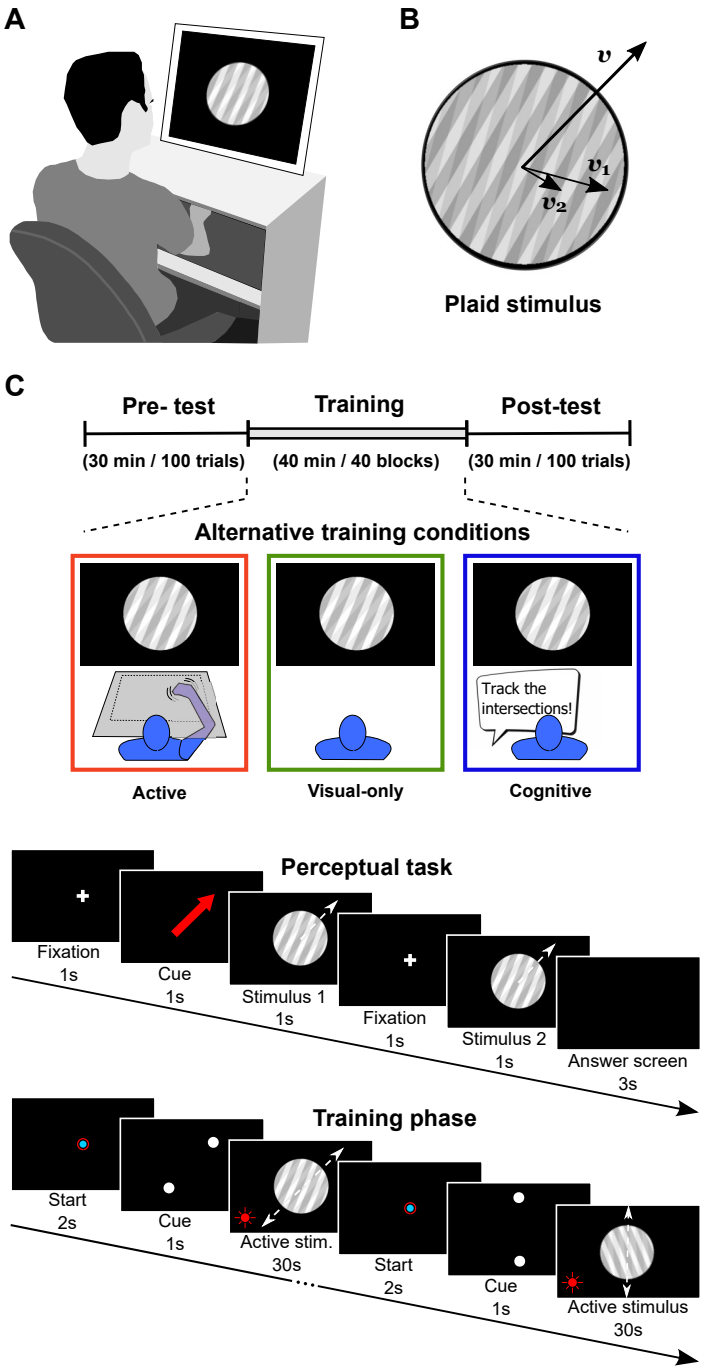

Figure 4.1 A: Experimental setup: The participant is seated in front of a screen and is exposed to moving visual stimuli (plaid). During active training they perform planar movements which result in motion of the plaid on the screen. Visual feedback of the arm is blocked. B: A plaid stimulus with velocity $\boldsymbol{v}$, composed of two gratings moving at velocities $\boldsymbol{v}_1, \boldsymbol{v}_2$. C: The experimental protocol has three phases: Participants start with a perceptual judgement task, then they perform a training task, and finally they repeat the perceptual task. Participants were divided in three groups, each with a different training condition: active, visual-only, and cognitive. The perceptual task is a 2AFC paradigm: Participants see two consecutive moving plaid stimuli, and are asked to choose which stimulus is moving in a direction more similar to that of the red arrow. During training participants are exposed to moving plaids: Participants in the active group perform planar hand movements to control the plaid motion on the screen, while participants of both the visual-only and cognitive groups observe played-back motions. In the cognitive condition, participants are instructed to track the intersections of the gratings.

each grating. The overall plaid image was defined as:

$$L(\boldsymbol{x},t) = L_0[1 + C_1 g_1(\boldsymbol{x},t) + C_2 g_2(\boldsymbol{x},t)]$$

where L_0 is the mean background intensity, g_1 and g_2 are the functions that defined the two component gratings, and C_1 and C_2 are the gratings' contrast levels, respectively (Stoner et al., 1990). The total contrast $C = C_1 + C_2$ was kept constant, and the relative contrast difference between the gratings of each plaid was defined as $\Delta c = |C_1 - C_2|/C$. In all experiments we set $C = 0.5$. Participants were instructed to maintain fixation at the center of the stimulus during the entire duration of stimulus presentation. Stimuli were generated using Psychophysics Toolbox for Matlab (Brainard, 1997; Kleiner et al., 2007).

4.2.4 Experimental Protocol

The experimental procedure had three phases; see Figure 4.1C (top). Participants were initially administered a perceptual judgement task (pre-training test). Next, they underwent a training phase under a variety of conditions (see below). After training, they repeated the perceptual judgement task (post-training test).

Perceptual judgement task

The purpose of this test was to quantify the ability to correctly assess the direction of plaid motion as the relative contrast difference of the two gratings (Δc) was varied. The test used a 2-alternative forced-choice (2AFC) paradigm; see Figure 4.1C (middle). Each trial started with a fixation point (black screen with a white cross at the center) displayed for 2 s. Then a red arrow with a $\theta_a = 45$ deg direction, was displayed for 1 s. Finally, two different plaids were presented for 1 s each, separated by a 1 s fixation point. The two plaids were identical and both moved in the direction $\theta = 45$ deg, but had different Δc. At the end of the trial, participants were asked to choose which of the two plaids had a movement direction which was most similar to that denoted by the red arrow. They had to provide an answer by pressing the left or right arrow on the keyboard within a 3 s time limit to indicate the first or the second plaid, respectively. Throughout the entire test, one plaid (Reference stimulus, R) had a constant contrast difference, $\Delta c_R = 0.8$, which facilitates the perception of gratings motion because of the great unbalance between the contrast of the composing grating. In the other plaid (Test stimulus, T), the contrast difference Δc_T changed on each trial, within a 0-0.8 range. The Test and Reference plaids were presented in random order.

We used a Bayesian adaptive procedure – Ψ (Psi) method (Kontsevich and Tyler, 1999; Prins, 2013) – to select the value of Δc_T on the current trial, based on the participant's answers in the previous trials. We took the selection of the Test stimulus as the correct answer. Every time the subject answered correctly, the Δc_T value was increased, so that it gradually became more and more similar to Δc_R.

The entire perceptual judgment test took a total of 100 trials to complete, which corresponded to a duration of about 30 min.

Active motor training

Participants were instructed to perform out and back planar arm movements between two briefly presented visual cues, in a target direction θ_T; see Figure 4.1C (top, left). The motion of a plaid on the screen was continuously yoked to the instantaneous direction of hand movement, $\theta(t)$, so that the two gratings moved in directions $\theta_1(t) = \theta(t) + \Delta\theta_1$ and $\theta_2(t) = \theta(t) + \Delta\theta_2$ while their relative orientations with respect to plaid motion, i.e. $\Delta\theta_1$ and $\Delta\theta_2$ remained constant.

The training phase was organised into a series of trials, each characterized by a different target hand direction.

At the beginning of each trial, participants had to place the hand (depicted as a blue cursor on the screen) inside a start region (circle on a black background) and hold it there for 2 s. Then both the start region and the cursor disappeared, and a circular aperture was displayed. Two white circles placed just outside the aperture, were displayed for 1 s, at opposite sides with respect to the center of the aperture, 28 deg of visual angle from one another with respect to the participant. The circles indicated the target hand direction for that trial.

As the circles disappeared, a plaid appeared inside the aperture. Participants were instructed to move the hand back and forth in the target direction, between the two remembered circle positions. Participants were encouraged to maintain a speed no greater than 5 deg/s – the speed of the plaid used in the perceptual judgement task. To aid in maintaining the correct speed, participants continuously received visual feedback on movement speed (circular spot in the bottom left corner of the screen; green if the speed was ≤ 5 deg/s, red otherwise). Each trial had a fixed duration of 30 s.

During training, participants were prevented from seeing their arm, so that the only visual information about their movement direction was provided by the plaid motion. During the movement training phase, the relative contrast difference Δc in the plaid was set to that subject's threshold level, as estimated at the end of the pre-training perceptual judgement task.

The entire training protocol involved four target directions (0 deg, 45 deg, 90 deg, 135 deg) each repeated 10 times in pseudo-random order, for a total of 40 trials and an approximate duration of 40 min.

Visual-only training

Participants were instructed to observe on the screen a plaid moving through an aperture, while performing no movements. The plaid stimulus was the playback of a stimulus generated by another participant in the active training group; see Figure 4.1C (top, middle). Again, the total duration of this phase was about 40 min.

Cognitive training

As in the visual-only training condition, participants had to observe on the screen a plaid while performing no movements. In addition, they were provided a hint to estimate the plaid movement direction – track the movements of the grating intersection points which have the same direction and speed of the plaid; see Figure 4.1C (top, right). Again, the total duration was about 40 min.

4.2.5 Data analysis

For each subject, we quantified performance in the perceptual judgement tasks before and after training by estimating a psychometric curve using a Bayesian adaptive Ψ (psi) method (Kontsevich and Tyler, 1999; Prins, 2013) and assuming a normal cumulative distribution function. We used the threshold and slope of the estimated psychometric curve as measures of perceptual performance. The threshold value is defined as the Δc_T value corresponding to 75% probability of selecting the Test stimulus, whereas the slope is defined as the inclination value of the psychometric curve at the threshold point. It is important to note that the number of trials (i.e. 100) chosen for the perceptual judgement task allows full convergence for the perceptual threshold values, but not for the slope estimates (Kontsevich and Tyler, 1999). We then assessed whether perceptual performance was affected by training in the active, visual or cognitive training conditions. To do this, we took perceptual threshold and slope before training (th_{pre}, slope_{pre}) as the baseline perceptual performance. We then looked at the threshold and slope after training (th_{post}, slope_{post}). For each quantity and for all experimental conditions, we first assessed normality (Anderson-Darling test). If normality was not ruled out for perceptual thresholds and/or slopes, we ran a repeated measures 2-way

ANOVA with time (PRE, POST) and experimental condition (active, visual, cognitive) as within- and between-subject factors.

In case the normality assumption had to be rejected, we used a non-parametric test (Kruskal-Wallis) to assess differences among conditions in the perceptual baseline (th_{pre} and slope_{pre}). We then focused on the training-related change ($\Delta\text{th} = \text{th}_{post} - \text{th}_{pre}$; same for slope). We tested for differences among experimental conditions, using 1-way ANOVA if normality was not ruled out; a non-parametric test (Wilcoxon Rank Sum) otherwise. Post-hoc analyses were conducted using pairwise t-test, with a Bonferroni-Holm correction.

Finally, we examined movements of the hand in the active motor training condition. For each trial, we calculated the statistical distribution of hand velocities (direction and magnitude), by separately accounting for forward and backward movements. We subtracted the target direction from the distribution of movement directions and then took the mean (bias) and standard deviation of the directional error for each block and each subject. We assessed how these quantities changed over the course of training (correlation with block number) and whether these changes correlated with changes in perceptual performance.

4.2.6 Computational Model

Plaid geometry

Plaid geometry is completely specified by the overall plaid velocity, $\boldsymbol{v}$ and by the directions of the two gratings, θ_1 and θ_2. The velocity of one single grating, $\boldsymbol{v}_i$, $i = 1,2$ is calculated as the projection of the plaid velocity onto the grating's normal direction: $\boldsymbol{v}_i = \boldsymbol{u}_i \cdot (\boldsymbol{u}_i^T \cdot \boldsymbol{v})$ where $\boldsymbol{u}_i = [\cos\theta_i \sin\theta_i]^T$, $i = 1,2$; see Figure 4.1B. The above expression can be rewritten as

$$\boldsymbol{v}_i = (\boldsymbol{u}_i \cdot \boldsymbol{u}_i^T) \cdot \boldsymbol{v} = U_i \cdot \boldsymbol{v}. \tag{4.1}$$

Sensory system

We assumed that the perceived velocity of each grating, $\boldsymbol{m}_i, i = 1,2$, is affected by additive zero-mean Gaussian noise, so that:

$$\begin{cases} \boldsymbol{m}_1 = \boldsymbol{v}_1 + \boldsymbol{\eta}_1 = U_1 \cdot \boldsymbol{v} + \boldsymbol{\eta}_1 \\ \boldsymbol{m}_2 = \boldsymbol{v}_2 + \boldsymbol{\eta}_2 = U_2 \cdot \boldsymbol{v} + \boldsymbol{\eta}_2 \end{cases} \tag{4.2}$$

where $\boldsymbol{\eta}_i \sim \text{Normal}(0, Q_i)$, $i = 1,2$ and the noise covariance matrix, Q_i, is defined as

$$Q_i = R(\theta_i)^T \cdot \begin{bmatrix} \sigma_{i\perp}^2 & 0 \\ 0 & \sigma_{i\parallel}^2 \end{bmatrix} \cdot R(\theta_i) \tag{4.3}$$

where $\sigma_{i\perp}^2$ and $\sigma_{i\parallel}^2$ are the noise variances in directions that are perpendicular and parallel to grating i, and $R(\theta_i)$ is a rotation matrix. As in Hedges et al. (2011), we set $\sigma_{i\parallel}^2 = h\,\sigma_{i\perp}^2$ with $h = 0.3$, so that the covariance matrix is aligned toward the grating's normal direction. As a consequence, we have that $p(\boldsymbol{m}_i|\boldsymbol{v}) = \text{Normal}(\boldsymbol{m}_i; U_i \cdot \boldsymbol{v}, Q_i)$.

Perception of a single grating is known to be affected by contrast. We assume that the noise variance is proportional to the inverse power of the relative contrast $c_i = C_i/C$, i.e. $\sigma_i^2 = s^2/c_i^q$, where $q > 0$ is the power exponential and s^2 is the variance corresponding to a relative contrast $c_i = 1$. This model is consistent with the findings of Hürlimann et al. (2002), who derived a similar expression. This expression also predicts that zero contrast (i.e., no grating) corresponds to an infinite noise variance. As a consequence, the covariance matrix of each grating is a function of the contrast: $Q_i = Q_i(c_i)$.

Bayesian generative model of plaid perception

We used a Bayesian framework to model the way humans perceive plaid motion (Hedges et al., 2011; Hürlimann et al., 2002; Stocker and Simoncelli, 2006). The optimal estimate of plaid velocity, $\boldsymbol{v}$, from the observed gratings velocities, $\boldsymbol{m}_1$ and $\boldsymbol{m}_2$, is the one which maximizes the posterior probability of $\boldsymbol{v}$, given $\boldsymbol{m}_1$ and $\boldsymbol{m}_2$:

$$\hat{\boldsymbol{v}} = \arg\max_{\boldsymbol{v}} p(\boldsymbol{v}|\boldsymbol{m}) \tag{4.4}$$

From Bayes' theorem, the posterior probability is given by: $p(\boldsymbol{v}|\boldsymbol{m}_1, \boldsymbol{m}_2) \propto L(\boldsymbol{v}) \cdot p(\boldsymbol{v})$, where $L(\boldsymbol{v}) = p(\boldsymbol{m}_1|\boldsymbol{v}) \cdot p(\boldsymbol{m}_2|\boldsymbol{v})$ is the likelihood of $\boldsymbol{v}$ given the observations ($\boldsymbol{m}_1$ and $\boldsymbol{m}_2$), whereas $p(\boldsymbol{v})$ is the velocity prior, which reflects prior experience of the subject with observation of moving stimuli. Several studies have reported a perceptual bias toward low-velocity stimuli, which was modeled as a zero-mean, exponential (Stocker and Simoncelli, 2006) or power-law (Hedges et al., 2011) probability density function. Here, we assume a Gaussian dependence: $p(\boldsymbol{v}) = \text{Normal}(\boldsymbol{v}; \boldsymbol{0}, I\sigma_p^2)$.

The above perceptual model implies that the contrasts of the gratings affect plaid velocity estimation through the gratings covariances, $Q_i(c_i)$. In fact, when the two gratings have the same contrast they equally activate the corresponding Fourier (bandpass) motion channels

and they equally contribute to the perception of the moving plaid. However, there is some evidence that perceiving the velocity of a single grating is affected by vision of another moving grating with a different contrast (Champion et al., 2007; Stone et al., 1990). Hence in the case of contrast unbalance, i.e. $\Delta c \neq 0$, one grating systematically affects the perception of the other. To incorporate this effect, we tentatively assumed that the perceptual system uses an inaccurate representation of plaid geometry, $\hat{U}_i$, thus generating inaccurate predictions of the grating velocities. We specifically set $\hat{U}_i = U_i + \Delta U_i$, where $\Delta U_1 = k U_2 \Delta c$ and similarly $\Delta U_2 = k U_1 \Delta c$, in which k denotes the amount of cross-talk. A consequence of this inaccurate representation of plaid geometry is that each grating is perceived as slightly rotated toward the other, in a way that is proportional to the relative contrast difference. In conclusion, our Bayesian perceptual model assumes that contrast unbalance has both a systematic and a random effect (on U_i and Q_i, $i = 1,2$, respectively).

The optimal estimate of plaid velocity, $\hat{\boldsymbol{v}}$ is a random variable (different $\boldsymbol{m}_i$'s give a different estimate) with a normal distribution, in which both mean and covariance depend on the relative contrast difference, Δc: $p(\hat{\boldsymbol{v}}|\boldsymbol{v},\Delta c) = \text{Normal}(\hat{\boldsymbol{v}}; \boldsymbol{\mu}_v(\Delta c), \Sigma_v(\Delta c))$. Notice that, because of the prior, the estimate is biased – i.e., the estimator's expected value is not the true plaid velocity $\boldsymbol{v}$. Different from earlier Bayesian formulations (Hedges et al., 2011; Weiss et al., 2002), the proposed model predicts two key empirical findings about the error in perceived plaid direction: (i) the error decreases with the logarithm of the contrast ratio (Stone et al., 1990) and (ii) the error is directed towards the higher contrast grating at high plaid speeds, but when the speed decreases the perceived plaid direction is biased towards the low contrast grating (Champion et al., 2007); see Supplementary Information for details.

Perceptual judgement task

The probability of estimating a plaid direction $\hat{\theta}$ given a specific Δc is given by

$$p(\hat{\theta}|\Delta c) = \int_0^\infty p(\hat{\boldsymbol{v}}|\Delta c) \cdot |\hat{\boldsymbol{v}}| \cdot d|\hat{\boldsymbol{v}}| \tag{4.5}$$

The perceptual judgement task can be modelled as a binary decision between two possible answers, Test (T) or Reference (R). The probability of answering T as a function of the contrast difference Δc_T in the Test stimulus and Δc_R in the Reference stimulus, i.e. $\Pr(T|\hat{\theta},\Delta c_T,\Delta c_R)$, where $\hat{\theta} = \theta_a$ (45 deg in our experiment), can be calculated from Bayes' theorem:

$$\Pr(T|\hat{\theta},\Delta c_T,\Delta c_R) = \frac{p(\hat{\theta}|\Delta c_T)}{p(\hat{\theta}|\Delta c_T) + p(\hat{\theta}|\Delta c_R)} \tag{4.6}$$

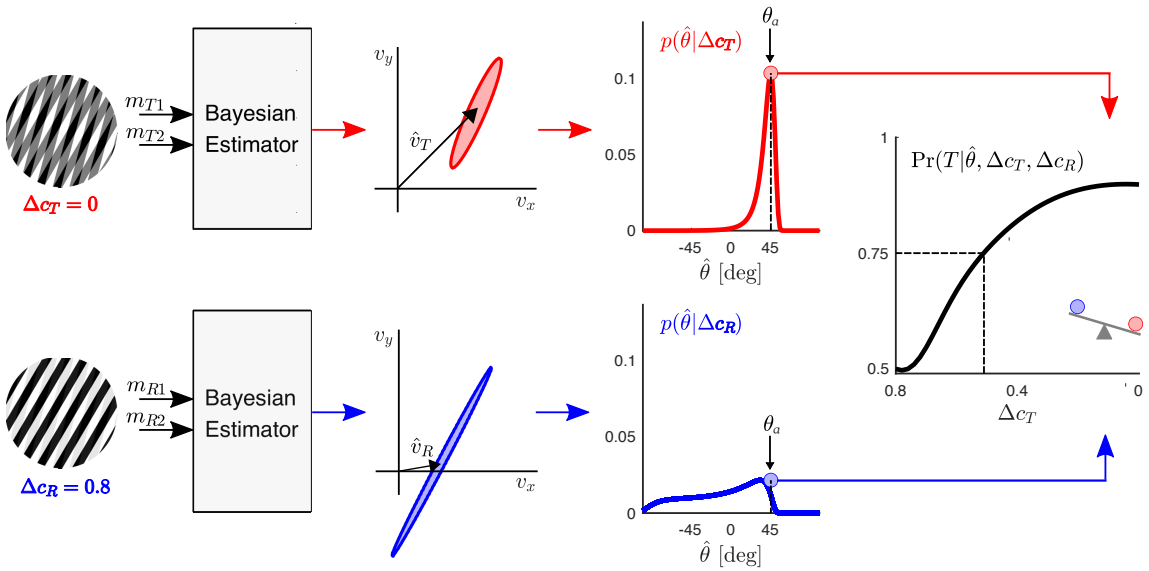

Figure 4.2 Bayesian model for the plaid estimation process and forced-choice paradigm. A Test (T) and Reference (R) plaids are shown, with $\Delta c_T = 0$ (top) and $\Delta c_R = 0.08$ (bottom). For each plaid, the optimal estimate of plaid velocity, $\hat{\mathbf{v}}$, is represented. $p(\hat{\mathbf{v}}|\mathbf{v}, \Delta c)$ has a normal distribution, in which both mean and covariance depend on the relative contrast difference, Δc. The probability of estimating a plaid direction $\hat{\theta}$ given a specific Δc is given by $p(\hat{\theta}|\Delta c)$. The psychometric curve represents the probability of answering T as a function of the contrast difference Δc_T and Δc_R, i.e. $\Pr(T|\hat{\theta}, \Delta c_T, \Delta c_R)$, where $\hat{\theta} = \theta_a$ (45 deg in our experiment).

Note that the model predicts that for $\Delta c_T = \Delta c_R$, the posterior probability is

$$\Pr(T|\hat{\theta}, \Delta c_T, \Delta c_R) = 0.5 \tag{4.7}$$

By decreasing Δc_T, the $\Pr(T|\hat{\theta}, \Delta c_T, \Delta c_R)$ is expected to be greater. Hence for a given value of Δc_R and $\hat{\theta}$, the function $f_T(\Delta c_T) = \Pr(T|\hat{\theta}, \Delta c_T, \Delta c_R)$ can be interpreted as a psychometric curve, whose magnitude ranges between 0.5 and 1.

Figure 4.2 summarizes the proposed Bayesian model of plaid perception. Relative contrast modulates the distribution of the estimated plaid velocity. Two relative contrast conditions, one fixed (R) and one variable (T), are used to build a psychometric curve which denotes the probability of selecting plaid T when asked which plaid among T and R exhibits a movement direction which is closest to the displayed cue.

Estimation of model parameters

The psychometric curve of Eq. 4.6 is a function of the model parameters $w = \left[s, q, \sigma_p^2, k\right]^T$, i.e. $\Pr(T|\Delta c_T, \hat{\theta} = \theta_a) = f_T(\Delta c_T; w)$. We identified the model parameters w from the perceptual judgement data before and after each of the training conditions. The available dataset, $D = \left\{(\Delta {c_R}^{(l)}, \Delta {c_T}^{(l)}, y^{(l)}), l = 1, \ldots, L\right\}$, was obtained from repeated forced-choice tests with different values of $\Delta {c_R}^{(l)}$ and $\Delta {c_T}^{(l)}$, where $y^{(l)}$ is the T/R answer to the l-th test trial (we assume that if T is chosen then $y^{(l)} = 1$; $y^{(l)} = 0$ otherwise). The answer y can be modeled as a random variable with a binomial distribution: $\Pr(y) = p^y \cdot (1-p)^{1-y}$, where $p = \Pr(y = 1|\Delta c_T, \hat{\theta} = \theta_a) = \Pr(T|\Delta c_T, \hat{\theta} = \theta_a) = f_T(\Delta c_T; w)$.

The optimal estimate of the model parameters given the data were obtained by maximizing the model log-likelihood, assuming that the L trials of the perceptual task are independent. The likelihood is given by:

$$\mathscr{L}(w) = \prod_{l=1}^{L} \left\{ f_T(\Delta {c_T}^{(l)}; w)^{y^{(l)}} \cdot \left[1 - f_T(\Delta {c_T}^{(l)}; w)^{1-y^{(l)}}\right] \right\} \tag{4.8}$$

For each subject and for each condition (before and after training), we estimated the model parameters w through numeric maximization of $\log \mathscr{L}(w)$.

4.3 Results

Figure 4.1 illustrates the experimental apparatus and procedure. Figure 4.1B shows the plaid stimulus, which is formed by two gratings with different orientations. When a single moving grating is observed through an aperture, only the component velocity perpendicular to its orientation can be perceived.

By adjusting the relative difference in the contrast of the two gratings, they appear either to be sliding one over the other in directions $\boldsymbol{v}_1$ and $\boldsymbol{v}_2$ or as a single plaid pattern moving in direction $\boldsymbol{v}$. In this way, the extent to which one perceives the coherent motion of a single plaid or two separate gratings can be manipulated. In the experiment participants undergo an initial perceptual judgement task to assess perception of plaid motion for different contrast values (see below). This is followed by a training phase, after which the perceptual task is repeated. In all conditions the plaid motion is seen through an aperture. Three different groups of participants were tested, see Panel 4.1C (top). In an active training condition the participant controls the plaid motion by moving their hand, such that the direction and velocity of the moving plaid corresponds to that of the hand; vision of the hand is blocked. In

a visual-only condition the participant sees a played-back moving plaid stimulus of another participant. In a cognitive condition the stimulus is identical to that in the visual-only condition, and in addition the experimenter instructs the participant to track the intersections of the two gratings. The motion of the intersections corresponds to that of the plaid. This provides participants with an explicit strategy that enables them to correctly estimate the plaid motion.

4.3.1 Perceptual judgement task

Figure 4.1C (middle) shows the perceptual task, which involves a two-alternative forced-choice (2AFC). Participants are presented with two consecutive moving plaids, which differ in the amount of the contrast difference. They are required to indicate which plaid is moving in a direction most similar to that shown by a red arrow. One of the two plaids, a Reference stimulus, has a fixed contrast difference between the two gratings Δc_R. In the other, a Test stimulus, the contrast difference is systematically varied Δc_T, and it is always less, which makes it easier to detect the plaid motion direction.

The results of perceptual task (the probability of selecting the Test stimulus as a function of the contrast difference Δc_T) and, in particular, training related changes in perception are presented in Figure 4.3A. Both threshold differences ($\Delta\text{th} = \text{th}_{\text{post}} - \text{th}_{\text{pre}}$) and differences ($\Delta\text{sl} = \text{slope}_{\text{post}} - \text{slope}_{\text{pre}}$) in the slope of the psychometric function are shown. Better perceptual performance is reflected in an ability to select the Test stimulus under conditions of greater contrast difference, that is for larger values of Δc_T. Both threshold and slope values were estimated using the adaptive Ψ procedure (see Methods). It is worth noting that the number of trials (100) chosen for the perceptual judgment task allows full convergence for perceptual threshold values, but not for the slope estimates (see Methods) (Kontsevich and Tyler, 1999). The values of the perceptual slope are shown for completeness and to allow for qualitative analysis of the results. Figure 4.3B shows psychometric threshold differences and slope differences for all participants in each experimental condition. It can be seen that there are changes in the psychometric threshold for the active group, and no changes in slope in any of the experimental conditions. Statistical analyses were conducted using difference scores which were found to be normally distributed ($P > 0.05$; Anderson-Darling test), whereas the pre-training and post-training perceptual values were not normally distributed ($P < 0.05$). We ran nonparametric tests (Kruskal-Wallis) to verify that baseline values for threshold and slope did not differ. We tested for differences in both the threshold (Δth) and the slope (Δsl) of the psychometric curves. We observed a highly significant difference in threshold between

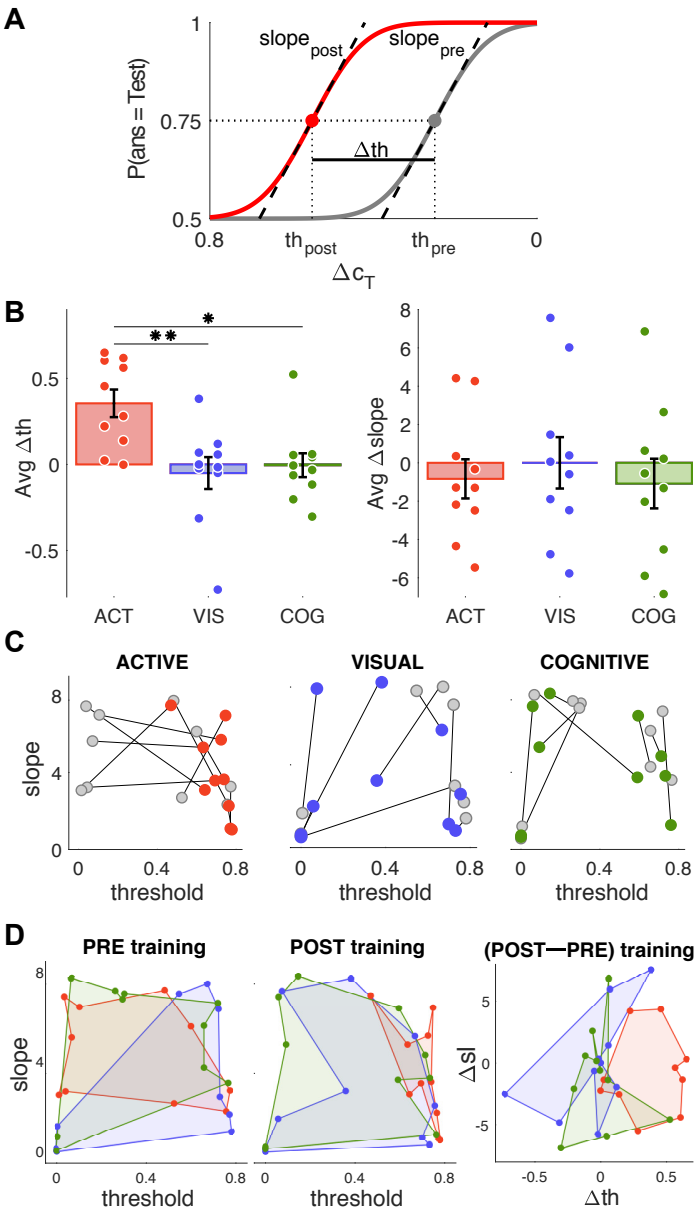

Figure 4.3 Results of the perceptual judgement task. A: Representative psychometric curves. Each curve represents the probability that the participant chooses the Test stimulus over a range of relative contrast differences Δc_T. Grey curve represents the perceptual baseline of a representative subject (pre-training), whereas the colored curve indicates the perceptual change (post-training). Solid lines represent the average values, the filled circles indicate the 75% threshold value (th_{pre}, th_{post}), and the dashed black lines show the slope of the curves at the threshold point ($slope_{pre}, slope_{post}$). The horizontal black segment displays the threshold difference, $\Delta th = th_{post} - th_{pre}$. B: Colored bars represent the average values of threshold differences Δth and slope differences Δsl over subjects of all three experimental conditions. Dots represent the individual values for each subject. Error bars denote standard errors. The average value of Δth in the active group is significantly greater than in the visual-only ($P = 0.003$) and the cognitive ($P = 0.019$) groups. C: Qualitative analysis of inter-subject variability is shown in terms of threshold and slope changes for the individual subjects in each condition. In all three conditions, the grey-colored dot pairs represent the pre-training values. D: Qualitative analysis of inter-subjects variability is shown in terms of the minimum polygons enclosing all data points in each group (active: red; visual-only: blue; cognitive: green).

experimental conditions (P = 0.0002; F(2,27) = 7.45; One-way ANOVA), and no reliable difference in slope. Post-hoc analyses (Bonferroni-Holm) revealed a significant difference in the threshold of the active and visual-only conditions (P = 0.003) and between the active and cognitive conditions (P = 0.019).

Figure 4.3C,D summarizes inter-subject variability. After training, all subjects in the active group exhibit a threshold value which is close to the maximum value of 0.8, in other words they correctly select the Test stimulus throughout the entire range of Δc_T. In contrast, subjects in the visual and cognitive groups exhibit no consistent trend in either threshold or slope. Figure 4.3D displays inter-subject variability in terms of the minimum polygons enclosing all data points in each group. Before training, the subjects within each group exhibit a similar amount of variability. After training, the subjects in the active group display a polarization towards greater threshold values. The distribution of the differences between PRE and POST values in both thresholds and slopes shows for the three training conditions a different clustering in three distinct regions of the $\Delta\text{th} - \Delta\text{sl}$ plane.

4.3.2 Training phase

Participants in the active training condition were instructed to make continuous movements back and forth between two circles that were presented briefly at the start of a continuous movement trial. During the trial the subject is presented with the plaid, whose motion direction and velocity match those of the hand. The contrast difference Δc between the single gratings that form the plaid is based on the individual threshold estimated from the pre-training perceptual task.

Figure 4.4 shows results of the active motor training. Panel 4.4A shows the frequency distribution of movement directions for a typical subject across all trials of the first and last blocks for all movement directions (each of the 4 directions, back and forth, is represented with a different color). We note that even though subjects are only presented with target circles at the very beginning of each trial sequence, variability of subsequent movements is relatively small, averaging 10-15 deg in each direction, and decreases from the first to the last block. Panel 4.4B shows mean directional bias and standard deviation of hand movement across subjects in each of 10 repetitive training blocks averaged over the 4 movement directions tested in this study. Both directional bias ($R^2 = 0.50$, P = 0.02), and directional standard deviation ($R^2 = 0.52$, P = 0.01) change significantly over the course of training. Moreover, we found a highly reliable relationship between the perceptual change from before to after training (Δth), and the change in movement direction (Δbias) that occurred in conjunction

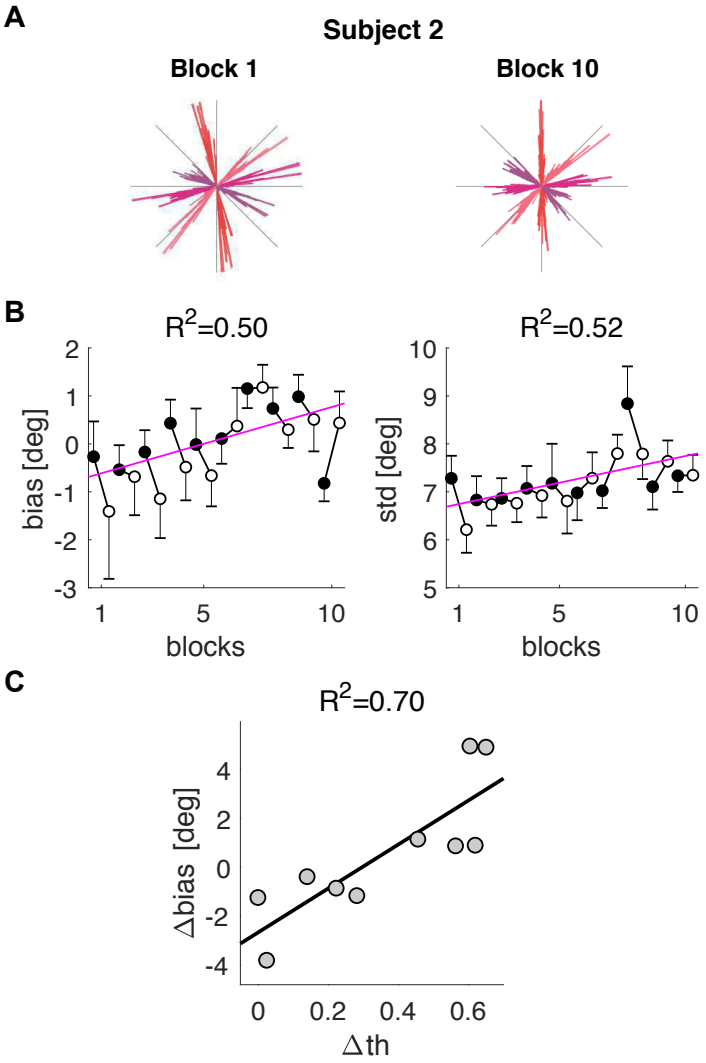

Figure 4.4 Results of active motor training. A: For a typical subject, the frequency distribution of directional errors across all trials of the first and last block for all movement directions (each of the 4 directions, back and forth, is represented with a different color). Grey lines represent the tested directions. B: Directional bias and standard deviation of hand movement, across subjects and directions for each individual training block. White and black circles refer respectively to early and late trials within each block. Error bars denote standard errors. The regression slope (pink line) shows training related changes across training blocks for both directional bias ($R^2 = 0.50$, $P = 0.02$) and directional standard deviation ($R^2 = 0.52$, $P = 0.01$). C: Relationship between perceptual change from before to after training (Δth), and the change in movement direction (Δbias) that occurred in conjunction with training ($R^2 = 0.70$, $P = 0.002$).

with training ($R^2 = 0.70$, $P = 0.002$); see Figure 4.4C. Specifically, subjects whose change in movement direction was more toward the direction of plaid motion were also those who showed greater change in the contrast difference over which they could see a moving plaid.

Computational model

A Bayesian framework was used to model the way humans perceive plaid motion. We specifically assumed that perception is affected by both random and systematic effects. In particular, the noise variance on the perception of a single grating velocity is affected by contrast, according to a power law: s is the minimal standard deviation of the noise for maximum contrast, and q is the exponent of the power law. We also assumed a reciprocal influence of one grating on the perception of the other grating's velocity (cross-talk), proportional to their contrast imbalance through a parameter k At last, we assumed a Gaussian prior for grating velocities with zero mean and variance ${\sigma_p}^2$. As a whole, the model is fully characterized by the parameter vector $w = [s, q, k, {\sigma_p}^2]^T$, (see Methods, for further details). The perceptual judgement task was modelled as a binary decision between two possible alternatives, Test (T) or Reference (R). The probability of choosing T as a function of the estimation od plaid direction, $\hat{\theta}$, and the contrast difference Δc_T in the test stimuli, i.e. $\Pr(T|\hat{\theta}, \Delta c_T)$, is calculated from the Bayes' theorem (see Methods, Eq. 4.6). The psychometric curve for this equation is a function of the model parameters w, i.e. $\Pr(T|\hat{\theta}, \Delta c_T) = f_T(\Delta c_T, w)$.

We fitted the model to the data and estimated the model parameters w before and after each of the training conditions. Figure 4.5 summarizes the results of model fitting. Figure 4.5A shows the average value of each model parameter among subjects, before (grey boxes) and after (colored boxes) each training condition. We found a significant change in σ_p^2 ($P = 0.01$), k ($P = 0.026$), and s ($P = 0.025$) parameters in the active group, only. Perceptual threshold values for the model are estimated at the 75th percentile (see Methods) and show a high correlation with the threshold values in the experimental tests (see Figure 4.5B). Figure 4.5C shows psychometric threshold differences ($\Delta\text{th} = \text{th}_{\text{post}} - \text{th}_{\text{pre}}$) calculated from model fitting for all the participants in each experimental condition (see Eq. 4.6). It can be seen that as in the empirical results there are significant changes in the psychometric thresholds in the active group alone. These observations are confirmed by statistical analysis. We tested for differences in threshold (Δth) of the psychometric curves. We observed a significant difference in threshold between experimental conditions ($F(2,27) = 7.76$; $P = 0.002$). Post-hoc analyses (Bonferroni-Holm) revealed a significant difference in the threshold of the active and visual-only conditions ($P = 0.003$) and between the active and cognitive conditions

(P = 0.024). These results on the perceptual threshold of the curves obtained by fitting the data with the Bayesian generative model are in agreement with those found in the results of the perceptual judgement task by fitting the data with the cumulative Gaussian function, as shown in Figure 4.5C; see Methods. Moreover, we found a highly reliable relationship between the change in the model parameter k (Δk) from before to after training, and the perceptual change from before to after training (Δth) ($R^2 = 0.81$, P = 0.0004); see Figure 4.5D. This means that for subjects with greater perceptual changes the model predicts a higher decrease in the cross-talk parameter k.

4.4 Discussion

The present study shows that active interaction with an ambiguous visual stimulus alters the subsequent perception of stimulus motion. Three groups of participants performed the same perceptual task before and after training. An active group generated plaid motion by performing planar movements. This was designed to assess whether perceptual decisions regarding plaid movements were affected by actively interacting with the stimulus. A visual-only group observed played-back plaid motion that was generated by another subject. This condition quantified the effect of prolonged exposure to the moving plaid stimulus. A cognitive group experienced the same stimuli as the visual-only group. These subjects were additionally instructed to track the gratings intersections and thus had an explicit strategy which would enable them to follow the coherent plaid motion. We found that the perceptual threshold for the direction of plaid motion changed significantly following training only in the active movement condition, where it showed more robust perceptual integration against contrast imbalance in the plaid. There were also practice related changes to movement. Movement direction changed over the course of training presumably because the plaid, which effectively serves as a cursor showing movement direction, is more easily seen by subjects as moving in the remembered target direction. We found that the change in perceptual threshold was strongly correlated with the change in movement direction measured during the active training, consistent with the idea that the perceptual change is tied to motor training. A quantitative model suggests that movement training affected perceptual judgement by improving the accuracy of the internal representation of the plaid geometry. The findings indicate that motor training resolves visual perceptual ambiguity and contributes to changes in visual perceptual ability.

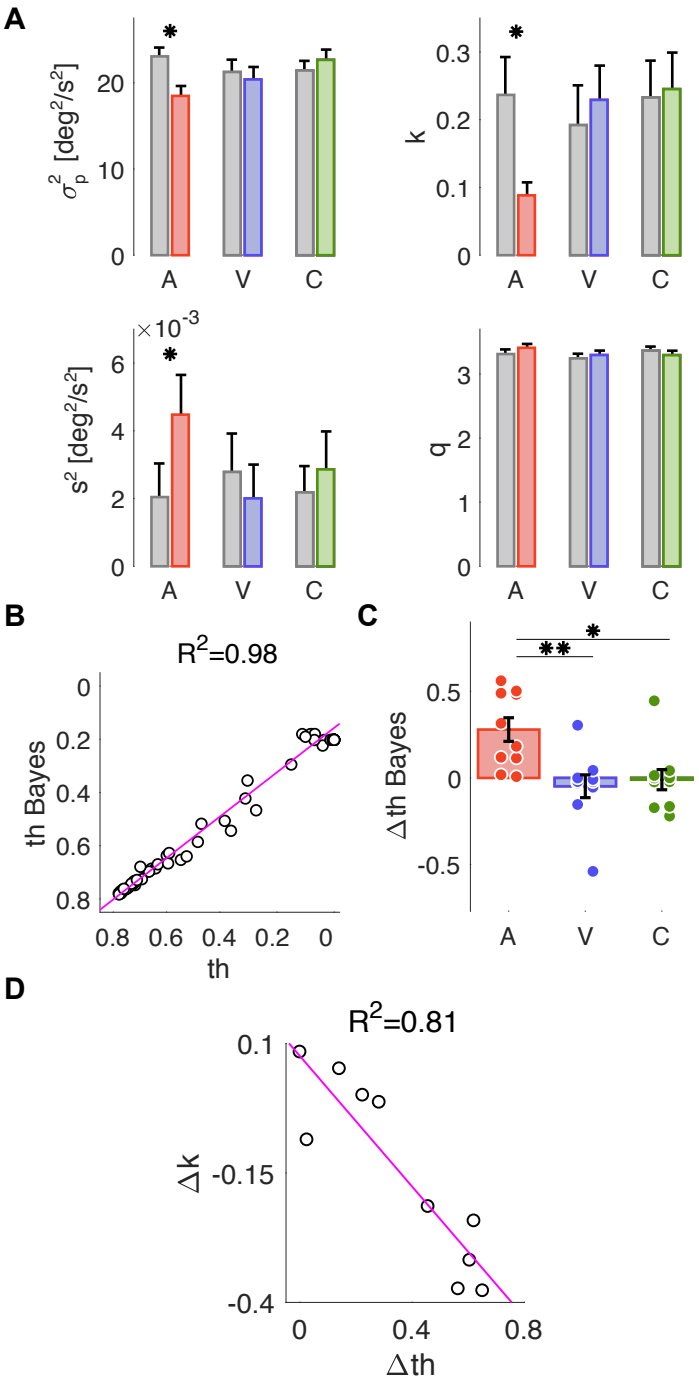

Figure 4.5 Results of model fitting. A) Comparative parameter fitting for the different training conditions. Grey and colored boxes refer to pre- and post-training conditions, respectively. σ_p^2 (Anderson-Darling test for normality: $P > 0.05$, T-test P=0.01 for the active group), k (Anderson-Darling test for normality: $P > 0.05$, T-test $P = 0.026$ for the active group), s (Anderson-Darling test for normality: $P = 0.003$, Wilcoxon rank sum test $P = 0.025$ for the active group), and q. B) Correlation between thresholds estimated using perceptual test data and from the Bayesian generative model ($P = 0.001$). C) Average thresholds of Bayes' model psychometric curves over all subjects of each group. D) Correlation between the perceptual threshold change (pre- *vs.* post-training), Δth, and the corresponding variation of the cross-talk parameter, Δk, ($P = 0.004$).

Motor training implications on perceptual discrimination

A small number of studies have examined the effects of motor learning on vision. Brown et al. (2007) found that movement initiation toward a moving object, that was to be intercepted, differed depending on the direction of a previously learned force field, indicating that expectations regarding visual motion are altered as a result of learning. Beets et al. (2010a) showed that when participants trained to make movements that violated to different degrees the 2/3 power law, there were improvements in visual discrimination of movements that corresponded to those which they experienced during training. These studies indicate that motor learning can induce a bias in visual perception. The present study suggests that movement training plays an even more pivotal role. Indeed, visual perception is inherently ambiguous. Movement training leads to a reduction in perceptual uncertainty, and to a change of perceptual sensitivity which in the present case is related to a stimulus parameter (gratings' contrast difference) that is not directly controlled during training. Both movement training and perceptual change occur here without feedback motor error provided to participants during training. Changes in movement direction within single training blocks and over the entire training session are significantly correlated with the observed perceptual change (between pre- and post-training perceptual tasks) suggesting that the two kinds of learning are cross-related. Visual motion perception may be based upon an empirical strategy which serves to resolve perceptual uncertainty (Purves et al., 2014; Sung et al., 2009). Accordingly, the perceived motion direction is determined by accumulated experience. Perceptual decisions regarding motion direction provide, in turn, sensory evidence that instructs behaviour. Our results suggest that visual function over time can be adapted with training, which is provided by interaction with the stimulus.

Modeling the fine-tuning of internal representation of plaid geometry

Several studies (Hedges et al., 2011; Weiss et al., 2002) used a Bayesian framework to model the perceptual task of estimating the velocity of the plaid from the perceived velocities of the two gratings. These models posit that prior information and an internal (neural) representation of plaid geometry are combined to obtain the expected value of plaid velocity (Hedges et al., 2011). Prior information captures the participant's prior experience with observing moving patterns and is summarized by the statistical distribution of the plaid velocities. The representation of plaid geometry approximates the mapping from plaid to gratings' velocities. Accordingly, inaccurate perception of plaid motion may be due to (i) an inaccurate representation of plaid geometry (sensory model), (ii) an inaccurate perception

of the velocity of each grating (noise variance), (iii) the bias introduced by previously experienced plaid motions (the prior); or a combination of the above.

Later studies suggest that this Bayesian formulation cannot account for key observations in the way the perception of plaid direction is affected by speed (Champion et al., 2007). With respect to those earlier formulations, we made a number of specific assumptions on how the gratings' contrasts affect the perceived plaid velocity. First, consistent with previous findings (Hürlimann et al., 2002) we assumed that the variance of sensory noise in perceiving the velocity of a grating is proportional to an inverse power of the grating contrast. This is reflected in two model parameters: the variance at maximum contrast and the power exponent. With these simple additions our model predicts those same observations (Champion et al., 2007) that have been claimed to falsify Bayesian models of plaid perception. We also posited an additional effect in the representation of plaid geometry: if two gratings have different contrasts, the represented direction of a grating affects that of the other – this was denoted by the 'cross-talk' parameter (cf. (Stone et al., 1990)). This effect results in a systematic error in the representation of plaid geometry.

For each participant we estimated the parameters that maximise the model likelihood given the data from the perceptual judgement task. For each experimental condition, we then assessed the model parameters changes from before to after training. Significant changes in the model parameters were obtained for the active training condition alone. Specifically, we found that participants in this condition exhibited a significant decrease in the cross-talk parameter and an increase of the power law exponent. The reduction in cross-talk leads to a more accurate representation of the direction of the gratings and therefore a more accurate representation of plaid geometry. The increase of the power law exponent leads to a decreased sensitivity of sensory noise to contrast.

Note that the cross-talk decrease exhibits a strong correlation with the observed change in perceptual threshold. That is, participants who exhibit greater perceptual changes also show a greater reduction in the cross-talk. This finding suggests that motor training in this task leads to a fine-tuning of the internal representation of plaid geometry.

Why does movement improve the sensory model while observation on its own does not? One possible explanation is that during movement, the sensory model predicts the sensory consequences of movements – the expected movements of the gratings. The mismatch between these predictions and the observed movements of the gratings – sometimes called sensory prediction error – is the source of information which can be used to adapt the sensory model. This information is not available during passive observation of plaid movements. Consistent with this view, sensorimotor adaptation to dynamic or visual perturbations has

been reported to critically depend on the availability of a sensory prediction error signal (Haith et al., 2009; Krakauer and Mazzoni, 2011).

4.4.1 Implications for neural representations of complex visual motion

As plaid stimuli are composed of a minimal number of one-dimensional Fourier components (two), each selectively recruiting narrow early vision oriented band-pass frequency channels, they can contribute to understanding how these channels are involved in the perceptual learning of coherent sensorimotor dependencies.

Finding a solution to the plaid motion problem can be related to the evidence from component-motion and pattern-motion cells, observed respectively in striate and extrastriate areas along the primary visual motion pathway, such as area V3A and middle temporal area (MT or V5) (Albright and Stoner, 1995). Ultimately, the steps in the formation of perceptual decisions and/or guidance of visual behaviours can be linked to higher-level brain areas (e.g., lateral intraparietal cortex and prefrontal cortex), which are often described as 'evidence accumulators' (Latimer et al., 2015; Law and Gold, 2008; Zhang and Tadin, 2019). The present model simulation suggests a reduction, after training, of the cross-talk between the two gratings in the corresponding sensory channels, when the gratings contrasts are unbalanced, as well as a reduction of the noise variance. The decrease in cross-talk magnitude would be consistent with an early neural instantiation of the perceptual learning process, which might occur at the coding stage of the component motion directions (cf., contrast normalization processes in V1). On the other hand, since the cross-talk in the model acts on gratings' velocities, it requires a pooling of the responses of different oriented channels, and its change might occur at pattern motion coding in an extrastriate area. Notably, the null effect of visual-only training leads us to exclude a role of a oculomotor-specific, but rather a reach-specific sensorimotor cortical area. Specific experiments and recordings of neural correlates would be necessary to disambiguate the different hypotheses. From a broader perspective, this study suggests a shift in focus to pattern and motion vision investigation, which includes continuous interaction with visual stimulation.

4.5 Supplementary Information

In order to provide additional support for the proposed Bayesian model of plaid perception here we compare the model predictions with two sets of empirical observations about the way perception of plaid direction is affected by absolute and relative contrast (Stone et al.,

1990) and by the grating speeds (Champion et al., 2007). The comparison will be also used to highlight the role of the individual model parameters in the estimated plaid direction.

4.5.1 Model summary

The Bayesian model of plaid perception assumes that perception of a single grating is affected by its contrast. The model also assumes a Gaussian plaid velocity prior, with variance σ_p^2, and a cross-talk parameter, k, which accounts for the conjecture that, in a plaid stimulus, the perception of the direction of each individual grating is biased toward the direction of the other.

4.5.2 Effect of gratings contrast on perception of direction

We compared the model predictions with the findings of (Stone et al., 1990). They used a plaid moving upwards (θ = 90 deg) at 2 deg/s and consisting of two gratings, moving in directions θ_1 = 90 - 60 = 30 deg and θ_2 = 90 + 60 = 150 deg with equal velocities (1 deg/s). In their experiment, they used different values of total contrast, C: $\{5\%, 10\%, 20\%, 40\%\}$ and for each C they varied the contrast ratio $a = c_1/c_2$. For each combination of C and a, they looked at the perceptual bias between the perceived and actual plaid direction, $\Delta\theta = \hat{\theta} - \theta_1$. They found that the perception of the plaid direction is biased toward the higher contrast grating. As a consequence, the bias increases with both the contrast ratio and decreases with total contrast.

We used the model to simulate the same experiment. The model predicts the probability density function of plaid direction as a function of the relative contrast of the two gratings (Eq. 4.5). From this expression it is possible to derive the mean and variance of the estimated plaid direction, $\hat{\theta}$. In our simulations we set q=2.5, 3 and 3.5, σ_P^2 = 1, 4, and 9 deg^2/s^2 and k=0 (no cross-talk) and 0.15. We also assumed that the noise variance of a grating at a maximum contrast is inversely proportional to the total contrast, I.e. $s^2 = h/C$. We set $h = 3 \cdot 10^{-3}$ deg^2/s^2. These values are similar to the estimates obtained from our data (main paper, Figure 4).

The simulation results are summarized in Figure 4.6, which has exactly the same format as the figures in (Stone et al., 1990). In particular, the model correctly captures the dependence of direction bias on contrast ratio. When the contrast ratio is greater than 1 – grating 1 has greater contrast than grating 2 – the perceived direction is biased toward grating 1, and vice versa; see Figure 4.6 (top). The bias also depends on total contrast (greater contrast, lower bias); see Figure 4.6 (bottom).

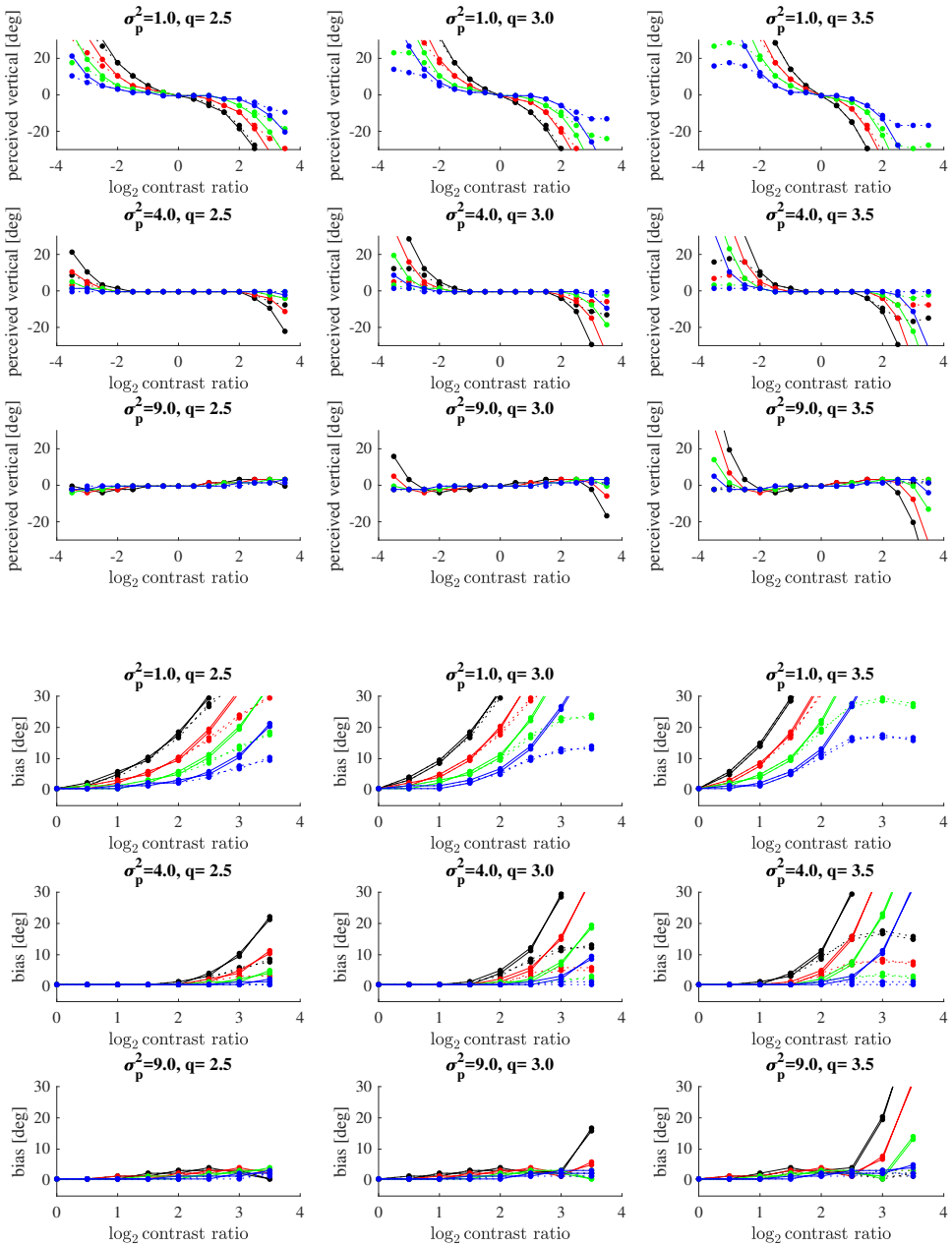

Figure 4.6 Predicted effect of contrast on perception of plaid direction (Stone et al., 1990). Perceived vertical (top) and bias (bottom) as functions of total contrast and contrast ratio. The colors refer to different total contrast magnitudes: C =5̇ % (black), 10 % (red), 20 % (green) and 40 % (blue). The different panels refer to different combinations of power exponent (q) and variance of the velocity prior (σ_p^2). Continuous and dashed lines refer to different amounts of cross-talk (k): 0 (continuous) and 0.15 (dashed).

The model also predicts that the contrast dependence of the direction bias is increased by a lower prior variance (σ_P^2) and by a greater power exponent (q). In contrast, the effect decreases when cross-talk (k) is present.

4.5.3 Effect of speed on perceived plaid direction

The work of Champion et al. (2007) complements the previous study. Specifically, they assessed how the perceived direction of a plaid which is composed of gratings with different contrasts is affected by the gratings' speed. They reported that the perceived plaid direction is biased toward the direction of the high-contrast grating. However, at low speeds (around 1 deg/s) the effect tends to reverse (bias toward the low-contrast grating). This result is in contrast with Stone et al. (1990) who used low speeds but found no such reversal.

We used our model to simulate Experiment 2 in their study. As in their study, we used a high contrast grating (C_1=60 %) with θ_1 = 90 - 45° and a low contrast grating (C_2 = 30 %) with θ_2 = 90 + 45°. This corresponds to a total contrast C = 90 % (greater than in Stone et al. (1990)) and to a relative contrast difference $\Delta c = 0.33$. As in the previous section, we used Eq. 4.5 to provide the most likely estimate of plaid direction. As in the previous section, in our simulations we set q=2.5, 3 and 3.5, σ_P^2 = 1, 4, and 9 deg^2/s^2 and k=0 (no cross-talk) and 0.15. As in the previous section, we set $h = 3 \cdot 10^{-3}$ deg^2/s^2. The simulation results are summarized in Figure 4.7 (black).

These simulations predict an almost zero directional bias over the whole range of speeds. This is indeed consistent with Stone et al. (1990), who found that the directional bias tends to dissappear as the total contrast increases. Nevertheless, if in the model the noise variance of the individual gratings is increased ($h = 6 \cdot 10^{-2}$ deg^2/s^2) – Figure 4.7 (red trace), the model predictions closely resemble the findings of Champion et al. (2007).

Looking at the roles of the individual model parameters in determining this finding, bias reversal seems to require a combination of higher power exponent (q) in the model of grating noise variance, and higher prior variance (σ_P^2), corresponding to a greater role of the gratings' likelihood in comparison with the velocity prior.

4.5.4 Conclusions

These results suggest that, in contrast with the conclusions of Champion et al. (2007), their results are consistent with a Bayesian model of plaid perception. It should be noted, however, that the two studies use very different contrast values (C=90 % vs C=5-40 %).

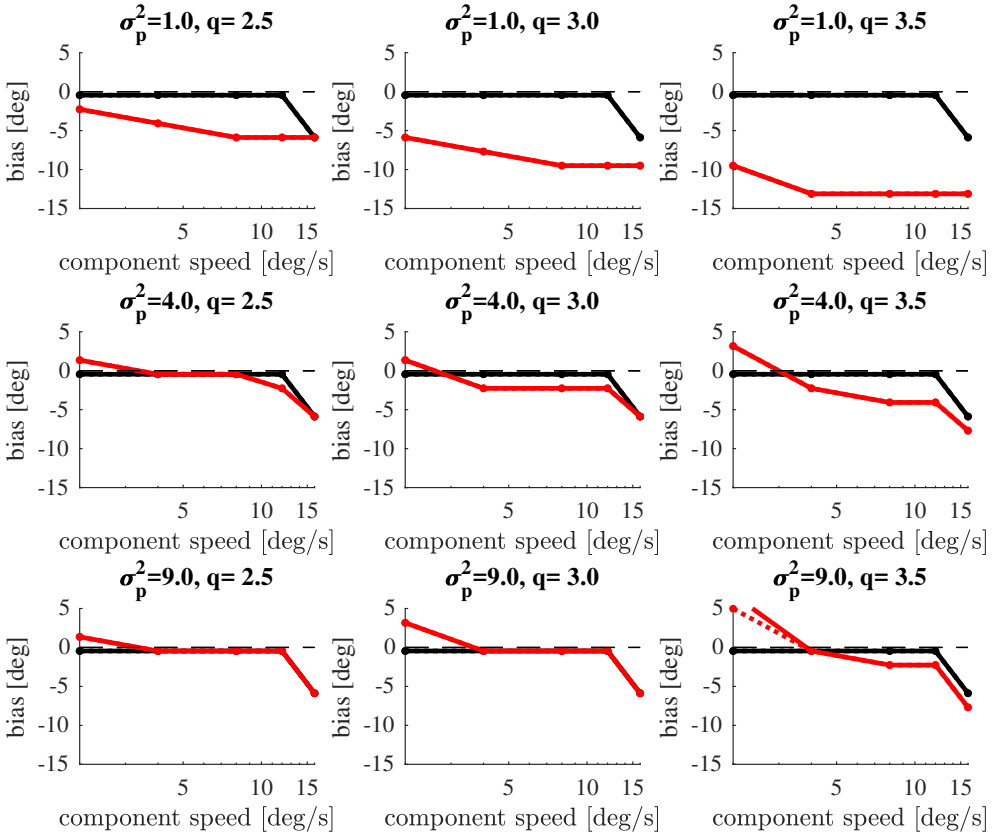

Figure 4.7 Dependence of the directional bias on the component (grating) speed as in Experiment 2 in Champion et al. (2007). The perceived plaid direction is biased toward the high-contrast grating (negative bias) at greater speeds, but the effect tends to reverse (bias toward low-contrast grating) at lower speeds. Black and red lines correspond, respectively, to $h = 3 \cdot 10^{-3}$ deg^2/s^2 and $h = 6 \cdot 10^{-2}$ deg^2/s^2. Continuous and dashed lines refer to different amounts of cross-talk (k): 0 (continuous) and 0.15 (dashed).

Chapter 5

Movements with ambiguous visual stimuli induce both visual and somatosensory changes [1]

5.1 Introduction

Studies of sensorimotor adaptation often describe perceptual and motor learning as two faces of the same coin, because they have been observed to occur together (Ostry and Gribble, 2016). This interpretation suggests that the two processes are intimately linked and can modify both sensory networks and motor areas in the brain.

Typical contexts such force-field learning Haith et al. (2009); Mattar et al. (2012); Ostry et al. (2010); Vahdat et al. (2011), visuomotor (Cressman and Henriques, 2009; Volcic et al., 2013) and prism adaptation (Beckett, 1980; Harris, 1963) show that both somatosensory and visual changes occur in conjunction with motor adaptation. This joint effect is supported by the presence of reciprocal neuroanatomical pathways between cortical motor and somatosensory areas, and confirmed by changes in functional connectivity in sensory networks of the brain shown in neuromaging studies (Andrew et al., 2015; Nasir et al., 2013; Pleger et al., 2003; Vahdat et al., 2011).

In vision, the visual control of movement has been deeply investigated, but the functional roles of cortical connections relaying information from the motor system to the visual system are still tentative (Nakayama, 1985). The way vision affects the motor outcome

[1] *A manuscript with material from this chapter is in preparation as Sedda, G., Sanguineti, V., Sabatini S. P., and Ostry, D. J. (2020). Movements with ambiguous visual stimuli induce both visual and somatosensory changes.*

is certainly better known than the effect of movement on visual perception. The above studies indicate that motor adaptation elicits lasting and concurrent changes to motor, visual, and somatosensory networks, but how movement influences perception remains relatively unclear.

In the literature on motion perception, there is evidence that predictions of visual motion are biased by relevant information stored by the motor system (Brown et al., 2007; Zago et al., 2004). During training the motor system acquires information on movement dynamics and builds a predictive model of the environmental forces (e.g. gravity) (Shadmehr and Mussa-Ivaldi, 1994). This information can be used to predict the visual characteristics of movement (Brown et al., 2007; Kim and Spelke, 1992). For example, Brown et al. (2007) found that during an object interception task after force-field learning, participant's movements showed an altered bias in interception timing and success which was based on force-direction applied to the hand during the training (see also Port et al. (1997); Zago et al. (2004)). The magnitude of this effect increases under longer viewing time conditions.

Taken together, these studies also suggest that in order to actively interact with the environment hand and eye movements need to be coordinated in a closed loop fashion. Several studies, consistent with this view, found that eye movements in a finger tracking task with self-generated motion are more accurate than when participants are required to track an externally-generated motion (Bock, 1987; Chen et al., 2016; Steinbach and Held, 1968). In both cases tracking accuracy is unaffected even when the reliability of visual perception is critically reduced, for example by using blurring the stimuli. Blur perturbs visual tracking performance, but eye-hand coupling is not disrupted (Maiello et al., 2018).

The above findings suggest that conditions that perturb or impoverish visual information can be used to highlight how movement affects visual perception and vice versa. For instance, in my study on moving ambiguous stimuli presented in Chapter 4. I found that movement training affects the way we make sense of complex visual information. For this purpose I designed an experiment that uses plaid stimuli, which we know can be perceived either as a single moving pattern or as two sliding gratings. Participants were trained to make movements between remembered target locations in which the direction of their hand movements was displayed as a moving plaid. I found that, as a result of movement training, perception of the plaid movement direction was less sensitive to contrast difference, and changes in movement were correlated with the perceptual changes. Perceptual changes were not observed when vision of the plaid was provided without movement, neither when participants viewed the visual stimulus without movement nor when they were provided with a cognitive strategy to facilitate the single pattern perception. Starting from these results, I hypothesized that during

motor training the ambiguous visual feedback of plaid motion may bias the proprioceptive decisions related to participants' arm movements.

Here, I present an experimental procedure involving motor training and both visual and proprioceptive tests, in which the perceptual tests are repeated before and after the motor training to identify any changes in participants' perception. During motor training, participants grasped a robot handle to actively control the motion of a plaid stimulus during a reaching task in which visual feedback of the arm itself was blocked. Preliminary results show that self-generated movements in conjunction with ambiguous stimuli can induce both visual and somatosensory changes, which can be interpreted as a perceptual skill learning.

5.2 Materials and Methods

5.2.1 Subjects

A total of 60 right-handed participants (16 males and 44 females, 18–35 years old) were recruited. Participants reported that they had normal or corrected-to-normal vision, and did not have any history of neurological disease. All participants were naïve with regards to the purpose of the experiment. Each participant was randomly assigned to one of the two groups (15 participants per each group). The research conforms to the ethical standards laid down in the 1964 Declaration of Helsinki that protects research participants and was approved by the McGill University Faculty of Medicine Institutional Review Board. Each participant signed a consent form conforming to these guidelines.

5.2.2 Apparatus

In a dimly lit room, participants were seated in front of a 2-degree-of-freedom robotic arm (In Motion2, Interactive Motion Technologies) coupled with a horizontal 46-inch LCD monitor (Samsung LN46B540) at 1920×1080 pixels; see Figure 5.1. Visual stimuli were refreshed on the screen at 60 Hz, and they were projected on the mirror that was about 10 cm below the screen. The semi-silvered mirror consists of a glass plate that reflects about half of the incident light of the stimulus and transmitted the other half, so that the plaid image formed under the mirror, corresponded to the 'true' position of the stimulus on the screen. By adjusting the distance between the mirror and the screen it was possible to reproduce the image of the plaid on the work plane of the hand. The seat height was adjusted for each participant separately in order to have the same vertical distance (about 30 cm) between the eyes and the plane of the robotic arm and the same horizontal distance (about 43 cm) between

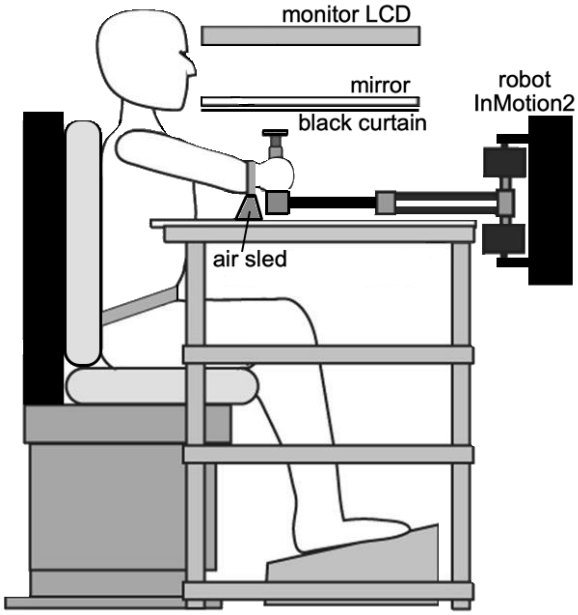

Figure 5.1 Experimental apparatus. In a dimly lit room, participants were seated in front of a 2-degree-of-freedom robotic arm coupled with a horizontal screen. A black curtain stretched under a semi-silvered mirror blocked the vision of the arm and the robot handle. Visual stimuli were projected on the mirror which was placed below the screen. An air sled was used to support the arm during hand movements.

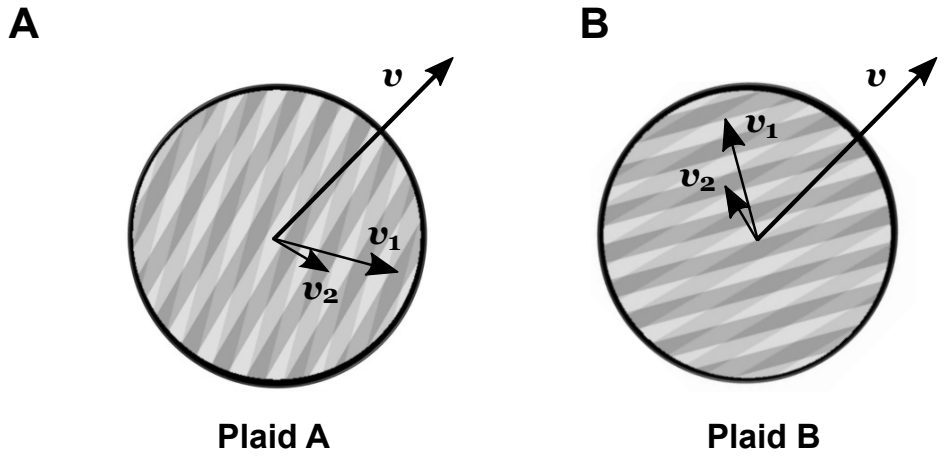

Figure 5.2 Plaid stimuli moving at velocity $\boldsymbol{v}$, are composed of two gratings sliding over each other at $\boldsymbol{v_1}$ and $\boldsymbol{v_2}$ respectively. In plaid A , $\boldsymbol{v_1}, \boldsymbol{v_2}$ are oriented to the right of the plaid velocity $\boldsymbol{v}$, whereas in plaid B they fall on the left of $\boldsymbol{v}$.

the eyes and the starting position. The width of the whole display was 118 deg of visual angle relative to the distance from the center of the stimulus.

In the active movement phase of the experiment (see below), participants held the handle of the robot with their right hand to actively drive the motion of the visual stimulus by moving in a horizontal plane, so that visual stimulus and the hand movements were in the same plane. The center point of the screen was mapped into the center of the robot work space, with a 1:1 scale factor. Optical encoders recorded the position of the hand (0.0055 deg resolution, Virtual Absolute Encoder, Gurley Precision Instruments).

5.2.3 Stimuli

A plaid stimulus moving at velocity $\boldsymbol{v}$, and composed by two square-wave gratings sliding over each other at velocities $\boldsymbol{v_1}$ and $\boldsymbol{v_2}$ respectively, was presented through a circular aperture about 18 cm in diameter on a black background. The plaid design is the same as reported in Chapter 4.

Two different configurations of the stimulus were designed, named *plaid A* and *plaid B*, as shown in Figure 5.2. In plaid A (left), gratings' velocities $\boldsymbol{v_1}, \boldsymbol{v_2}$ are oriented to the right of the plaid velocity $\boldsymbol{v}$, whereas in plaid B (right) they fall on the left of $\boldsymbol{v}$. Both plaids moved at speed $v = 5$ deg/s in the direction $\theta = 45$ deg (from the lower left corner of the screen to the upper right corner). The normal directions of the two component gratings of each plaid are called θ_1 and θ_2. $\Delta\theta_1 = \theta_1 - \theta =$ -60 deg and $\Delta\theta_2 = \theta_2 - \theta =$ -75.5 deg defined the relative directions of individual gratings with respect to the direction of the plaid A, whereas

$\Delta\theta_1 = \theta_1 - \theta = 60$ deg and $\Delta\theta_2 = \theta_2 - \theta = 75.5$ deg defined the relative directions of the gratings with respect to the direction of the plaid B. In both geometric arrangements, the ratio between the two gratings speeds was $\cos(\Delta\theta_1)/\cos(\Delta\theta_2)$. For each plaid, the luminance of the black background outside the aperture was 0 cd/m^2. Stimuli were generated using the Matlab Psychophysics Toolbox (Brainard, 1997; Kleiner et al., 2007).

5.2.4 Experimental Protocol

The experimental procedure involved three phases; see Figure 5.3A. Participants were initially administered a perceptual judgement task (pre-training test). After, they underwent a motor training phase. After training, they repeated the perceptual judgement task (post-training test). I tested for changes in visual and somatosensory perceptual function associated with motor training with ambiguous plaid stimuli. Two different perceptual tasks, visual and proprioceptive, assessed the visually perceived direction of ambiguous stimuli and the sensed limb position, respectively. Participants were divided into four different experimental conditions (indicated as VA, VB, PA, PB), based on the perceptual task: visual (V) or proprioceptive (P), which they had to perform and the plaid stimulus (A or B) which was presented during the experiment. Participants in each experimental condition repeated the same perceptual task before and after the motor training.

5.2.5 Visual judgement task

The purpose of this test was to quantify individuals' ability to assess the direction of plaid motion in reference to the direction of a red arrow.

I used a 2-alternative forced-choice (2AFC) paradigm; see Figure 5.3B. Each trial started with a fixation point (a red dot at the starting position) displayed for 2 s. Then, a plaid stimulus was presented for 1 s, moving in the reference direction $\theta_R = 45$ deg from the lower left corner of the screen to the upper right corner. The plaid was the same on all trials. The stimulus was followed by an oriented red arrow (displayed for 1 s), separated by an interval of 1 s (i.e. a black window with a red dot). The test direction of the arrow (θ_a) changed at each trial. Participants were asked to judge if the arrow was pointing to the left or to the right of the imaginary straight line that connected the visual target to the starting position. Participants were instructed to maintain fixation at the center of the stimulus during the whole duration of stimulus presentation. At the end of each trial they had a maximum time of 3 s to answer verbally.

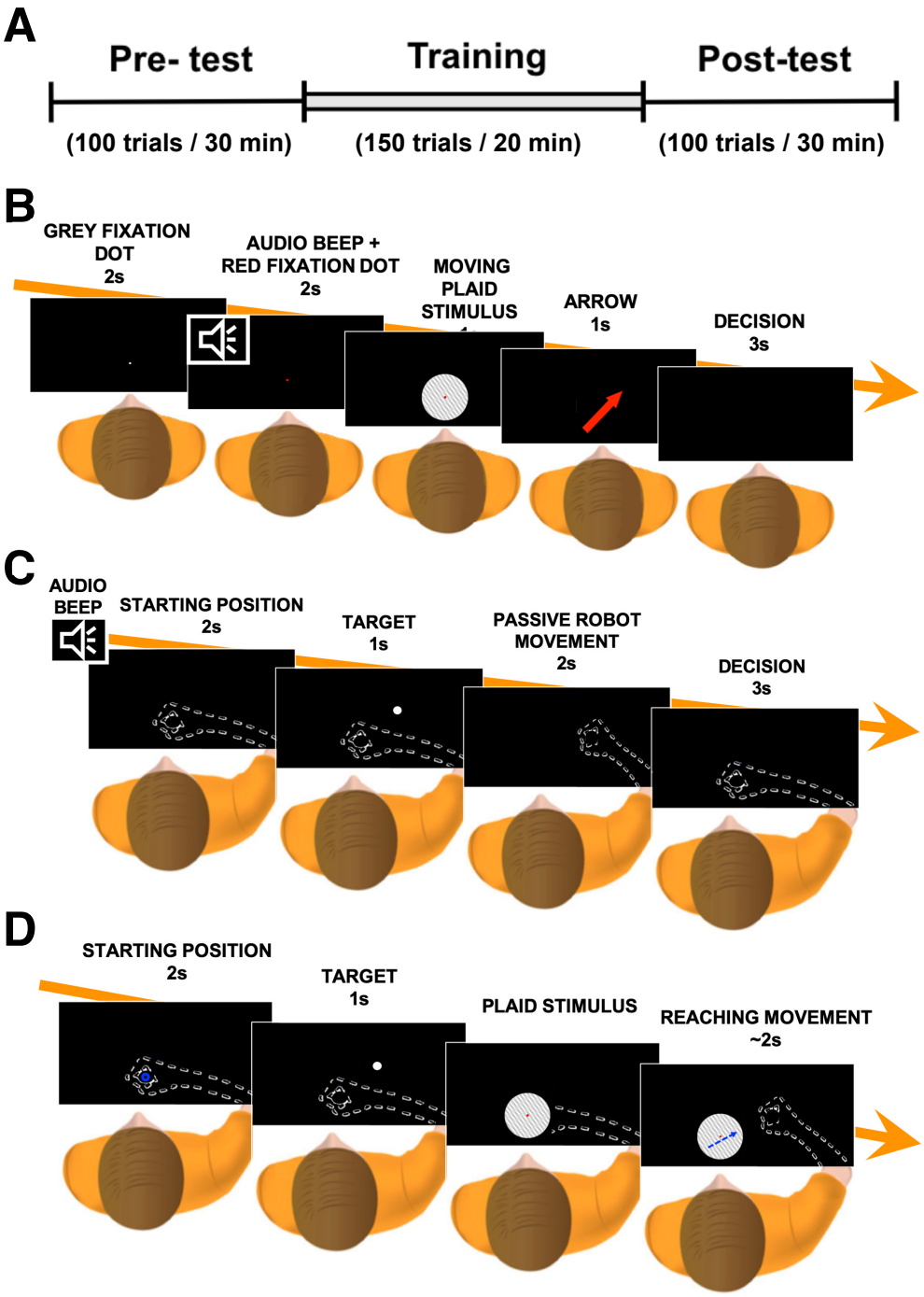

Figure 5.3 (A) The experimental protocol consisted of a perceptual test (visual or proprioceptive) repeated before and after the motor training. (B) During the visual perceptual task, participants were asked to judge if the displayed red arrow was pointing towards the right or the left of the direction of a moving plaid which was presented beforehand. (C) During the proprioceptive task, the robot moved the hand outward with vision of the arm blocked. Participants were asked to judge whether the hand was moved to the right or to the left of a visual target which was presented before the movement. (D) During the motor training, participants reached towards a briefly presented target beyond the far edge of the aperture by moving the robot handle. At the same time they moved a plaid stimulus displayed on the screen. The direction of plaid motion corresponded to the direction of the hand movement. The arm was occluded and there was no cursor. The only visual feedback was from the direction of plaid motion.

The visual judgement task took a total of 100 trials to complete, corresponding to a whole duration of about 30 min. The procedure for selecting stimulus directions is described below.

It is important to note that the visual condition of the participants is completely different from that of the visual perceptual test presented in the previous chapter. In this experiment, I wanted to evaluate the visual perceptual judgment on the same operating plane as the proprioceptive judgment, which corresponds to the working space of the hand. This testing condition adds some difficulty to the visual perceptual judgment of complex stimuli such as plaids: the local features of visual perception change slightly in the direction of depth, and this creates perceptual imbalances that make the perception of coherent plaid more difficult.

5.2.6 Proprioceptive judgement task

The aim of this test was to quantify the participants' ability to assess the direction of their hand motion during passive movement.

I used a 2-alternative forced-choice (2AFC) paradigm; see Figure 5.3C. At the beginning of each trial participants held the robotic arm and the robot moved their hand to the starting position. Afterwards a visual target (white filled circle, about 3 deg of diameter) appeared for 1 s at the reference direction $\theta_R = 45$ deg at 18 cm of distance from the starting position, then the robot moved the hand outward with vision of the arm blocked. Participants were asked to judge whether the hand was moved to the right or left of the imaginary straight line that connected the remembered visual target to the starting position. The test direction of the hand (θ_h) changed at each trial. At the end of each trial participants had a maximum time of 3 s to answer verbally.

The proprioceptive judgement task took a total of 100 trials to complete, corresponding to a whole duration of about 30 min.

5.2.7 Motor training

Participants were instructed to perform reaching movements toward a target; see Figure 5.3D. The motion of a plaid on the screen was continuously yoked to the hand movement direction, $\theta(t)$, so that the two gratings moved in directions $\theta_1(t) = \theta(t) + \Delta\theta_1$ and $\theta_2(t) = \theta(t) + \Delta\theta_2$ while their relative orientations with respect to plaid motion, i.e. $\Delta\theta_1$ and $\Delta\theta_2$, remained constant.

The training phase was organised into a sequence of trials, each characterized by the same target position. At the beginning of each trial, participants held the handle of the robot, which brought the participant's hand to the starting position and blocked all movement for 2 s.

Then both the start position and the cursor disappeared, and a visual target (white filled circle, about 3 deg of diameter) appeared for 1 s at 45 deg and 18 cm of distance from the starting position. As the target disappeared, a plaid appeared inside a circular aperture. Participants were instructed to move the hand in order to reach the remembered target position with a single smooth movement, as precisely as possible. At the participants moved, the direction of plaid motion corresponded to the direction of the hand movement, with a 1:1 movement ratio. The only visual feedback of the hand movement direction was from the plaid motion. When the subject stopped movement, the robot brought their hand back to the start position. The relative difference of contrast Δc in the gratings that formed the plaid was set to 0.4 (which is the average threshold level estimated at the end of the pre-training perceptual visual task on contrast difference presented in Chapter 4).

The motor training task lasted about half an hour during which participants performed a total of 150 trials subdivided in 3 blocks; at the end of each block participants rested for about 1 min.

5.2.8 Data analysis

The Bayesian adaptive Ψ (Psi) method (Kontsevich and Tyler, 1999; Prins, 2013) was used to select the value of θ_a for visual test and θ_h for proprioceptive test on the current trial, based on the participant's answers in the previous trials. For each participant, I quantified performance in the perceptual judgement task before and after training by estimating a psychometric curve assuming a normal cumulative distribution function. I took threshold values of the estimated psychometric curves as measure of perceptual performance. Threshold value for visual condition was defined as the angle value corresponding to 75% of probability that the direction pointed by the arrow, θ_a is greater than the reference direction of the plaid, θ_R, whereas threshold for proprioceptive condition was defined as the angle value corresponding to 75% probability that the hand direction, θ_h, is greater than the reference direction of the target, θ_R, which means that θ_h is to the left of θ_R. I then assessed whether perceptual performance for each group (VA, VB, PA, PB) was affected by movement training. To do this, I took perceptual thresholds before training (th_{pre}) as the baseline perceptual performance. I then looked at the threshold after training (th_{post}). For each quantity and for all groups, I first assessed normality (Anderson-Darling test). If normality was not ruled out for perceptual thresholds, I ran a repeated measures 2-way ANOVA with time (PRE, POST) and group (plaid type) as within- and between-subject factors, separately for visual and proprioceptive conditions. In case the normality assumption had to be rejected, I used a non-parametric test

(Kruskal-Wallis) to assess group effects on the perceptual baseline (th_{pre}). I then focused on the training-related change ($\Delta\text{th} = \text{th}_{post} - \text{th}_{pre}$). I tested for group differences (plaid type), using t-test if normality was not ruled out, separately for visual and proprioceptive conditions; a non-parametric test (Wilcoxon Rank Sum) was used otherwise. In all statistical tests, I took $P = 0.05$ as the threshold for significance.

Finally, I examined movements of the hand during motor training for each group, separately. For each trial, I calculated the hand directions, from which I subtracted the target direction. Then, I took the average of the directional error (bias) for each trial across all participants and for each group separately. I also evaluated how these quantities changed over the course of training (correlation with trial number over time, including resting phases). I fitted the following exponential model:

$$y = A + Be^{Cx} \tag{5.1}$$

to the performance time series, where x are the average data of the directional bias, separately for each experimental condition. The model has a total of 3 parameters: A, B, C.

5.3 Results

5.3.1 Perceptual results

Visual judgement task

The results of perceptual task are presented as psychometric functions, which give the probability that the direction pointed by the arrow, θ_a, is greater than the reference direction of the plaid, θ_R. $\theta_a - \theta_R$ represents the directional visual bias (Vbias). Thresholds (th) of psychometric curves are estimated using the adaptive Ψ (Psi) procedure (see Methods). Participants who have better perceptual performance should have a threshold value closer to the motion direction of the plaid. Figure 5.4 (left) shows the psychometric functions for two representative subjects, who performed the visual judgement task with plaid A (top-left) or plaid B (bottom-left). The pre-training curve is in blue and post-training curve is in red. Vbias = 0 corresponds to when the arrow direction, θ_a, is equal to the direction of the moving plaid, $\theta_R = 45$ deg.

Results related to plaid A (top-left) show a negative (i.e. rightward) pre-training threshold, and a large positive (i.e. leftward) shift occurs in the post-training tests. In contrast, plaid B (bottom-left) shows a leftward pre-training threshold, and a large rightward shift occurs in

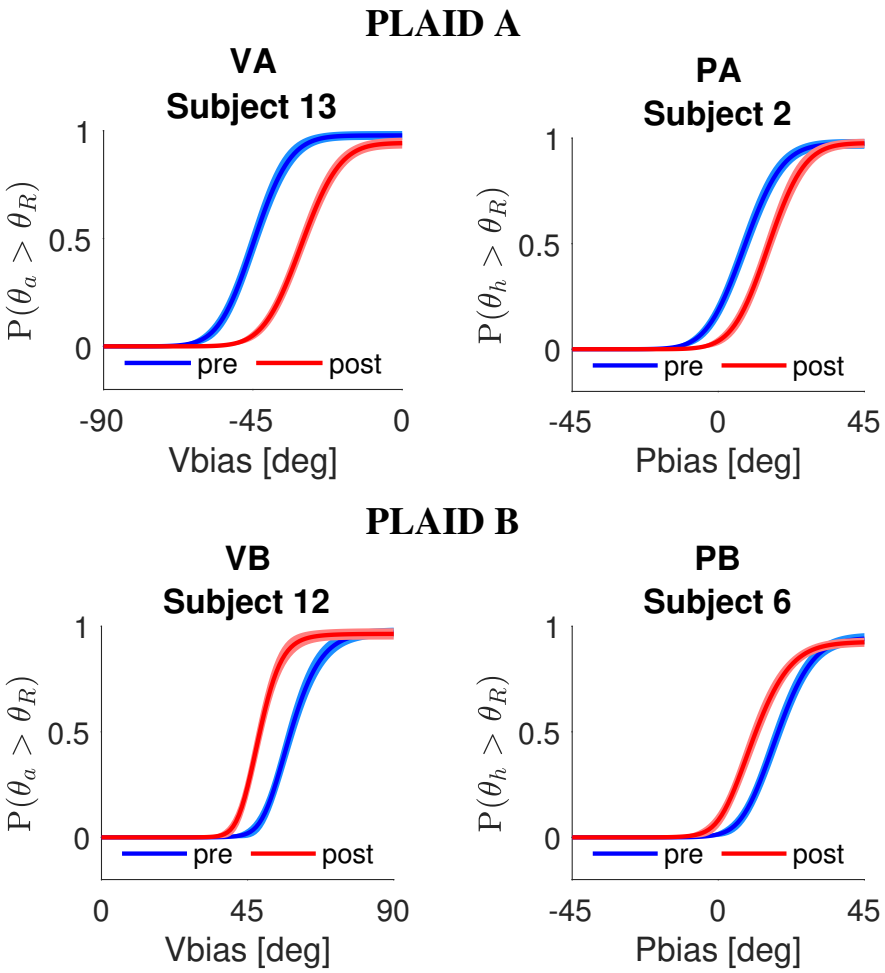

Figure 5.4 Representative perceptual results for all groups: visual (V, left) and proprioceptive (P, right). On the top the psychometric curves for two typical subjects are shown for plaid A, whereas on the bottom the results of the same perceptual tests are shown for two typical subjects using plaid B. Thick lines represent the fitted curves related to the perceptual pre-test (blue) and post-test (red). For the visual curve, Vbias = 0 on the x-axis when the arrow direction θ_a is equal to that of the moving plaid $\theta_R = 45$ deg. For the proprioceptive curve, Pbias = 0 on the x-axis corresponds to when the hand direction θ_h is equal to that of the target $\theta_R = 45$ deg.

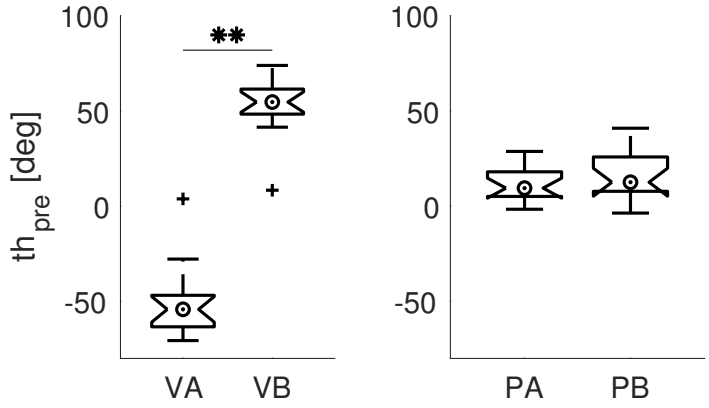

Figure 5.5 The average values of pre-training perceptual thresholds over all participants are compared for both visual (left) and proprioceptive (right) conditions. In each box, the central mark indicates the median, and the bottom and top edges of the box indicate the 25th and 75th percentiles, respectively. I observed a highly significant difference in pre-training visual thresholds between conditions using plaid A and B ($P < 0.0001$; Kruskal-Wallis test); no difference was found in pre-training proprioceptive thresholds.

the post-training tests. It is worth noting that the post-training shift in both plaid A (leftward) and plaid B (rightward) are towards the direction of coherent plaid motion, in relation to the experimental setup (cf. different geometrical configuration of plaid A and B).

These observations are confirmed by statistical analysis. The analyses were conducted using difference scores which were found to be normally distributed ($P > 0.05$; Anderson-Darling test), whereas the pre-training and post-training perceptual values were not normally distributed ($P < 0.05$). Figure 5.5 (left) compares the average of psychometric pre-training thresholds (th_{pre}) over all participants in visual conditions with plaid A and B , VA and VB respectively. The figure shows that the two visual conditions have a significantly different pre-training threshold depending on the plaid type ($P < 0.0001$; Kruskal-Wallis test).

Furthermore, Figure 5.6 (left) compares the average of threshold differences (Δth) from before to after training over all participants in visual conditions with plaid A and B, VA and VB respectively. I found a significant threshold difference with respect to zero (time effect, t-test) in the visual condition with both plaid A ($P = 0.004$) and plaid B ($P = 0.0162$). In addition, a significant difference found between the two visual threshold difference scores depending on plaid type ($P = 0.0015$; pairwise t-test).

5.3.2 Proprioceptive judgement task

The results of perceptual task are presented as psychometric functions, which give the probability that the hand direction, θ_h, is greater than the reference direction of the target,

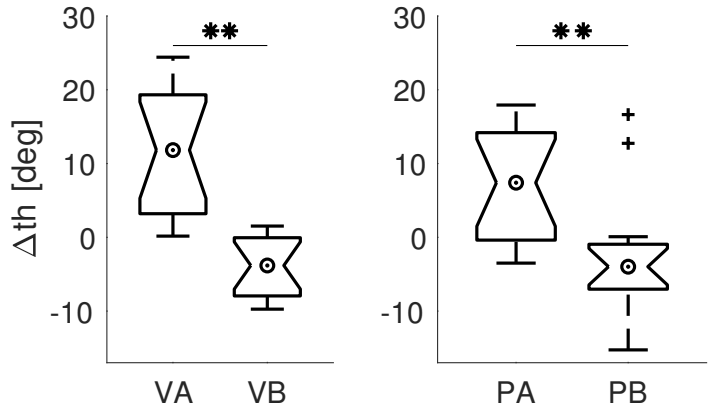

Figure 5.6 The average values of perceptual threshold differences over all subjects in both visual (left) and proprioceptive (right) conditions. In each box, the central mark indicates the median, and the bottom and top edges indicate the 25th and 75th percentiles, respectively. I observed a highly significant difference between threshold difference scores depending on plaid type, both for visual ($P = 0.0015$; pairwise t-test) and proprioceptive ($P = 0.0046$; pairwise t-test) groups.

θ_R, which means that θ_h is to the left of θ_R. $\theta_h - \theta_R$ represents the directional proprioceptive bias (Pbias). Thresholds (th) of psychometric curves are estimated using the adaptive Ψ procedure (see Methods). Participants who have better perceptual performances have threshold values which are closer to the target direction. Figure 5.4 (right) shows the proprioceptive psychometric functions for two representative subjects, who performed the visual judgement task with plaid A (top-right) or plaid B (bottom-right). The pre-training curve is blue and post-training curve is red. $\text{Pbias} = 0$ occurs when the threshold hand direction in the psychophysical tests, θ_h, is equal to the direction of the target, $\theta_R = 45$ deg. Results related to plaid A (top-right) show a leftward pre-training threshold, and a slightly leftward shift in the post-training tests. In contrast, the results related to plaid B (bottom-right) show a leftward pre-training threshold, and a slightly rightward shift in the post-training tests.

These observations were confirmed by statistical analysis. The analyses were conducted using difference scores which were found to be normally distributed ($P > 0.05$; Anderson-Darling test), whereas the pre-training and post-training perceptual values were not normally distributed ($P < 0.05$). Figure 5.5 (right) compares the average of psychometric pre-training thresholds (th_{pre}) over all participants in the proprioceptive tests with plaid A and B, PA and PB respectively. No difference is found between proprioceptive conditions depending on plaid type (Kruskal-Wallis test). Furthermore, Figure 5.6 (right) compares the average of threshold differences (Δth) from before to after training over all participants in proprioceptive

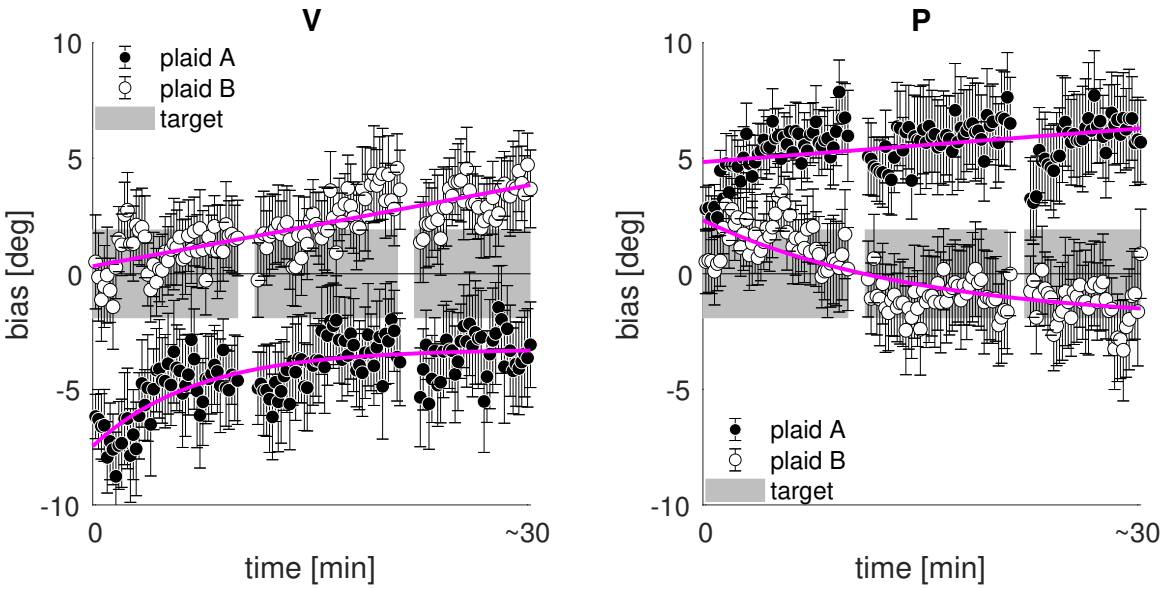

Figure 5.7 Results of motor training. Time series of the average directional bias across subjects over time for both visual (left) and proprioceptive (right) conditions, with both plaid A (black circles) and plaid B (white circles). Each of the three training blocks consists of 50 trials (grey patches), separated by 1 min of rest. Pink lines represent the exponential fitting for each condition; the estimated model parameters and the related coefficient of determination (R^2) are reported in Table 5.1.

testing associated with plaid A and B, PA and PB respectively. I found a significant threshold difference with respect to zero (time effect, t-test) in the proprioceptive tests with both plaid A (P = 0.008) and plaid B (P = 0.0163). In addition, a significant difference is found between the proprioceptive threshold values depending on plaid type (P = 0.0046; pairwise t-test).

5.3.3 Motor training

Participants in the motor training condition were instructed to make reaching movements to a target that was briefly presented at the start of each movement trial. During the trial the only visual information is a plaid, whose motion direction and velocity match those of the hand.

Figure 5.7 shows the time series of the average directional bias of hand movements across subjects of each group over time. Each of the three training blocks consists of 50 trials (grey patches), separated by 1 min of rest. When the directional bias is equal to 0, it means that the hand direction during movement is equal to that of the previously displayed target. Results of visual conditions (left) show a significant leftward change of the directional bias over time increasingly positive values) for both plaid A (black circles; $R^2 = 57.3\%$) and plaid B (white circles; $R^2 = 64.5\%$). Looking at movement directions immediately after the perceptual

Table 5.1 Summary of estimated model parameters.

Perceptual task	Plaid type	A	B	C	R^2 %
V	A	-3.2	-4.2	$-2.8 \cdot 10^{-2}$	57.3
V	B	$-1.5 \cdot 10^2$	$1.5 \cdot 10^2$	$1.4 \cdot 10^{-4}$	64.5
P	A	$-2.6 \cdot 10^2$	$2.6 \cdot 10^2$	$3.6 \cdot 10^{-5}$	20.2
P	B	$9.5 \cdot 10^2$	$-9.5 \cdot 10^2$	$1.6 \cdot 10^{-5}$	47.8

test, they start with a rightward bias for plaid A, and no bias for plaid B, but no correlation is found between the perceptual threshold measures and motor bias measures in either of the visual conditions. The results of proprioceptive conditions (right) show a significant leftward change in the directional bias over time for plaid A (black circles; $R^2 = 20.2\%$), and a significant rightward change for plaid B (white circles; $R^2 = 47.9\%$). Looking at movement directions immediately following the initial perceptual test, they start with a leftward bias for plaid A, and no bias for plaid B, but no correlation is found between proprioceptive perceptual threshold measures and motor bias measures in either of the visual conditions.

I fitted an exponential model to the performance time series of each training block for each group (see Methods). The model has a total of 3 parameters: A, B, C. Table 5.1 shows the estimated model parameters and the related coefficient of determination (R^2) over time for each group.

5.4 Discussion

The present study shows that interactive motor training with an ambiguous visual stimulus changes the subsequent visual perception of stimulus motion and the somatosensory perception of hand movement. Four groups of participants performed the same motor training task with two possible types of visual motion feedback (plaid A or plaid B) and with two different perceptual tests (visual or proprioceptive), which preceded and followed the movement training session.

During the visual perceptual test, participants were asked to judge if a displayed red arrow was pointing towards the right or the left of the direction of a moving plaid which was presented before. During the proprioceptive task, the robot moved the hand outward with vision of the arm blocked. Participants were asked to judge whether the hand was moved to the right or to the left of a visual target that was also presented before. During motor training, participants reached towards a briefly presented target beyond the far edge of the aperture by

moving the robot handle. At the same time they moved a plaid stimulus displayed on the screen. The direction of plaid motion corresponded to the direction of the hand movement. The arm was occluded and there was no cursor. The only visual feedback was from the direction of plaid motion. This training was designed to assess whether perceptual decisions regarding plaid movements (visual judgement test) or hand movements (proprioceptive judgement test) were affected by actively interacting with the stimulus.

5.4.1 Motor training implications on perceptual changes

The idea that motor learning is involved in neural plasticity in both motor and sensory systems is widely supported in literature. There is substantial evidence of somatosensory changes (Henriques and Cressman, 2012; Ostry and Gribble, 2016), which may be the result of the repeated pairing of somatic input and movement. Training-related changes to movement and motor cortex are accompanied by somatosensory plasticity. Similarly, in the context of speech motor learning there is a demonstrated contribution of the effects of motor learning on auditory perception of speech (Henriques and Cressman, 2012; Ostry and Gribble, 2016).

In the literature on vision, motor priming of visual motion perception was presented preliminarily by (Ishimura, 1995; Ishimura and Shimojo, 1994). They demonstrated that movement can affect simultaneous visual motion perception, and this phenomenon was called *action capture*. Other online changes to visual perception which accompany movement have also been reported (Müsseler, 1999; Schütz-Bosbach and Prinz, 2007a), based on the idea that movement is controlled by the anticipation of its intended effects.

More recently, several studies have presented evidence that the visual perception of a moving stimulus can be shaped by both movement execution (Beets et al., 2010b; Zwickel et al., 2007) and movement planning (Wohlschläger, 2000). Several studies have shown that practising a movement can improve visual discrimination of the same movement (Beets et al., 2010b; Hecht et al., 2001; Zwickel et al., 2007); in addition, observation of movement leads to increased activity of the related cortical motor areas (Calvo-Merino et al., 2005; Engel et al., 2008; Reithler et al., 2007).

In contrast, a small number of studies have examined the effects of motor learning on vision. For instance, Brown et al. (2007) found that expectations regarding visual motion are changed as a result of learning. Beets et al. (2010a) demonstrate that motor learning can induce a bias in visual perception.

5.4.2 Motor training with ambiguous stimuli induce both visual and somatosensory changes

The perceptual tests show significantly different pre-training perceptual thresholds; see Figure 5.5. Visual pre-training thresholds differ in accordance with plaid type, so this suggests that the perceptual threshold depends on the geometrical arrangement of the moving stimulus used in each condition (plaid A or plaid B). In constrast, the proprioceptive pre-training threshold is always leftward, such as in the baseline of visuomotor (Cressman and Henriques, 2009; Volcic et al., 2013) or prism adaptation (Beckett, 1980; Harris, 1963) studies, suggesting that this bias is due to the biomechanical configuration of the arm and occurs when its movement feedback is occluded (Bagesteiro and Sainburg, 2002; Uno et al., 1989).

The motor bias at the beginning of the movement training task seems to reflect the related pre-training perceptual threshold (see Figure 5.7), even if no correlation is found between motor bias and perceptual thresholds in all conditions.

I found that both visual and somatosensory perceptual thresholds changed significantly following training. Figure 5.6 shows that the threshold differences from before to after training depend both on the plaid type and perceptual test. Results related to plaid A show a leftward shift in the post-training tests for both visual and proprioceptive groups (VA, PA). Results related to plaid B shows a rightward shift in the post-training tests (VB, PV). It is possible that the different geometric arrangement of the two plaids can affect perceptual changes observed. The two plaids were designed in order to have the same global velocity, in terms of both amplitude and direction, but their component gratings move in opposite directions with respect to the plaid motion direction.

Moreover, participants showed greater changes of directional bias with plaid A than plaid B. Both pattern motion and gratings' motion direction of plaid A are from left to right, whereas in plaid B gratings' motion direction is from right to left. This aspect could increase the perceptual ambiguity of plaid B, because the participant tries to find perceptive coherence in an apparently more ambiguous situation. Perception of plaid A can have greater changes also because of spatially directional reading habits: habitual reading-related biases might guide participants' gaze and motor behaviour (left-to-right reading direction in Western societies) (Werner et al., 2019).

5.4.3 Motor training with ambiguous stimuli induce practice-related changes to movement

Movement direction changed over the course of training, presumably because the plaid effectively serves as a ‘cursor’ showing movement direction. The esults showed that the perceptual ambiguity of plaid motion is overcome by subjects by interacting with the stimulus. In this way, participants likely can experience the sensorimotor contingencies caused by the concurrent self-generated plaid motion and its perceptual consequences. As both visual and proprioceptive inputs are provided during the interaction, they contribute with contingent information so that a prediction is created on the perceptual consequences caused by the plaid motion (see (Gibson, 1979; Held and Hein, 1963; O’Regan and Noë, 2001)).

Part II

Computational models of stroke recovery through exercise-based training

Chapter 6

State of the Art [1]

6.1 Introduction

A cerebrovascular accident (stroke) elicits in the nervous system a complex series of reorganization processes at molecular, cellular, neural population, behavioral (sensorimotor and cognitive) and social interaction levels, with temporal scales that range from hours, to months, to years (Nudo, 2006). Animal models and human studies suggest that functional recovery after a stroke is mediated by use-dependent reorganization of the preserved neural circuitry. A key to neuromotor recovery and the basis of many neurorehabilitation interventions - including robot-assisted exercise - is the movement associated with a task and with volitional effort (Timmermans et al., 2010). Several studies have modeled the evolution of sensorimotor performance through exercise (motor learning); much fewer studies have specifically addressed the neuromotor recovery process (Casadio et al., 2013). Models of motor learning focus on a set of variables that summarize task performance within a single trial - for instance, motor error, smoothness, or average speed. The goal of modeling is to describe the trial-by-trial evolution of performance and its underlying mechanisms. Variants of the power law of practice have often been used to describe the trial-by-trial evolution of motor performance. However, these descriptions do not address the underlying mechanisms. Also, they do not consider the effect of exogenous variables - like task difficulty or physical guidance - which likely affect motor performance and/or learning speed. As a consequence, they can only be used to describe spontaneous learning (or recovery). Here, I use a more general formulation, based on state-space models (Ueyama, 2017). These models have

[1] *Parts of the content of this chapter has been published as Sedda, G., Summa, S., and Sanguineti, V. (2018). Computational models of the recovery process in robot-assisted training. In Rehabilitation Robotics, pages 117–135. Elsevier.*

been first proposed to describe the temporal evolution and the mechanisms underlying the sensorimotor adaptation and motor learning. Only recently, these same techniques have been used to describe neuromotor recovery.

6.2 Computational models of motor learning

6.2.1 Models of sensorimotor adaptation

The use of the state-space dynamic system models to describe the trial-by-trial dynamics of sensorimotor adaptation (Cheng and Sabes, 2006; Donchin et al., 2003; Scheidt et al., 2001; Thoroughman and Shadmehr, 2000) is now well established. A perturbation during targeted movements induces an adaptation process, consisting of the development of an "internal model" of the perturbation so that future motor commands take this prediction into account. This trial-by-trial process can be described in terms of a dynamic model. Model formulation requires specific assumptions on the signal or signals that drive adaptation. To identify the actual adaptation mechanism, alternative models of the same process may be compared (Cheng and Sabes, 2006) to select which model best describes the data. Most trial-by-trial models of adaptation assume that hand position on the t-th trial, $h(t)$, is determined by the movement (motor command) $u(t)$, plus a force perturbation $f(t)$:

$$h(t) = u(t) + D \cdot f(t) \tag{6.1}$$

In many studies, the perturbation $f(t)$ is a velocity-dependent force field (Shadmehr and Mussa-Ivaldi, 1994). Parameter D can be interpreted as the arm compliance (the inverse of arm stiffness, $K = 1/D$) (Donchin et al., 2003). Note that here I am only interested in modeling the component of the motor command and of hand position that relates to perturbations, whereas the components that are supposed to be responsible for reaching the target are assumed to be unaffected by the perturbation. In velocity-dependent force fields, the perturbation is always orthogonal to the movement, so that $h(t)$ is a measure of lateral deviation of the movement with respect to the straight line from starting point to target. The "motor command," $u(t)$, can be interpreted as the lateral deviation observed when the perturbation is removed ($f = 0$). I also assume that the perceived hand position, $y(t)$, is modeled as the actual hand position, plus some sensory (e.g., visual) noise, $n_v(t)$:

$$y(t) = h(t) + n_v(t) = D \cdot f(t) + u(t) + n_v(t) \tag{6.2}$$

In case the perturbation is visual, that is, it affects the way the hand is displayed (e.g., a rotation), the displayed ("cursor") position of the hand on the t-th trial, $c(t)$, is obtained as the hand position $h(t)$ plus the visual perturbation $r(t)$:

$$c(t) = h(t) + r(t) \tag{6.3}$$

Again, I assume that the visually perceived position, $y_v(t)$, is equal to the actual visual (cursor) position plus some sensory (e.g., "visual") noise $n_v(t)$:

$$y_v(t) = c(t) + n_v(t) = h(t) + r(t) + n_v(t) = r(t) + u(t) + n_v(t) \tag{6.4}$$

where the motor command $u(t)$ denotes the hand position without perturbation.

Both models may incorporate proprioception-based information on hand position, $y_p(t)$, expressed as the true hand position $h(t)$, plus sensory (proprioceptive) noise, $n_p(t)$:

$$y_p(t) = h(t) + n_p(t) \tag{6.5}$$

Proprioception is affected by force perturbations but not visual perturbations. In this case, the overall sensory information available to the nervous system would include both vision and proprioception, so that $y(t) = [y_v(t) y_p(t)]^T$. Proprioceptive perturbations could be also provided, for instance, by muscle vibration. In this case, the extension of the model would be straightforward. Both dynamic and kinematic perturbations might be applied at the same time (Summa et al., 2012). In this case, the overall disturbance would be denoted as $x = [f r]^T$ and the overall execution noise term as $n_y = [n_v n_p]^T$ with $n_y \sim N(0, R)$. I would end up with

$$y(t) = H \cdot x(t) + G \cdot u(t) + n_y(t) \tag{6.6}$$

where H and G combine Eqs. 6.2, 6.4.

A "controller" is assumed to determine the motor command $u(t)$ on the basis of the dynamic and/or kinematic perturbations, that is, $x(t)$. The nervous system does not have a direct access to perturbations, but may estimate their effects adaptively based on the available evidence, that is, the sensory information $y(t)$. Estimation of the disturbance is a dynamic process, which can be described by a state-space equation

$$\hat{x}(t+1) = A \cdot \hat{x}(t) + B \cdot e(t) + n_x(t) \tag{6.7}$$

where $\hat{x}(t)$ denotes the estimated disturbance. Eq. 6.7 indicates that the predicted disturbance at the next trial is a combination of the current estimate and an "adaptation" term proportional to a "driving" signal, $e(t)$. A noise term, $n_x(t) \sim N(0,Q)$, or process noise models the extent to which perturbation can be predicted. Coefficients A and B denote, respectively, the "retention rate", the extent to which a given estimate is retained at the next trial (for stability, A should be $0 < A < 1$), and the "learning rate", the extent to which the estimated perturbation is sensitive to the driving signal. Different hypotheses have been formulated on the nature of $e(t)$. Empirical studies (Shadmehr et al., 2010) have suggested that adaptation is driven by the mismatch between actual and predicted perturbation, that is, $e(t) = x(t) - \hat{x}(t)$. A Bayesian approach, optimally combining all the available evidence, can be used to identify the ideal adaptation mechanism. In this way, a model of adaptation can be derived from general principles, with no need to make specific hypotheses on the driving signals, and then compared with empirical evidence. Haith et al. (2009) first proposed a Bayesian approach to model the adaptation to a velocity-dependent force field. In a Bayesian framework, an optimal estimate of the perturbations, $\hat{x}(t)$, can be derived by combining prior belief and the available measures, that is, $y(t)$ and $u(t)$. I denote prior belief as $\hat{x}^-(t)$ and model it as

$$\hat{x}^-(t+1) = A \cdot \hat{x}^-(t) + n_x(t) \tag{6.8}$$

where $0 < A < 1$ is a decay parameter. Basically, I am assuming that the best we can do in absence of new information is to predict the future perturbation in terms of the current estimate. Sensory information, that is, $y(t)$, is a potential source of information on the perturbation. To make sense of it, we need to quantify the sensory consequence $\hat{y}^-(t)$, of the predicted state, $\hat{x}^-(t) : \hat{y}^-(t) = H \cdot \hat{x}^-(t) + G \cdot u(t)$.

An unbiased minimum-variance posterior estimate of the state, $\hat{x}^+(t)$, would take the form of a combination of prior belief and error correction based on sensory information:

$$\hat{x}^+(t+1) = \hat{x}^-(t+1) + K(t) \cdot [y(t) - \hat{y}^-(t)] = A \cdot \hat{x}^+(t) + K(t) \cdot [y(t) - \hat{y}^-(t)] \tag{6.9}$$

The gain $K(t)$ is computed iteratively through the Kalman algorithm. The overall computational model is depicted in Figure 6.1. In the case of force or visual perturbation alone, motor commands are simply calculated as the opposite of the predicted perturbation, that is, $u(t) = -\hat{x}(t)$. Other control schemes may be plausible, for instance, involving a combination of prediction (of the perturbation) and resistance to it (achieved, for instance, by increasing arm stiffness) or a trade-off between error and effort (Emken et al., 2007).

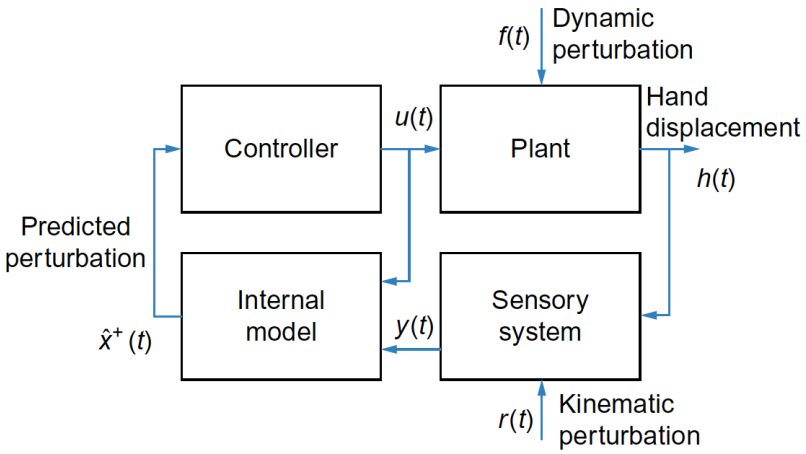

Figure 6.1 Computational model of sensorimotor adaptation.

In all cases, the model predicts that asymptotic cancellation of the perturbation is not complete because the forgetting term, A, counteracts adaptation. Large values of A lead to slower forgetting and more adaptation; lower values of A result in fast forgetting and less adaptation. If both visual and proprioceptive modalities are taken into account, the Bayesian model of adaptation also predicts that forcefield adaptation would introduce not only a change in the motor commands that incorporate a prediction of the perturbation but also a sensory bias in proprioception (Haith et al., 2009). This prediction has been confirmed experimentally (Ostry et al., 2010), thus emphasizing the interplay between motor and sensory (proprioceptive) adaptation. The Kalman framework confirms the empirical finding that sensorimotor adaptation is optimally driven by the discrepancy between actual and predicted perturbation, which is equivalent to the discrepancy between actual and predicted sensory output; see Eq. 6.9.

Multirate adaptation

Empirical findings (Smith et al., 2006) have suggested that the nervous system may keep multiple internal representations of the perturbations, each with their own time constant. The basic model (Eqs. 6.3, 6.9) is easily extended to account for multiple internal representations if we posit more internal models, each with their own dynamics equation. Specifically, Smith et al. (2006) suggested that two internal representations, with different time constants (“fast”

and "slow," i.e. $B_f > B_s$ and $A_f < A_s$)

$$\begin{aligned} \hat{x}_f(t+1) &= A_f \cdot \hat{x}_f(t) + B_f \cdot y(t) \\ \hat{x}_s(t+1) &= A_s \cdot \hat{x}_s(t) + B_s \cdot y(t) \\ y(t) &= D \cdot f(t) + u(t) \end{aligned} \tag{6.10}$$

with $u(t) = -\hat{x}_f(t) - \hat{x}_s(t)$, account for the observation that in repeated adaptation-washout cycles, subsequent adaptations tend to be faster and more persistent than those observed in naive subjects—the so-called "savings" property. Adaptation mostly relies on implicit mechanisms, which do not need voluntary control to take place. More recently, explicit (Taylor et al., 2014) and reward-based (see Izawa and Shadmehr (2011) and below) components of adaptation have been identified. Specifically, explicit and implicit components of adaptation have been related (McDougle et al., 2015) to the fast and slow components above.

Spatial generalization

Movements during an adaptation trial may differ in terms of starting position, amplitude, and/or direction. In particular, many studies have been focusing on movements with the same starting position and amplitude, but different directions. An important issue is whether and to what extent adaptation to perturbations in a specific movement generalizes, that is, affects the adaptation to perturbations applied to similar movements. Models of adaptation often assume that movements in each direction $\theta_1, ..., \theta_D$ are specified by a different "motor memory" or motor commands. In other words, there is a different $\hat{x}_d$ for each movement direction, $d = 1, \ldots, D$, and making one movement is assumed to affect the motor memories of similar movements (directional generalization). In principle, all model parameters may be direction-dependent. For more details, see Chapter7.

Sensorimotor adaptation is widely used as experimental model for exercise-driven motor plasticity. Robot-assisted neuromotor recovery cannot be simply reduced to a form of adaptation, but adaptation paradigms are often used in rehabilitation to clarify how neurological diseases affect motor plasticity. Robots are essential tools to study the adaptation to perturbations, and models can be used to draw specific conclusions. For instance, empirical studies using adaptation models have suggested that persons with cerebellar atrophy, but not Huntington's disease, exhibit a near-zero learning rate,and are therefore unable to adapt to a force field (Smith, 2005). Persons with multiple sclerosis and little or no disability have intact adaptation capabilities but defective motor performance, as shown by the large variance of the output noise, (Casadio et al., 2008).

6.2.2 Model of motor skill learning

Sensorimotor adaptation is a specific form of learning, driven by the discrepancy between a perturbation and its internal representation. The goal of motor skill learning is to develop a "motor command" or action that maximizes its long-term benefit or "value" in relation to a specific task. To quantify the compliance of movements to the task, there is no available motor error. Rather, the environment provides a scalar or even binary "reward" signal, and the long-term benefit is expressed in terms of the expected future rewards. Different from sensorimotor adaptation, this creates the need for active exploration of the action space, that is an explicit trial-and-error search for "good" behaviors.

Learning of actions based on a reward is usually referred as reinforcement learning (RL); see Sutton and Barto (2018) for a comprehensive presentation. RL models have been largely used in modeling cognitive tasks, in which the "action" consists of a decision among a discrete number of options. Much less often, these models have been applied to describe the trial-by-trial dynamics of learning a motor skill. Here, I only summarize the main concepts and the formulations that are most relevant to the development of state-space models of motor skill learning. In an RL scenario, the environment responds to each motor command $u(t)$ with a scalar reward signal, $r = r(u)$. The agent's goal is to gradually develop a policy that maximizes the long-term benefit or action "value," defined as the weighted sum of the rewards obtained in the current and future trials - the expected cost to go:

$$V(t) = E\{r(t) + \gamma \cdot r(t+1) + \gamma^2 \cdot r(t+2) + ... + \gamma^{T-t} \cdot r(T)\} \tag{6.11}$$

where parameter γ is the discount rate, quantifying the relevance of future rewards ($\gamma = 0$ indicates that only the current reward matters), and T is the total number of trials. If T is sufficiently large, the following property holds $V(t) = r(t) + \gamma \cdot V(t+1)$. I assume that the learning agent maintains a model of the action value, $\hat{V}(t)$ - usually referred as the "critic". The quantity $\hat{V}(t) - \gamma \cdot \hat{V}(t+1)$ can be interpreted as the expected reward at time t, so that we can define a reward prediction error (RPE) at the t-th trial: $\delta(t) = r(t) - \hat{V}(t) + \gamma \cdot \hat{V}(t+1)$. The critic can be learned through the temporal difference (TD) learning rule (Sutton and Barto, 2018):

$$\hat{V}(t+1) = \hat{V}(t) + \alpha_c \cdot \delta(t) \tag{6.12}$$

where α_c is the critic's learning rate. As regards the selection of the next action, we can assume that the agent develops a separate representation of the next action (an "actor" in RL terminology). This is called the actor-critic (AC) model. Similar to the critic, optimal action may be developed in terms of a TD learning rule. Various rules are possible; for instance,

Izawa and Shadmehr (2011) assumed that the motor command $u(t)$ is a combination of an "action" $a(t)$ and an "active search" or "exploration" noise, that is, $u(t) = a(t) + n_a(t)$. The action update in the "actor" learning rule was assumed to be proportional to the exploration noise (Izawa and Shadmehr, 2011) - more exploration leads to a greater change:

$$a(t+1) = a(t) + \alpha_a \cdot \delta(t) \cdot n_a(t) = a(t) + \alpha_a \cdot \delta(t) \cdot [u(t) - a(t)] \tag{6.13}$$

where α_a is the actor's learning rate. Izawa and Shadmehr (2011) used this formulation to identify the relative contributions of error-based and reward-based learning in the adaptation to visual rotations.

The above formulations are suitable in stationary situations, in which there is one action to learn and the environment is stable. In more general situations, the environment may change - this includes, for instance, perturbations or changes in task parameters, for example, task difficulty. If the environment state is denoted by $x(t)$, the long-term benefit is denoted by an action-value function, $Q(u,x)$. The critic's goal is to learn a model of this function, $\hat{Q}(u,x)$, which may depend on a number of parameters. At each time step, an action is selected as a trade-off between exploitation (maximizing $\hat{Q}(u,x)$) and exploration of the action space. The Gibbs softmax procedure is often used:

$$p(u|x) \propto e^{\hat{Q}(u,x)/\lambda} \tag{6.14}$$

where λ is a "temperature" parameter that regulates the amount of exploration (greater λ implies more variability and therefore more exploration). RL models are appropriate for describing situations in which learning occurs through trials and errors and is driven by reward. This is the case, for instance, of many of the exercise games (exergames) used in neuromotor rehabilitation. RL models based on TD learning can be expressed as state-space linear or nonlinear models; therefore, they fit well in this general framework.

6.2.3 Models of neuromotor recovery

Similar to motor skill learning, exercise-based neurorehabilitation aims at gradually improving performance through repeated exercise. However, different from motor learning, poor performance depends not only on insufficient skill but also, first and foremost, on the presence of an impairment. Therefore, the problem is not primarily to learn a skill but, rather, to achieve satisfactory performance despite the existing impairment. Redundancy in the musculoskeletal system plays a key role in recovery: as the motor system has more

degrees of freedom than task variables, the same functional behavior may be achieved with different movements. The pressure toward regaining functional independence may lead to the development of compensatory strategies that, although adequate for carrying out activities of daily life (ADLs), may be energetically inefficient and may ultimately prevent true recovery (Cirstea and Levin, 2000; Levin, 1996). For instance, an excess use of the nonparetic limb may have a negative influence on the process of cortical reorganization (Avanzino et al., 2011) by further reinforcing the imbalance between the impaired and nonimpaired hemispheres. Understanding the complex set of interactions among the neural structures that underlie voluntary movements is of paramount importance to understand neuromotor impairments and to identify treatments that facilitate recovery (Casadio et al., 2013). A model of neuromotor recovery must build on specific assumptions on the nature of the impairment and on the way it affects performance. In other words, to model motor recovery, we need to account for both motor learning and neural plasticity (and recovery) mechanisms (Reinkensmeyer et al., 2016).

6.2.4 Models of recovery at neural level

Reinkensmeyer et al. (2003) developed a model of cortical damage and its consequences on arm-reaching movements. Based on experiments on nonhuman primates (Georgopoulos et al., 1982), neurons in the motor cortex are assumed to collectively encode the initial direction of the movement (population vector coding). Specifically, each neuron's firing rate is assumed to be a function (truncated cosine) of the difference between the actual movement direction and the "preferred direction" for that neuron plus a noise term, whose standard deviation is proportional to the deterministic part of the cell response (signal-dependent noise). The overall encoded (i.e., internally represented) movement direction is the sum of the preferred directions of each individual neuron, weighted by their activity levels. Cortical lesions were simulated by eliminating a fraction of the neurons (cell death) - hence resulting in underrepresented or nonrepresented preferred directions. Movement performance was measured in terms of the discrepancy between intended and encoded movement direction. These authors specifically looked at the variability of the directional error within the same intended direction and across directions and how these quantities are affected by cell death. They found that both error measures are inversely correlated to the fraction of surviving cells. In a number of experimental studies with stroke survivors, the same indicators exhibit similar relationships with the subjects' clinical impairment measures (Kamper et al., 2002; Reinkensmeyer et al., 2002; Takahashi and Reinkensmeyer, 2003).

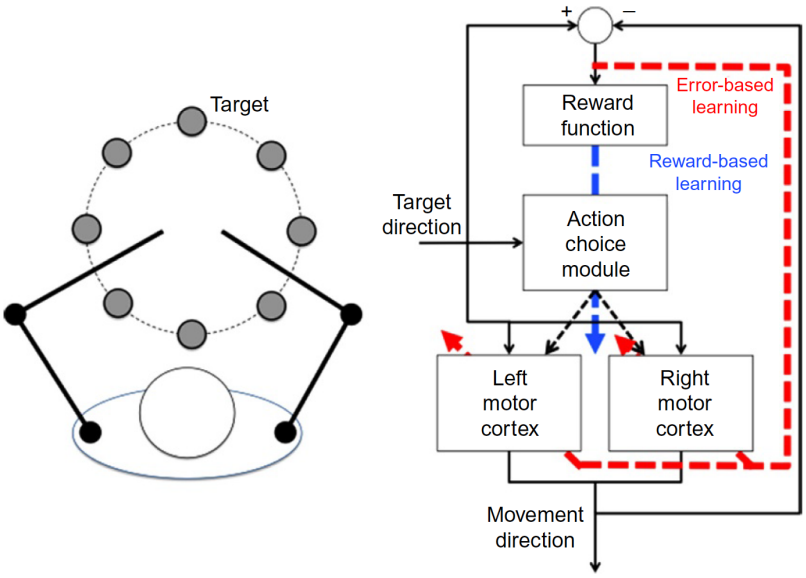

Figure 6.2 Model of spontaneous recovery after stroke. The model focuses on reaching movements (left), for which subjects spontaneously select what arm to use. The model (right) includes a model of the motor cortex (both hemispheres) and an action selection module. Modified from Han et al. (2008)

The above study addresses how cortical damage results in impaired movements, but does not address the mechanisms of recovery. Han et al. (2008) used the same model of lesions in cortical motor areas to understand how lesions affect the mechanisms of arm selection to achieve a goal (reaching a target) and how impairment evolves through spontaneous arm use. Therefore, the model accounts for both motor cortical dynamics (both hemispheres) and action selection; see Figure 6.2.

The effect of a stroke was modeled by eliminating part of the neurons within one hemisphere's motor cortex. Activity-dependent cortical reorganization is modeled by a Hebbian mechanism, in which the preferred directions of each neuron are assumed to adapt as a function of activity. Adaptation has two aims: (i) shifting the actual encoded direction closer to the desired direction (supervised component) and (ii) shifting the preferred directions of the individual neurons toward the desired direction (self-organizing component). The process of deciding which arm to use is modeled in terms of the RL framework. An action selection module accounts for the process of selecting the hand that will actually make the movement. After every movement, a reward signal is provided, defined as the sum of two terms, respectively, reflecting (i) how close the cortex's encoded direction is to the desired movement direction and (ii) the fact that the left hand is more likely chosen for leftward movements, whereas the right hand is more likely selected for rightward movements. A

model of the action-value mapping, based on radial basis functions, generates the expected reward as a function of the direction of the actual movement. The hand corresponding to the maximum expected reward is selected to execute the movement. After each trial, the action-value model is updated to minimize the difference between actual and expected reward (TD learning).

The impaired side is initially unlikely to be selected for movements on that side, and the lack of use makes its selection even less likely. Forced use of the impaired side induces reorganization, so that the intact portion of that hemisphere gradually shifts its preferred directions toward those that were once covered by the impaired portion. In summary, the model addresses the mechanisms of interaction between activity-driven cortical reorganization and functional compensation, that is, the change in the motor strategy (in this case, from the impaired to intact arm) that is driven by the need to preserve functional performance (e.g., a high reward). The model predicts that recovery will self-sustain if the amount of spontaneous use of the impaired arm reaches a certain threshold. If this is not the case, the impaired arm will be less likely selected, and recovery (if any) will gradually wash out. The model makes an important qualitative prediction - an activity threshold is a necessary condition for recovery to self-sustain. This may explain the mechanisms of action of rehabilitation strategies that rely on forced use of the impaired arm. Observations from a rehabilitation trial based on constraint-induced movement therapy (CIMT) are indeed consistent with the "threshold" notion (Schweighofer et al., 2009). The model also suggests a criterion to personalize the therapy - aiming to achieve an "activity threshold" rather than providing a fixed amount of training. This model is important, because it is a first attempt to address the interplay between the cortical reorganization and the development of compensatory strategies.

Unilateral spatial neglect (USN) is a neuropsychological syndrome described as a "failure to report, orient toward, or respond to stimuli in contralesional space, which cannot be attributed to primary motor or sensory dysfunction" (Heilman and Valenstein, 1979), which is often observed in right-hemisphere stroke patients. Recently, Leigh et al. (2015) proposed a neural model that qualitatively describes cortical lesions and predicts the resulting neglect symptoms. The model reproduced a few symptoms of neglect, like the line bisection behavior and the beneficial effect of prism adaptation (Rossetti et al., 1998). However, model predictions are qualitative and cannot be used to explain individual behaviors.

6.2.5 Models of recovery at function level

Models of recovery at neural level may qualitatively predict the mechanisms and the determinants of recovery, but cannot be used as analytic tools to understand the recovery process of individual subjects. To do so, we need models of recovery that capture the main processes occurring at cortical level, but are expressed in terms of quantities that are directly observable, for example, sensorimotor performance. Hidaka et al. (2012) redefined Han's recovery model in terms of quantities that either are directly observable or can be estimated from observations. The functionality of the affected (A) and nonaffected (N) arm at time t is summarized into two variables, $u_A(t)$ and $u_N(t)$. A binary variable, $y(t)$, encodes the arm selected ($y = 1$, affected arm; $y = 0$ nonaffected arm). The probability of selecting the affected arm is modeled as a logistic function of u_A:

$$Pr(y(t) = 1|u_A) = \frac{1}{1 + e^{-[H \cdot u_A(t) + G]}} \tag{6.15}$$

where parameter H denotes the effect of function on arm use. The functionality of the nonaffected arm is assumed to be constant, and its effect on arm use is accounted by parameter G. The functionality of the affected arm is assumed to improve with use ($y = 1$) and to decline with nonuse ($y = 0$) - in the words from Hidaka et al. (2012), "use it and improve it, or lose it":

$$u_A(t+1) = A \cdot u_A(t) + B \cdot y(t) \tag{6.16}$$

where parameter B (recovery rate) captures the effect of arm use on arm function. To minimize the number of parameters, the decay time constant (retention rate, A) was assumed to be the complement of B, that is, $A = 1 - B$. The model was used to interpret the arm selection time series from the EXCITE trial (Schweighofer et al., 2009), in which stroke patients underwent constraint-induced movement therapy (CIMT) - subjects were forced to use their nonaffected arm for a fraction of their time. The available data were a questionnaire-based normalized arm use score and a measure of arm functionality based on movement time, assessed every 4 months during the 24-month trial. In two groups, a 2-week CIMT protocol was administered either at the beginning (immediate group) or at the end of the trial (delayed group). Model simulations suggested that the effect of function on arm use (parameter H) is the main determinant of the long-term increase of arm use. Comparisons with data before and after treatment also suggest that the main effect of CIMT therapy is to increase H.

Likewise, starting from Leigh's model of neglect (Leigh et al., 2015), Sedda et al. (2017) derived a computational model of recovery from neglect through exercise. The model

reproduces the main observations of prism adaptation experiments and was fitted to data from a rehabilitation trial based on a novel VR-based rehabilitation approach, involving reaching movements within an adaptive environment. For more details, see Chapter8.

6.2.6 Modeling the role of robot assistance

Robots can be used in many different ways to promote recovery. Robots may help completing the movement when the subject is unable to do it alone, thus increasing the administered exercise dose and/or intensity. In this case, the robot only plays an indirect role in the recovery process. Robots can also be used to increase movement variability, thus increasing the amount of exploration. More exploration leads to more accurate control in later movements (Patton et al., 2006). In other scenarios, robots continuously assist movements, very much like human therapists. Only few modeling studies have addressed how continuous robot assistance affects recovery. Emken et al. (2007) looked at adaptive changes in gait movements in the presence of assistive forces. The model specifically addresses the trial-by-trial evolution of performance. As in Figure 6.1 and similar to force-field adaptation experiments, a controller receives the desired trajectory as input and generated the motor command. One main assumption is that the motor system behaves as a "greedy" optimizer, that is, the motor command is generated through an optimization process, which accounts for a combination of motor error and effort. As the assistive force aims at reducing the error, it is gradually incorporated into the motor plan so that the motor command gradually reduces its magnitude while the performance level (e.g. a small error) is maintained. This decay mechanism has been termed "slacking" and is a consequence of the forgetting term in the adaptation equation.

Emken et al. (2007) also suggested that slacking may have adverse effects on recovery (the "slacking" hypothesis). As a consequence, in robot-assisted rehabilitation, assistance should be kept to a minimum (assist as needed). Furthermore, it has to be decreased—manually or automatically—as performance improves. A variety of techniques have been proposed to adaptively regulate the magnitude of assistive force as a function of the observed outcome. The "greedy optimizer" model has been highly influential to rehabilitation, but does not explicitly address the recovery mechanisms. In fact, it has been derived from studies on healthy subjects, and its implications for recovery are largely speculative. The slacking hypothesis has never been directly tested in clinical rehabilitation trials.

Casadio and Sanguineti (2012) developed a dynamic model to describe the trial-by-trial evolution of the motor performance in chronic stroke survivors who underwent a rehabilitation protocol based on a robot-assisted arm extension task. Similar to (Emken et al.,

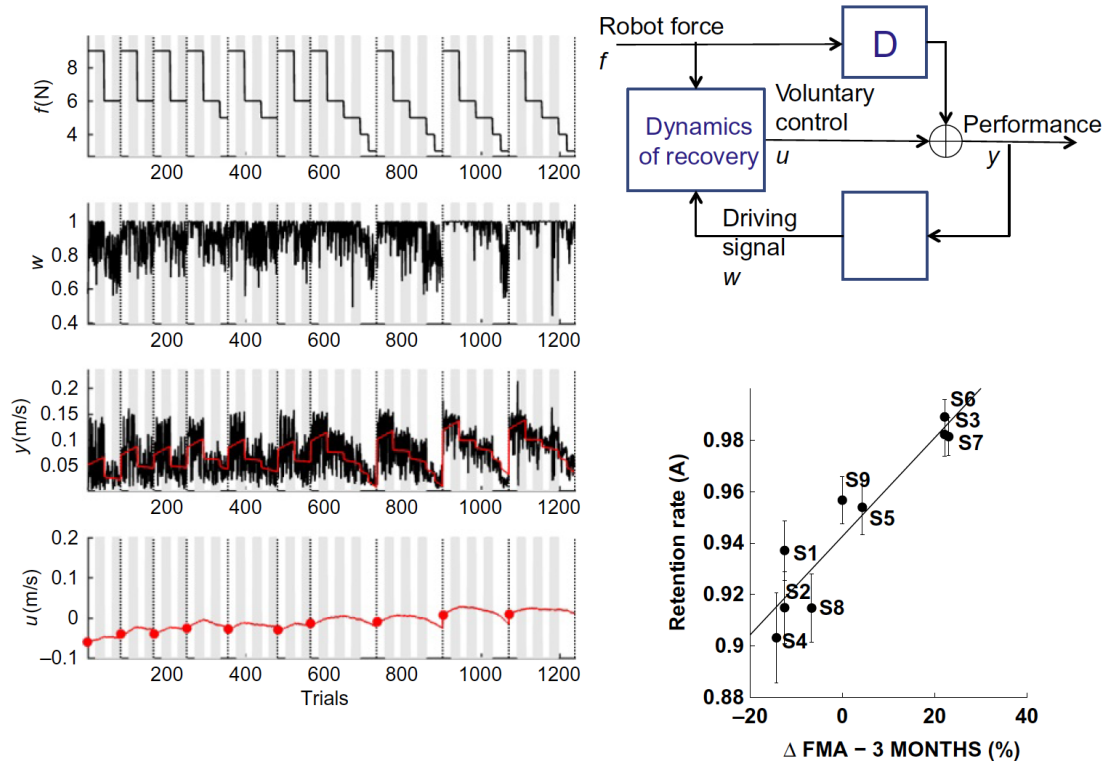

Figure 6.3 State-space model of stroke recovery through robot assistance. Left: fitting performance. Right: model schematic (top) and the main result that the model's rate of retention parameter predicts the long-term outcome—change in the Fugl-Meyer assessment (FMA) score in the 3 months following the end of the treatment (bottom). Modified from Casadio and Sanguineti (2012).

2007), the model assumed that in robot-assisted exercise, the robot and the subject cooperate toward a common goal - a form of shared control. Specifically, the model assumes that task performance, $y(t)$, is a function of a voluntary, human-generated command, $u(t)$, (taken as the model's state variable) and of a robot-generated assistive force, $x(t)$:

$$y(t) = u(t) + D \cdot x(t) \tag{6.17}$$

Average speed was taken as the task performance measure. Therefore, parameter D can be interpreted as hand mobility (the inverse of viscosity); see Figure 6.3, top right.

As regards the recovery process, the model assumes that the amount of voluntary control on the next trial is the sum of three components: (i) a "memory" or "retention" term, a fraction of the current amount of voluntary control; (ii) a "learning" component, proportional to a "driving" signal, a function w(t) of movement performance that can be interpreted as a reward; and (iii) an assistance-related component, proportional to the magnitude of the

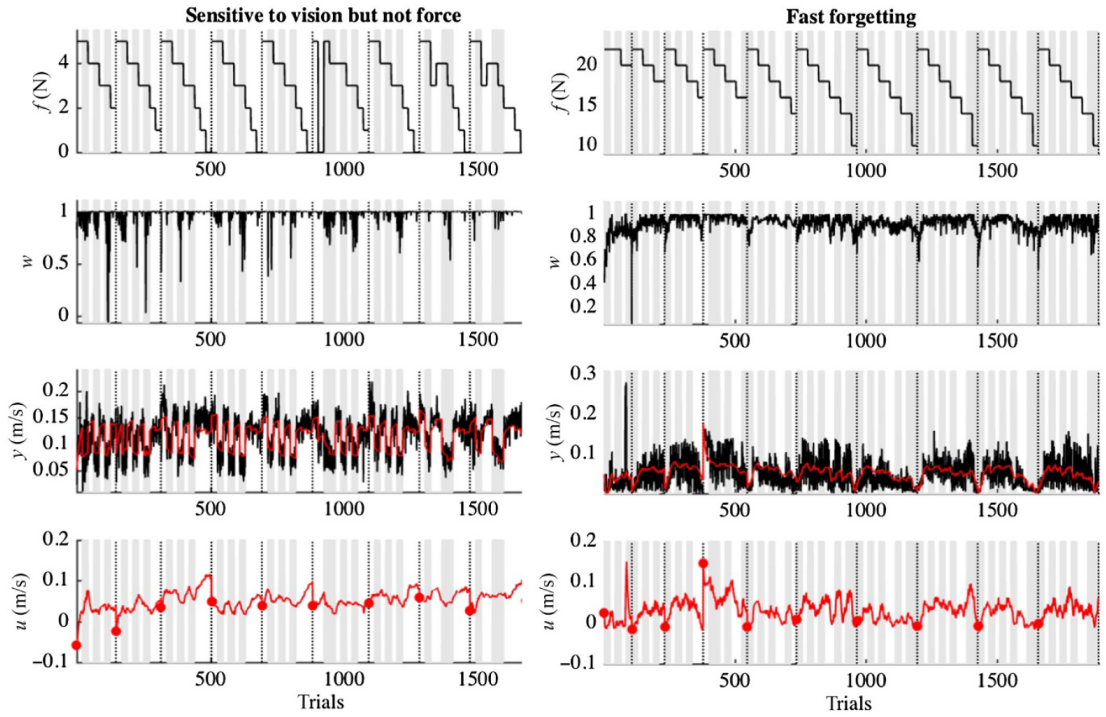

Figure 6.4 Fitting examples from the state-space model. Left: performance and model fitting in a subject who is a little sensitive to assistive force and is more sensitive to the presence/absence of arm vision (white and shaded areas). Right: performance and model fitting in a fast-forgetting (low retention) subject, who is unable to build up performance from trial to trial. Modified from Casadio and Sanguineti (2012).

assistive force:

$$u(t+1) = A \cdot u(t) + B \cdot w(t) - S \cdot x(t) \tag{6.18}$$

The three parameters denote, respectively, the retention rate A, the learning rate B, and the "slacking" rate S. Therefore, this model posits separate mechanisms for "retention" and for the effect of assistance, that is, the actual "slacking." These terms have often been used interchangeably; see Reinkensmeyer et al. (2009) for a review that specifically covers slacking models. The model was used to analyze the trial-by-trial time series of performance in nine chronic stroke survivors, who underwent a 10-session training protocol; see Figure 6.4, left.

As performance measure and driving signal, they took, respectively, the average speed and the fraction of amplitude covered by the first assisted submovement. The estimates of the model parameters for each subject suggested that recovery is determined by a complex interplay of memory (retention), performance, and slacking. One specific finding was that in severely impaired subjects, recovery is greater when the driving (reward) signal is greater;

hence, recovery improves when the performance - not the motor error - is greater. Another finding was that a greater assistive force has a negative impact on recovery (slacking). However, only a few subjects - the least impaired - exhibited a significant "slacking" effect. The single most important finding was that the retention rate (memory decay) parameter accurately predicts the long-term outcome of the rehabilitation trial (see Figure 6.3, bottom right). This finding is consistent with (Han et al., 2008): the hypothesis that recovery must reach a threshold in order to self-sustain implies a buildup mechanism that integrates the effect of repeated motor activities. High retention is an essential prerequisite of this mechanism. The mechanisms of recovery may differ in different subjects; see Figure 6.4.

Specifically, some subjects turned out to be little sensitive to assistive force, whereas their performance was much more affected by the presence or the absence of vision of the hand; see Figure 6.4 (left). Other subjects exhibited a large forgetting rate, so that the intertrial improvement in performance did not build up into a massive improvement; see Figure 6.4 (right). Intersubject differences call for an adaptive regulation of assistance, in which peculiarities of the individual subjects are to be taken into account. Again, this calls for an adaptive regulation of assistance, in which peculiarities of the individual subjects are to be taken into account.

6.2.7 Multirate and spatial generalization models of recovery

As noted in the introduction, neuromotor recovery results from the combination of various processes, each with their own timescale (Colombo et al., 2009; Massie et al., 2016). Models involving multiple recovery processes, with different time constants, like those used in sensorimotor adaptation, could capture these effects.

Neuromotor impairment is highly dependent on arm configuration and varies with movement direction (Huang and Patton, 2016). Likewise, the dynamics of recovery may be directiondependent, because the arm moving in different directions may exhibit a different sensitivity to assistance. These effects must be accounted for while analyzing the temporal evolution of the subjects' voluntary control in tasks that involve submovements in different directions. A way to do this is to use the same approaches used to account for spatial generalization in models of sensorimotor adaptation (see above).

6.2.8 System identification techniques

All the recovery models presented here take the form of state-space dynamic systems, either linear or nonlinear. Given reasonable values for the parameters, these models can be used to

simulate the dynamics of the recovery process. However, if suitable data are available, we can estimate the model parameters for a specific recovery process. The available data may include the following: (i) one or more measures of performance, these are the system outputs, denoted as $y(t)$; (ii) one or more external inputs or environmental states, for instance, the amount of robot assistance or measures of task difficulty or other task parameters, denoted as $x(t)$; and (iii) the reward $r(t)$ provided at the end of each movement. The "motor command" $u(t)$ that changes with exercise may be one of the performance variables or may not be directly observable - for instance, movement speed when no assistance is provided. In this case, it constitutes a "latent" model variable.

Most rehabilitation trials are organized into multiple training sessions. Each session is described by a specific time series. If we assume a stationary recovery process, the model parameters will be constant over sessions. Alternatively, model parameters may be separately identified within each session. The identification of parameters from data in state-space models can be formulated in Bayesian terms, as the maximization of a posterior probability or a model likelihood (Hidaka et al., 2012). If the state variables are not observable, model identification can be carried out through an expectation maximization (EM) algorithm, which alternates estimates of the state given the parameters (expectation or E-step) and estimates of the parameters given the state, through maximization of a quasilikelihood (maximization or M-step) (Cheng and Sabes, 2006; Ghahramani and Hinton, 1996). Alternative approaches involve prediction error methods (PEM) that rely on more general formulations, also suitable for nonlinear models (Ljung, 1998).

Not all models guarantee reliable identification of the model parameters. For instance, in a linear state-space model, stable parameter identification is problematic if the variance of the process (state) noise is large with respect to the variance of the sensory (output) noise (Cheng and Sabes, 2006). A number of software tools are available for the identification of state-space models. MATLAB's System Identification Toolbox uses PEM for identification of various classes of linear and nonlinear state-space models. An EM identification algorithm is available as supplementary material of (Cheng and Sabes, 2006). In many rehabilitation trials, robot assistance or task difficulty are adjusted to the actual subject's performance, on a trial-by-trial basis. In this case, recovery process and assistance control indeed constitute one single dynamic system. Identification must take both into account.

Finally, analytic tools are necessary to quantify the performance of one model, to compare multiple models, and in order to decide which one is best for our data. The variance accounted for (VAF) - or coefficient of determination (R^2) - is widely used. Comparing different models

may require to correct the performance measure to account for different numbers of model parameters - Akaike information criterion (AIC) is an example of these techniques.

6.3 Conclusion

A deeper understanding of the functional and physiological mechanisms underlying recovery would likely have a strong impact on neuromotor rehabilitation. Computational models may greatly contribute to this understanding (Huang and Krakauer, 2009; Reinkensmeyer et al., 2016). As a future development, adaptively estimated computational models of recovery might be incorporated into patient-specific interaction strategies with the robot. This would lead to more effective ways to maximize recovery, resembling a therapist who keeps an "internal model" of how the patient reacts to their manipulations and on this basis continuously adapts their actions.

Chapter 7

A computational model of recovery and spatial generalization during robot-assisted rehabilitation to predict outcome in patients after stroke [1]

7.1 Introduction

Stroke is a disabling disorder that in accordance with International Classification of Functioning, Disability and Health (ICF) framework, has a strong impact in terms of impairment, activity limitations and participation restriction (Langhorne et al., 2011). Stroke survivors often experience restriction in arm-hand and leg movements function and mobility, and will have to deal with important disabilities for the remainder of their life (Kwakkel et al., 2006). Specifically, they have difficulty in performing activities of daily living, a fact that severely affects their quality of life and independence (Kwakkel and Kollen, 2013). Robot-assisted rehabilitation, by delivering of high dosage, high intensity and task specific training protocols, has demonstrated to be effective for the recovery of motor function and reduction of impairment (Hsieh et al., 2012; Mehrholz et al., 2015).

The computational neurorehabilitation approach attempts to mathematically model the mechanisms underlying the rehabilitation process itself, in order to understand the recovery

[1] *Parts of the content of this chapter has been published as Sedda G., Franzosi R., Mazzone A., Sanguineti V., Colombo R. (2019) Robot Assisted Exercise: Modelling the Recovery Process to Personalise Therapy. In: Masia L., Micera S., Akay M., Pons J. (eds) Converging Clinical and Engineering Research on Neurorehabilitation III. ICNR 2018. Biosystems & Biorobotics, vol 21. Springer, Cham.*

of motor behavior mediated through restitution (i.e. the restoring of normal biological structures and functions) and compensation (i.e. the use of biological structures and functions different from those originally involved before the injury) (Reinkensmeyer et al., 2016). These models critically depend on detailed kinematic and kinetic data characterizing the motor performance and patients' outcome, that modern rehabilitation technologies, and particularly robot devices, make available (Balasubramanian et al., 2012). Thanks to the sensors included in these devices, the models take as input quantitative descriptions of sensorimotor activity achieved during therapy and try to describe through a mathematical procedure the mechanisms underlying recovery. They produce as outputs a number of quantitative variables that vary with the time and relate to patient's functional outcome. Their aim is mathematically to describe the so called "activity-dependent plasticity" i.e. the changes in the motor system that are caused by sensorimotor activity practiced during training (Krakauer, 2006). In addition, they allow to simulate the effect of variations of some rehabilitative parameters, thus allowing the design and implementation of potentially more effective experiments and training programs. In other words, they allow to speed-up the process of optimization of the rehabilitation programs. Furthermore, the optimization of therapy should allow implementation of training customized to individual subjects, in terms of dosage, scheduling, timing and type of task-specific exercise. Recent literature presents different example of computational neurorehabilitation models that can be broadly divided in two categories: a) prognostic regression models and b) theory-driven mechanistic dynamical models. The first category includes those models supporting clinical decision making for an early management of patients during rehabilitation (Kwakkel and Kollen, 2013; Nijland et al., 2010; Stinear, 2010; van Kordelaar et al., 2013). The second incorporates dynamical models of plasticity and learning mechanisms underlying recovery (Casadio and Sanguineti, 2012; Han et al., 2008; Hidaka et al., 2012; Jarrassé et al., 2012; Reinkensmeyer et al., 2012).

Generalization refers to the concept that training on one task can improve performance on other tasks that were not specifically object of training (Dipietro et al., 2009; French et al., 2016; Gandolfo et al., 1996; Shadmehr and Mussa-Ivaldi, 1994). Generalization is a key aspect of motor learning that computational models need to account for and the organization of practice may determine how much generalization occurs (Schmidt, 2003). Recently, Panarese et al. (2012) demonstrated that generalization of motor recovery can only be expected on movements falling within the workspace spanned by the movements executed during training. However, in view of optimizing the training process, further information regarding how to adapt the rehabilitation protocol to the individual directional patterns of impairment is lacking. In addition, much is known about various neurobiological processes

important to effective rehabilitation, however, the way these processes are integrated at different spatial and temporal scales is still unclear. Further, the early post-stroke period is interesting because is characterized by spontaneous biological recovery, but the interaction of this period with rehabilitation has not yet been well explored in terms of computational models.

In view of the potential offered by computational models, the aim of the present study was to verify if using a computational model, it is possible to predict the outcome of rehabilitation, in particular recovery and retaining, from motor performance during training. In addition, I assessed if spatial generalization of motor performance during training can provide information about mechanisms of motor recovery (see Sedda et al. (2018a,b)).

7.2 Materials and Methods

7.2.1 Subjects

Data were obtained through a retrospective analysis of 49 individuals after stroke, consecutively admitted for in-patient robot-assisted rehabilitation between September 2003 and November 2016 to the "Istituti Clinici Scientifici Maugeri", IRCCS, Rehabilitation Institutes of Veruno (NO). The study included patients admitted to a robotic rehabilitation program in both the subacute (cerebrovascular accident, CVA, occurred within 6 months) and chronic (CVA occurred after 6 months) phase.

The level of impairment and muscle spasticity of stroke patients was clinically evaluated through the upper-extremity portion of the Fugl-Meyer Scale (FM, score range = 0-66, see Fugl-Meyer (1980)) and the Modified Ashworth scale (MAS, see Bohannon and Smith (1987)), at the start (FM_{pre}), end (FM_{post}) of training and 3-month follow-up (FM_{fu}). Their functional status at the start and end of training was evaluated by the Functional Independence Measure scale (FIM) (Heinemann et al., 1993). Based on the initial FM score, I classified patients' impairment into severe (0-15) and moderate-mild (15-66), which resulted in two groups with similar size. Similarly, based on the improvement after the rehabilitation trial ($\Delta FM_{post} = FM_{post} - FM_{pre}$), I divided patients into weak ($\Delta FM_{post} < 6$) and strong ($\Delta FM_{post} >= 6$). Only 16 patients had the follow-up assessment of FM score. Before the start of the rehabilitation, most of participants presented a severe impairment (0-15), in particular chronic, see Figure 7.1. In the remaining participants the impairment was relatively mild. Following the rehabilitation, most patients exhibited an improvement in their conditions, corresponding to an increased FM score, i.e. they almost recovered the

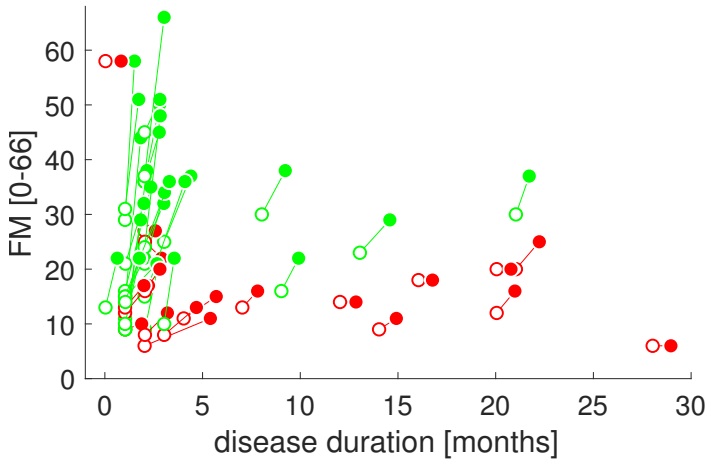

Figure 7.1 Disease duration vs patients' impairment. Patients are represented based on their Fugl Meyer scale (FM, 0-66), measured before (FM_{pre}, empty circles) and after (FM_{post}, filled circles) the robot training. Both slope and amplitude of segments make sense of patients' motor improvement: green segments indicate the patients with a clinically significant improvement ($\Delta FM > 5.25$, whereas red segments show the others.

motor performance they exhibited before stroke. Table 8.1 summarizes the participants' demographic and clinical data. The study conforms to the ethical standards laid down in the 1964 Declaration of Helsinki that protects research participants and was approved by the local scientific and ethics committees. Each participant signed a consent form conforming to these guidelines.

7.2.2 Experimental apparatus and protocol

Patients were seated in a chair in front of a 2-degree-of-freedom device, the robotic arm 'Braccio di Ferro" (BdF) (Casadio et al., 2006) (Celin s.r.l., Follo, SP, Italy) or the MEchatronic system for MOtor recovery after Stroke (MEMOS, in-house prototype) (Colombo et al., 2005), as shown in Figure 7.2. Each device was coupled with a computer monitor located above the robot work-space. Patients had their torso fastened to the back of the chair by a special restraint in order to limit movements. The patient's paretic limb was supported at the elbow by a low friction pad sliding along the surface of the robot work-space.

Patients had to make a sequence of point-to-point reaching movements in the horizontal plane; they were instructed to move the robot handle from the starting point to the end point following the straight line. At each time, only the next (current) target was made visible. The visual feedback of hand position was continuously displayed as a colored cursor (red circle) on the screen differently form the target (green circle). If the patient could not complete the

Table 7.1 Participants' demographic data and Fugl-Meyer assessment (FM).

	Demographic data				FM scale (0-66 range)		
ID	Sex	Age (years)	Impaired arm (L/R)	Time since acute event (month)	PRE	POST	FU
S1	M	56	L	1	14	44	65
S2	M	76	L	3	25	37	34
S3	M	69	L	2	27	27	33
S4	F	81	R	2	45	51	63
S5	F	46	L	21	20	25	–
S6	F	78	L	1	9	10	12
S7	M	62	L	2	21	34	45
S8	M	55	L	1	15	22	–
S9	M	86	R	1	16	35	–
S10	M	60	L	1	9	38	43
S11	M	85	L	2	25	22	–
S12	F	75	L	1	9	29	–
S13	M	72	L	2	37	66	66
S14	M	64	R	2	15	36	52
S15	M	44	L	28	6	6	–
S16	M	41	R	4	11	15	–
S17	M	56	R	3	8	13	18
S18	M	40	R	2	8	12	–
S19	F	52	R	8	30	38	40
S20	M	58	R	7	13	16	–
S21	M	82	L	–	9	17	–
S22	M	76	R	1	21	32	–
S23	M	73	R	3	10	22	–
S24	F	34	R	1	12	17	–
S25	F	75	R	1	10	22	–
S26	F	90	L	1	15	21	17
S27	F	86	R	2	24	48	–
S28	M	73	R	2	16	20	26
S29	M	71	R	1	15	36	61
S30	F	79	L	0	58	58	–
S31	M	52	L	13	23	29	–
S32	F	75	L	0	13	22	–
S33	M	60	L	1	13	17	–
S34	M	51	L	1	14	22	23
S35	F	60	R	1	31	51	61
S36	F	69	L	2	36	50	–
S37	F	42	R	14	9	11	–
S38	F	65	L	2	36	45	–
S39	M	45	L	20	12	16	–
S40	M	35	R	12	14	14	–
S41	F	55	R	2	24	32	–
S42	M	53	L	21	30	37	–
S43	M	51	R	2	6	11	–
S44	M	52	R	16	18	18	–
S45	F	29	R	1	29	58	–
S46	M	66	L	20	20	20	–
S47	M	72	L	2	9	22	–
S48	M	34	L	1	11	22	–
S49	M	43	L	9	16	22	–
		61.7 ±15.4		5.1 ±6.9	18.71 ±10.83	28.3 ±14.3	39.5 ±19.7

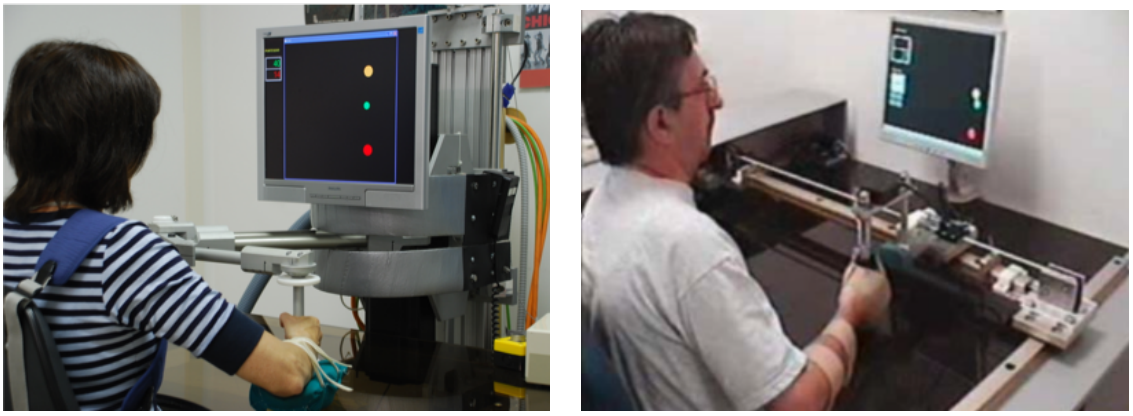

Figure 7.2 Experimental setup. Participants performed planar movements with the devices 'Braccio di Ferro" (BdF, left) (Casadio et al., 2006) or the MEchatronic system for MOtor recovery after Stroke (MEMOS, right) (Colombo et al., 2005) (in-house prototype).

movement by means of voluntary activity, the robot guided the patient's arm to the target position. Details of the administered motor tasks and procedures have been extensively reported elsewhere (Colombo et al., 2008, 2013).

The targets were arranged as the vertices of polygons. At the beginning of the rehabilitation process the targets were arranged according to a square path, hence resulting in four sub-movements, each in a different direction (0, 90, 180, 270 deg); see Figure 7.3 (left). The distance between the starting position and the target, i.e. the side of the square, was 150 mm. The center of the square was aligned with the shoulder of the patient and the position of the seat was adjusted in order to reach the farthest targets with an almost fully extended arm. An easy way to build a more difficult and more challenging task to perform is to add new secondary sub-movements in different directions (Cameirão et al., 2010). For this reason, if patients showed a significant motor improvement the therapist could decide to switch into a more complex diamond-shape path, involving 16 sub-movements with 8 different directions (0, 45, 90, 135, 180, 225, 270, 315 deg); see Figure 7.3 (right).

Patients underwent training twice a day and each training session consisted of 4 cycles of exercise lasting 5 min each, followed by a 3 min of resting period. All patients were treated 5 days a week for 3 weeks. In addition, on the same days as robot treatment, all patients underwent physical therapy performed by professional therapists according to the Italian Stroke Prevention and Educational Awareness Diffusion (SPREAD) guidelines, for 45 min/day.

When the patient completed the sub-movement without robot-assistance, i.e. by means of volitional control alone, the trial was considered successful. Otherwise, if during the task the

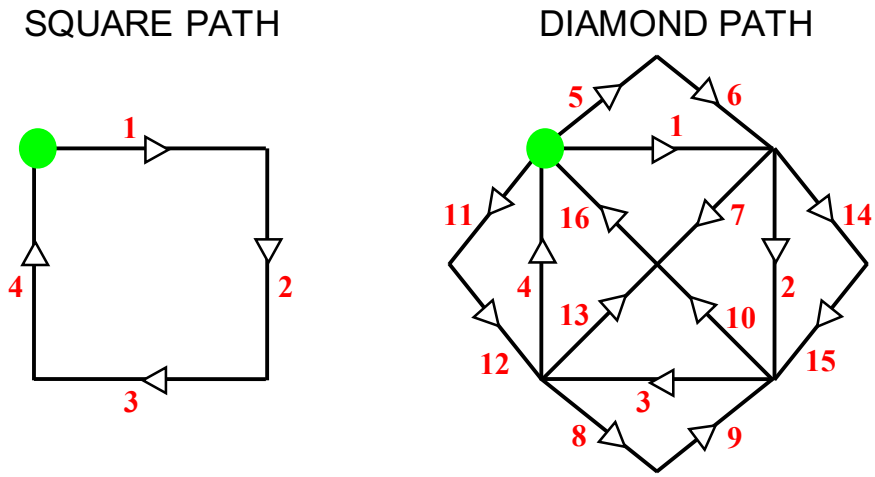

Figure 7.3 Point-to-point reaching tasks: patients had to perform a sequence point to point reaching movements in the horizontal plane; they had to move the robot handle from the starting position to the target. The target point was arranged as the vertices of the figure. The path to follow was initially a square (4 sub-movements, left). In case of significant motor improvement, the therapist could change the training into a more challenging one in which diamond-shaped path (16 sub-movements, right) has to be executed.

participant was unable to move the handle for a period of time greater than 3 s (failure), the robot guided patient's arm to the target position along a minimum path trajectory. At the end of each sub-movement (i.e. a trial), patients received a 0-10 score displayed on the screen; this score is calculated as the percentage of trajectory covered with an active movement within the time limit, this has been referred as the Active Movement Index (AMI) (Colombo et al., 2012; Panarese et al., 2012).

7.2.3 Computational Model

Motor adaptation is the process of tuning motor output to reduce the errors between planned and actual movements. During an adaptation trial, movements may differ in terms of starting position, amplitude, and/or direction. Several studies on motor adaptation have shown that motor learning generalizes: a movement in a given direction affects movements in nearby directions (Thoroughman and Shadmehr, 2000).

In stroke survivors, the degree of impairment is typically direction-dependent – movements in specific directions are more impaired than in others – but it is unclear if the recovery process exhibits spatial generalization phenomena similar to those occurring in sensorimotor

adaptation. To address this, I modelled the trial-by-trial dynamics of the recovery process through task-specific exercise, by accounting of how movement direction affects motor performance.

General model structure.

Following Panarese et al. (2012), I considered the AMI score as the performance or 'reward' measure $y(t)$ at the end of the t-th movement trial. In order to properly define the model of recovery for this rehabilitation trial, I assumed that voluntary control is determined by two factors: a memory component proportional to active movement and a recovery component proportional to an additional input, the driving signal $r(t)$. The dependence on these two factors is fully described by two scalar model parameters, the retention rate A and the recovery rate B:

$$x_i(t+1) = A_i \cdot x_i(t) + B_i \cdot r(t) \tag{7.1}$$

Equation (7.1) indicates that the predicted disturbance at the next trial is a combination of the current estimate and the 'adaptation' factor proportional to the 'driving' signal $r(t)$, which is the performance calculated during the previous trial. Parameter $0 < A < 1$ is the extent to which a given estimate is retained at the next trial, while B is the extent to which the estimated perturbation is sensitive to the reward, the driving signal of this model. Moreover, I assumed that during recovery the subjects independently improve the average speed ($v(t)$) of the end effector, the trajectory smoothness ($s(t)$), and the trajectory linearity ($l(t)$). Smoothness is measured as the Krebs parameter $s(t) = v(t)/V_{max}$ (speed metric, see Rohrer et al. (2002)). The model predicts that the smoothness parameter has an increasing trend and grows asymptotically towards positive values. Linearity is the path length normalized on projection of performed movement. I considered linearity, smoothness, and speed as three independent state variables of the recovery model, $x_l(t)$, $x_s(t)$ and $x_v(t)$, respectively. In conclusion, the recovery model is defined by speed, smoothness and linearity, whose evolution is driven by the reward, i.e. the previous t-th trial:

$$x_l(t+1) = A_l \cdot x_l(t) + B_l \cdot (x_L - x_s(t)) \cdot r(t) \tag{7.2}$$

$$x_s(t+1) = A_s \cdot x_s(t) + B_s \cdot (x_S - x_s(t)) \cdot r(t) \tag{7.3}$$

$$x_v(t+1) = A_v \cdot x_v(t) + B_v \cdot (x_V - x_v(t)) \cdot r(t) \tag{7.4}$$

where parameters A_l, A_s, A_v can be interpreted as the *retention rate* of linearity, smoothness and average speed, and B_l, B_s, B_v are the parameters linked to the *recovery rate*. Constant

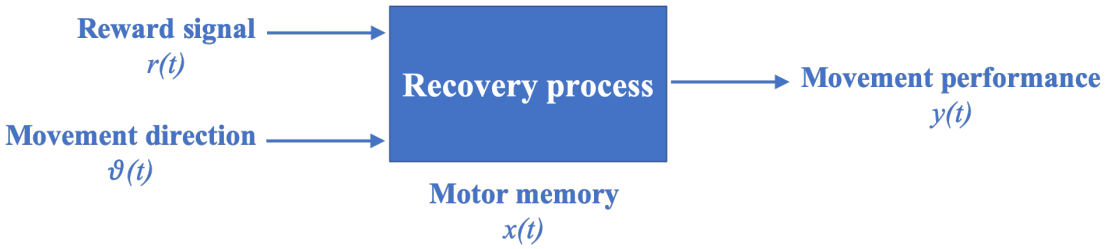

Figure 7.4 Computational model of stroke recovery process.

values x_L, x_S, x_V represent the maximum for each state variable: $x_L = 1$ (straight line), $x_S = 1$, $x_V = 150$ mm/s. The above equations assume that linearity, smoothness, and speed have different time constants - this is consistent with previous observations (Colombo et al., 2017). For insights on internal representations see Smith et al. (2006).

Spatial generalization.

Based on the previous equations, I developed a recovery model which takes into account the movement directions (spatial generalization), as summarized in Figure 7.4. During an exercise session, movements may have the same starting position and amplitude, but different directions. I assumed that for each movement direction θ_d ($d = 1, ..., D$) there is a different *motor memory* or motor command, $x_{l,d}$, $x_{s,d}$, $x_{v,d}$, for each state variable (linearity, smoothness, and speed). As in similar sensorimotor adaptation experiments, I modelled directional generalization by assuming that a movement in direction θ_d affects the motor memories in directions nearby, as shown in Figure 7.5. I considered that all the parameters involved in the recovery model may be direction-dependent. Arm compliance depends on directions (Smith, 2005). During all over the simulations, I considered $D = 4$ different motor memories, corresponding to $\theta_d = (0, 90, 180, 270$ deg).

To account for spatial generalization of recovery, I assumed that a movement in θ direction affects the motor memories in directions nearby. If the t-th movement is performed in direction $\theta(t)$, for all motor memories ($x_{l,d}$, $x_{s,d}$, $x_{v,d}$) and for each movement direction I can write:

$$x_d(t+1) = A(d) \cdot x_d(t) + B(d) \cdot (x_T - x_d(t)) \cdot r(t) \tag{7.5}$$

The recovery rate, B, reaches its maximum in the direction in which the movement is performed and gradually decays for the positions that are further away. For this reason, I

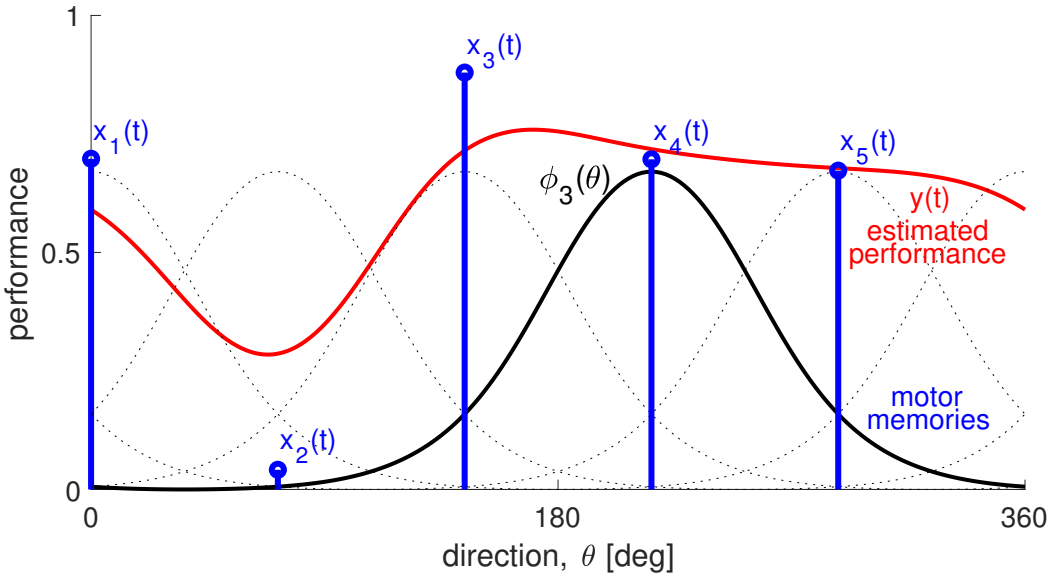

Figure 7.5 Performance (linearity, smoothness, and speed) of movements at a specific direction is determined by a generalization process which involves a combination of motor memories (in blue), each encoding motor capabilities at a given direction. The recovery process is described by the temporal evolution of such motor memories. The estimated performance $y(t)$ in the direction $\theta(t)$ is the red line. The black curves represent the directional selectivity, $\varphi_d(\theta)$, which is modelled as a Von Mises function.

assumed that recovery rate for the d-th motor memories is given by:

$$B(d,\theta) = B \cdot \varphi_d(\theta) \tag{7.6}$$

where $\varphi_d(\theta)$ is modelled as a normalized Von Mises function - the circular analogue of the Gaussian distribution (Bock, 2013) - defined so that $\phi(\theta_d) = 1$:

$$\varphi_d(\theta) = \frac{e^{k\cos(\theta-\theta_d)} - e^{-k}}{e^{k} - e^{-k}} \tag{7.7}$$

The function quantifies how much the current movement direction θ affects the d-th motor memory. The parameter k is a shape parameter known as 'concentration' (effectively equivalent to the standard deviation). When the k parameter is greater, the Von Mises's curve is more selective to the current direction of movement. The concentration parameter was kept fixed at $k = 6$, corresponding to a width of ± 90 deg in the function $\varphi_d(\theta)$. Parameter B indicates the maximum recovery rate that is achieved for $\theta = \theta_d$. If $B > 0$, training is always beneficial to motor memories, i.e. $B(d,\theta)$ is positive for all d. The retention rate, A, may exhibit a similar dependence on direction. However, A can never be zero value because it

would lead to a complete wash-out of the motor memory, see Eq. (7.5). Furthermore, sensorimotor adaptation experiments (Howard and Franklin, 2016) suggest an almost complete retention ($A \cong 1$) for movements whose directions are far from those of motor memory, whereas the retention rate is lowest corresponding to $\theta = \theta_d$. However, no information is available for recovery trials. I finally assumed that, given the state vector (motor memories), the performance (linearity or smoothness or speed) in direction θ is given by the reward $r(t)$ in the direction $\theta(t)$ and can be estimated from the motor memories as:

$$y(t) = \frac{\sum_d \varphi_d(\theta) x_d(t)}{\sum_d \varphi_d(\theta)} \tag{7.8}$$

This is the output equation of the recovery process, as represented in Figure 7.4. Based on previous observations that different aspects of performance exhibit different rates of the recovery (Howard and Franklin, 2016), I assumed that linearity, smoothness, and speed had different retention rates, A_l, A_s, A_v, and different recovery rates, B_l, B_s, B_v. Because of spatial generalization, the model is now non-linear in both states and output equations.

Model identification

For each of the 49 subjects who were able to complete the rehabilitation protocol (Panarese et al., 2012) previously described, I fitted the recovery model to the time series data. In particular, the model considered the reward $r(t)$ - i.e. the performance calculated during the previous trial - and the direction $\theta(t)$ as inputs, and the linearity, smoothness, and average speed ($y_l(t)$, $y_s(t)$, $y_v(t)$) as outputs. As reward $r(t)$ I took the AMI score and reflects the portion of movement that was actually performed by the patient's active movement. With the previous equations, I defined a non linear discrete-time state-space dynamical model in which the motor memories $x_l(t)$, $x_s(t)$, and $x_v(t)$ are independent state variables. I fitted the recovery model with four motor memories, $\theta_d = (0, 90, 180, 270\,\text{deg})$. Model parameters ($A_l$, A_s, A_v, B_l, B_s, B_v) were identified using a prediction error method (PEM). All estimations were carried out with MATLAB's System Identification Toolbox. Initial values of state variables at the beginning of each session were estimated from data. I treated the data from different sessions as separate experiments, but I assumed that the model parameters do not change during the whole multi-session treatment protocol. As a measure of fitting performance, I calculated the correlation coefficient, R, between the observed and predicted performance (separately for linearity, smoothness, and average speed), while its square, R^2, expressed in percent, can be interpreted as the fraction of variance accounted for (VAF) by the model.

Moreover, in order to identify model parameters best discriminating between weak and strong recovery, I used the Fisher's Linear Discriminant Analysis (LDA) on data, considering the following features: disease duration, severity, A_l, A_s, A_v, B_l, B_s, B_v.

Finally, I used the Naïve Bayes classifier to compare the model outcome prediction with diagnosis data (disease duration and impairment) and with the interaction between model predictions and diagnosis data. I trained a first classifier with model predictions, a second classifier with diagnosis data, and a third one with both. I compared classifier performances with their ROC curves and the related correct rate.

7.3 Results

7.3.1 Identification

I fitted the stroke recovery model to the performance time series of a total of 49 subjects. Each subject participated in a total of thirty (approximately) exercise sessions, each involving a minimum of four movements, i.e. in square path directions.

The model has a total of 6 parameters, 2 for linearity (A_l, B_l), 2 for smoothness (A_s, B_s), and 2 for average speed (A_v, B_v). The model is non-linear in parameters in both state and output equations. For each subject I fitted the recovery model to the time series of performance data (linearity, smoothness and speed).

The overall variance accounted for (VAF) was about 20 % for linearity, 22 % for smoothness, and 32 % for velocity, as shown in Figure 7.6 for all subjects. Consistent with previous studies (Casadio and Sanguineti, 2012), the model captures the main trends in the evolution of performance, but the average fitting (VAF range: 5%-70%) is more variable and lower than that observed in similar models of sensorimotor adaptation (70%-80%, see Donchin et al. (2003)). The estimated model parameters are summarized in Table 7.2.

7.3.2 Predicted versus observed time series

I used the stroke recovery model to evaluate the temporal evolution of the performance variables (linearity $l(t)$, smoothness $s(t)$, and speed $v(t)$) during the rehabilitation trial for all subjects. Figures 7.7, 7.8 summarize the time series of the observed performances (blue dots) and the model predictions (red dots) for two typical patients with different levels of improvement, poor ($\Delta FM \leq 6$) and strong (($\Delta FM > 6$)) respectively. The top panel depicts the reward time series, $r(t)$. It can be observed that for both subjects the model fitting follows qualitatively well the time course of the three performance indices.

Table 7.2 Summary of estimated model parameters.

ID	A_l	B_l $\cdot 10^{-2}$	R_l^2	A_s	B_s $\cdot 10^{-2}$	R_s^2	A_v	B_v $\cdot 10^{-2}$	R_v^2
S1	1.00	0.83	20	0.99	0.22	15	1.00	0.04	23
S2	1.00	1.92	59	0.87	38.6	30	1.00	0.33	52
S3	1.00	29.2	17	0.99	1.95	9	1.00	0.11	26
S4	1.00	100	14	0.99	0.21	23	0.99	0.008	20
S5	0.99	0.71	14	0.64	99.9	6	0.99	0.002	6
S6	1.00	0.03	15	0.99	0.18	12	0.99	0.001	36
S7	1.00	7.40	10	0.91	13.0	17	1.00	0.05	54
S8	1.99	12.16	8	0.99	0.26	7	0.99	0.06	35
S9	0.99	0.51	13	0.99	0.25	21	1.00	0.08	35
S10	1.00	0.24	5	0.99	0.24	14	1.00	0.09	41
S11	1.00	0.001	24	0.99	0.43	20	1.00	0.03	35
S12	1.00	97.66	4	0.99	0.22	14	1.00	0.19	32
S13	0.99	0.001	47	0.99	2.03	43	1.00	0.13	45
S14	0.99	0.001	47	0.99	0.17	62	1.00	0.10	63
S15	0.99	0.001	38	0.99	0.46	44	1.00	0.003	52
S16	0.99	0.001	48	0.99	0.22	51	1.00	0.08	53
S17	0.99	0.12	22	0.99	1.74	21	0.99	0.32	26
S18	0.99	0.41	23	0.99	1.32	18	0.99	0.09	28
S19	0.99	0.001	27	0.99	1.76	12	1.00	0.11	18
S20	0.99	0.001	25	0.99	0.74	20	1.00	0.05	29
S21	0.99	0.06	27	0.99	0.79	24	1.00	0.11	30
S22	0.99	0.28	59	0.99	0.06	51	1.00	0.01	41
S23	0.99	0.13	20	0.99	0.12	20	1.00	0.08	25
S24	0.99	0.02	22	0.99	0.09	32	1.00	0.04	28
S25	0.99	0.29	20	0.99	1.78	15	1.00	0.05	24
S26	0.99	0.17	20	0.99	0.51	18	1.00	0.02	35
S27	1.00	0.79	12	0.99	1.19	20	1.00	0.09	27
S28	0.99	0.001	14	0.99	0.23	20	1.00	0.08	15
S29	0.99	0.09	13	0.99	0.19	24	1.00	0.11	14
S30	1.00	0.001	12	0.99	0.13	10	1.00	0.04	13
S31	1.00	12.3	23	0.99	2.13	30	1.00	0.12	33
S32	1.00	0.001	28	0.99	0.21	29	1.00	0.01	32
S33	1.00	0.38	17	0.99	0.15	15	1.00	0.04	26
S34	1.00	44.6	7	0.99	0.23	14	1.00	0.05	15
S35	1.00	93.1	11	0.99	0.35	12	1.00	0.07	24
S36	1.00	51.3	9	0.99	0.78	5	1.00	0.03	30
S37	1.00	77.6	7	0.98	3.93	8	1.00	0.04	30
S38	0.99	0.09	14	0.99	0.10	22	1.00	0.07	27
S39	1.00	100	14	0.99	0.11	10	1.00	0.05	30
S40	1.00	0.03	14	0.99	0.48	29	1.00	0.10	42
S41	1.00	63.2	7	0.99	0.06	11	1.00	0.003	38
S42	1.00	0.001	10	0.99	0.22	17	1.00	0.001	42
S43	1.00	89.2	8	0.99	0.81	6	1.00	0.07	28
S44	1.00	39.3	11	0.81	35.4	6	1.00	0.03	36
S45	1.00	99	8	0.94	10.6	7	1.00	0.06	34
S46	0.99	0.001	40	0.99	2.03	39	0.99	0.05	58
S47	1.00	1.32	22	0.99	0.32	43	1.00	0.21	20
S48	1.00	0.001	18	0.99	0.19	46	1.00	0.10	23
S49	1.00	0.78	16	0.99	0.65	34	0.99	0.10	19

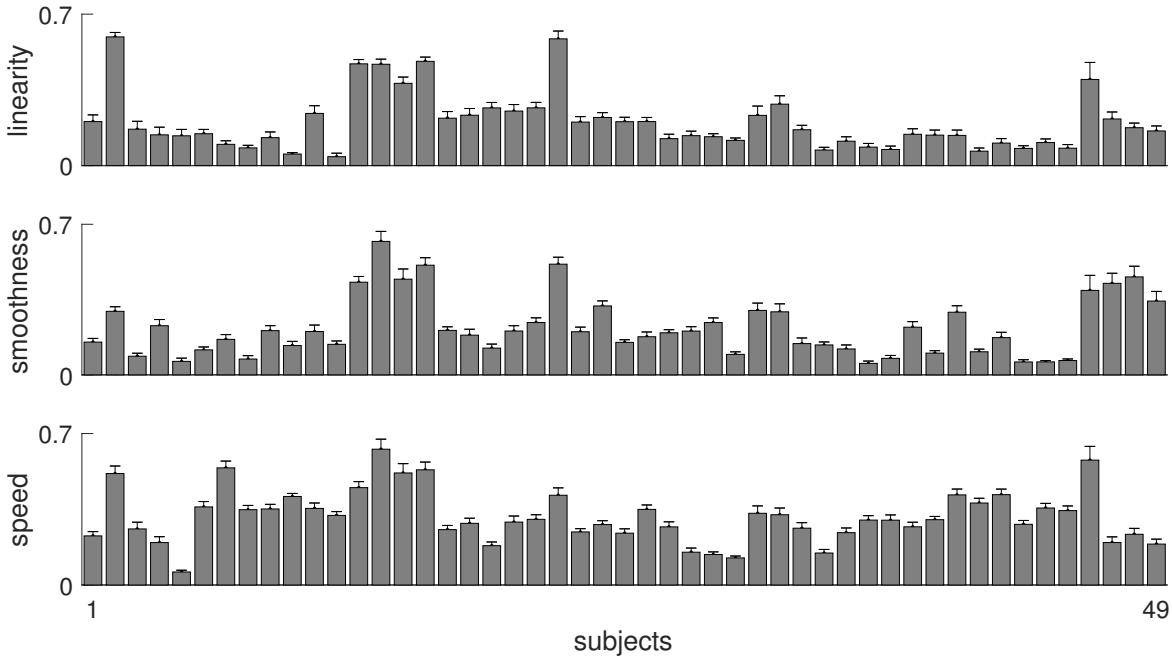

Figure 7.6 Summary of model fitting performance for all subjects: R^2, expressed in percent, is the fraction of variance accounted for (VAF) by the model. Black error bars represent the standard error of data.

7.3.3 Spatial generalization

Figures 7.9, 7.11 show the time series of the four motor memories for the same subjects. Motor memories are represented with respect to the days of the treatment sessions and with different colors ($\theta_d = 0$ deg in red, $\theta_d = 90$ deg in green, $\theta_d = 180$ deg in blue, and $\theta_d = 270$ deg in cyan). It can be observed that the discontinuities in the performance levels are mainly due to the uneven distribution of the treatments and occur when sessions are several days apart. Figures 7.10, 7.12 display the observed performances (linearity, smoothness and average speed - blue dots) and the related motor memories (pink dots) of both the first session (top line) and the last session (bottom line) of the treatment on a Cartesian plane, based on the direction of the performed movement. The filled circles with different colors show the directions of the motor memories $\theta_d = (0, 90, 180, 270$ deg), whereas the red curve represents the function $\varphi(\theta - \theta_d)$. It can be observed that the level of spatial generalization, i.e. both the width and shape of the function $\varphi(\theta - \theta_d)$, does not change from before to after training for the subject with poor recovery (see Figure 7.10), whereas the width of the curve increases and its shape becomes more regular from before to after training for the subject with strong recovery (see Figure 7.12).

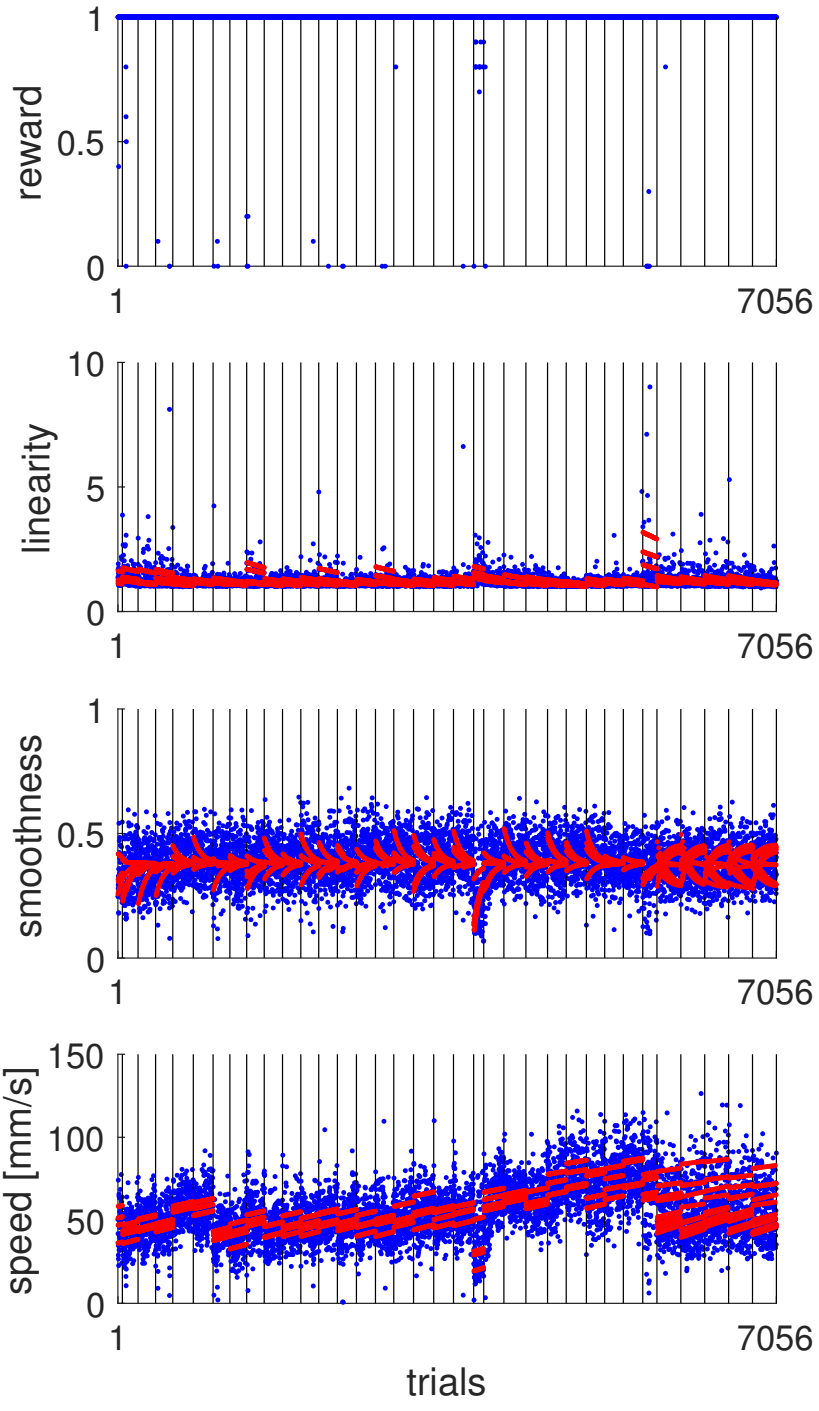

Figure 7.7 Model fitting of a subject with poor recovery ($FM_{pre} = 25$, $\Delta FM = -3$). Blue dots show single-trial performance, whereas red dots represent model predictions. Vertical black lines separate data from different session.

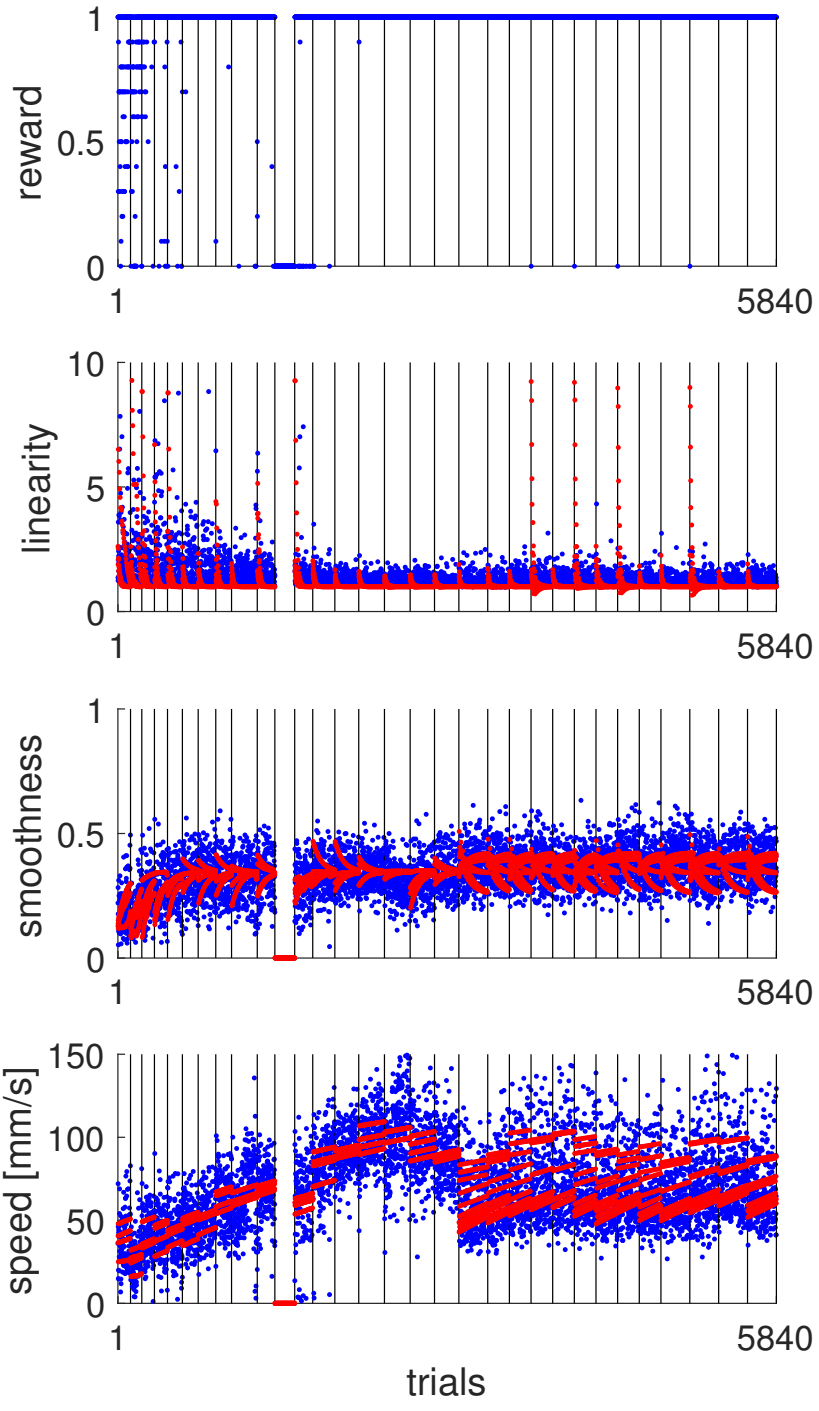

Figure 7.8 Model fitting of a subject with strong recovery ($FM_{pre} = 14$, $\Delta FM = 30$). Blue dots show single-trial performance, whereas red dots represent model predictions. Vertical black lines separate data from different session.

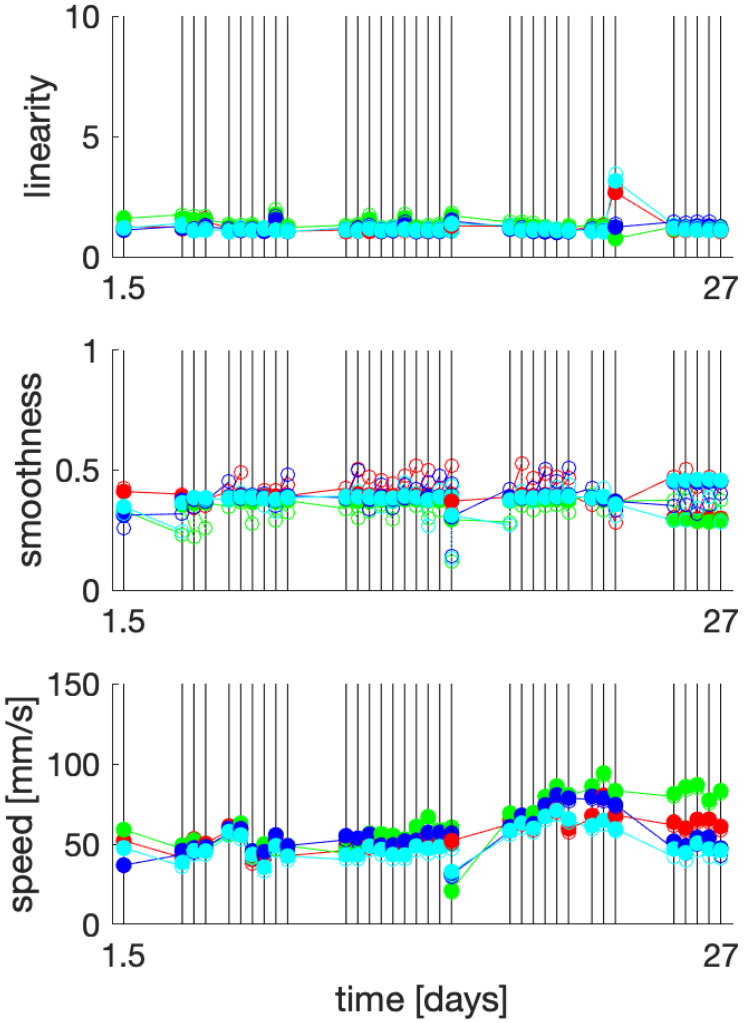

Figure 7.9 Time series of motor memories of a subject with poor recovery ($FM_{pre} = 25$, $\Delta FM = -3$). Motor memories in different directions are represented with various colors ($\theta_d = 0$ deg in red, $\theta_d = 90$ deg in green, $\theta_d = 180$ deg in blue, and $\theta_d = 270$ deg in cyan).

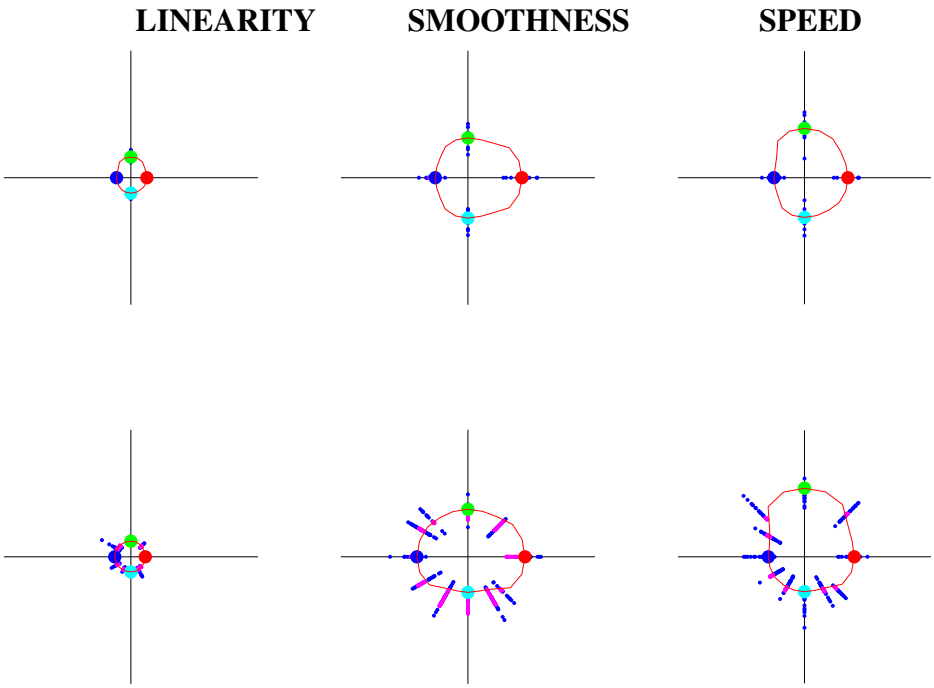

Figure 7.10 Spatial generalization of a subject with poor recovery ($FM_{pre} = 25$, $\Delta FM = -3$). The observed performances (blue dots) and the related motor memories (pink dots) of both the first session (top line) and the last session (bottom line) of the treatment are represented on a Cartesian plane based on the direction of the performed movement. Both axes of each graph have the same scale: 0-10 for linearity, 0-1 for smoothness, and 0-150 mm/s for speed. The filled circles with different colors show the directions of the motor memories ($\theta_d = 0$ deg in red, $\theta_d = 90$ deg in green, $\theta_d = 180$ deg in blue, and $\theta_d = 270$ deg in cyan), whereas the red curve represents the function $\varphi_d(\theta)$.

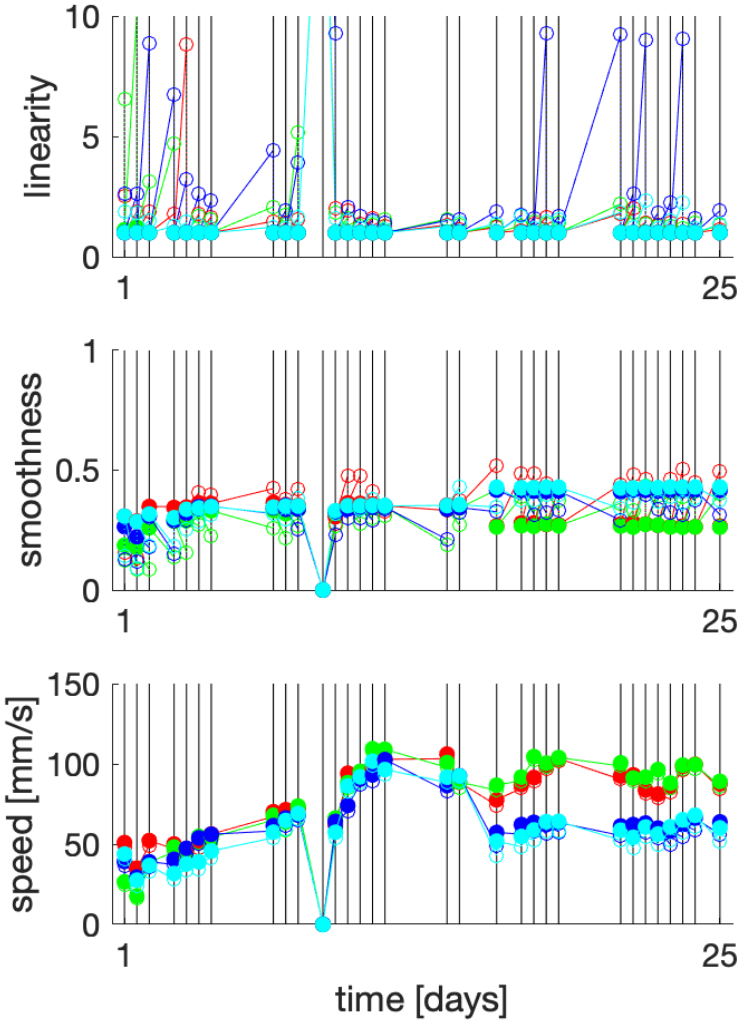

Figure 7.11 Time series of motor memories of a subject with strong recovery ($FM_{pre} = 14$, $\Delta FM = 30$). Motor memories in different directions are represented with various colors ($\theta_d = 0$ deg in red, $\theta_d = 90$ deg in green, $\theta_d = 180$ deg in blue, and $\theta_d = 270$ deg in cyan).

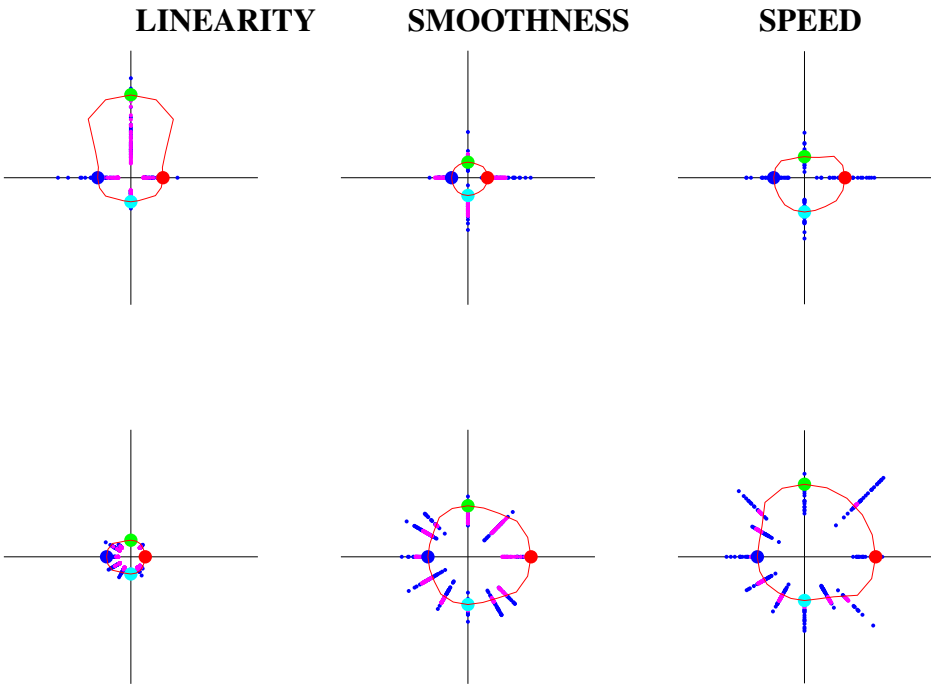

Figure 7.12 Spatial generalization of a subject with strong recovery ($FM_{pre} = 14$, $\Delta FM = 30$). The observed performances (blue dots) and the related motor memories (pink dots) of both the first session (top line) and the last session (bottom line) of the treatment are represented on a Cartesian plane based on the direction of the performed movement. Both axes of each graph have the same scale: 0-10 for linearity, 0-1 for smoothness, and 0-150 mm/s for speed. The filled circles with different colors show the directions of the motor memories ($\theta_d = 0$ deg in red, $\theta_d = 90$ deg in green, $\theta_d = 180$ deg in blue, and $\theta_d = 270$ deg in cyan), whereas the red curve represents the function $\varphi_d(\theta)$.

7.3.4 Model parameters best discriminating recovery

In order to identify the model parameters which best discriminate between weak and strong recovery, I used the Fisher's Linear Discriminant Analysis (LDA). My hypothesis was that within-session dynamics is able to predict recovery outcome. Figure 7.13 shows the results of the analysis: the most important parameters to evaluate recovery are disease duration, linearity recovery rate (B_l), smoothness retention rate (A_s) and recovery rate (B_s). This means that for this model the 'strong' recovery is determined by fast dynamics of trajectory curvature and slow dynamics of trajectory smoothness. These results are confirmed by statistical analysis. I calculated the average values of model parameters $B_l, B_s, B_v, A_l, A_s, A_v$ over all subjects with weak and strong improvement. Figure 7.14 show that a significant difference is found only in the average values of model parameters B_l (P = 0.03), B_s (P = 0.045), and A_s (P = 0.033).

To further relate these observations to the dynamics of recovery, we focused on the recovery model of Eqs. 7.2, 7.3, 7.4. In case the movement is directed along one motor memory direction and the reward is maximum ($r(t) = 1$), the equation becomes:

$$x_d(t+1) = A(d) \cdot x_d(t) + B(d) \cdot (x_T - x_d(t)) \tag{7.9}$$

which can be rewritten as:

$$x_d(t+1) = (A(d) - B(d)) \cdot x_d(t) + B(d) \cdot x_T \tag{7.10}$$

This suggests that in case of close-to-optimal performance the recovery time constant is determined by $(A-B)$ - greater $(A-B)$, faster recovery. We then calculated $A-B$ (recovery time constant) for all three indicators and both subjects groups. Figure 7.15 show that a significant difference is found in the average values of the time constant of both linearity $A_l - B_l$ (P = 0.03) and smoothness $A_s - B_s$ (P = 0.041).

7.3.5 Model improves outcome prediction

I trained three Naïve Bayes classifiers to compare the model outcome prediction with diagnosis data (disease duration and impairment) and with the interaction between model predictions and diagnosis data. I calculated the ROC curve and the related correct rate for each classifier, as shown in Figure 7.16: 67% of correct rate for the model alone ('model'), 71% for the diagnosis data ('diagnosis'), and 75% for the interaction of the model with diagnosis data ('diagnosis + model').

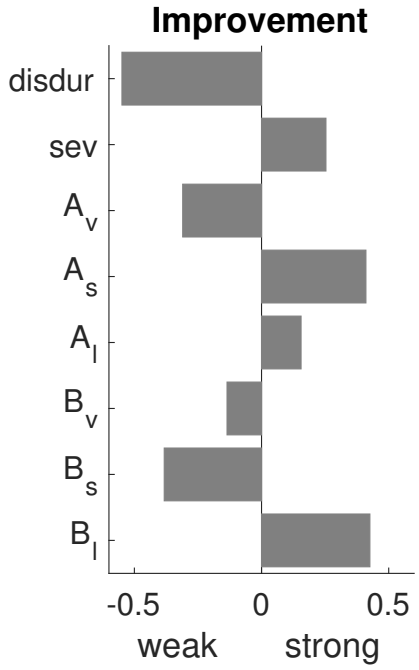

Figure 7.13 LDA technique identifies the model parameters which best discriminate between weak and strong recovery: B_l, B_s, A_s. The following parameters were considered for the analysis: disease duration (*disdur*), severity (*sev*), A_l, A_s, A_v, B_l, B_s, B_v.

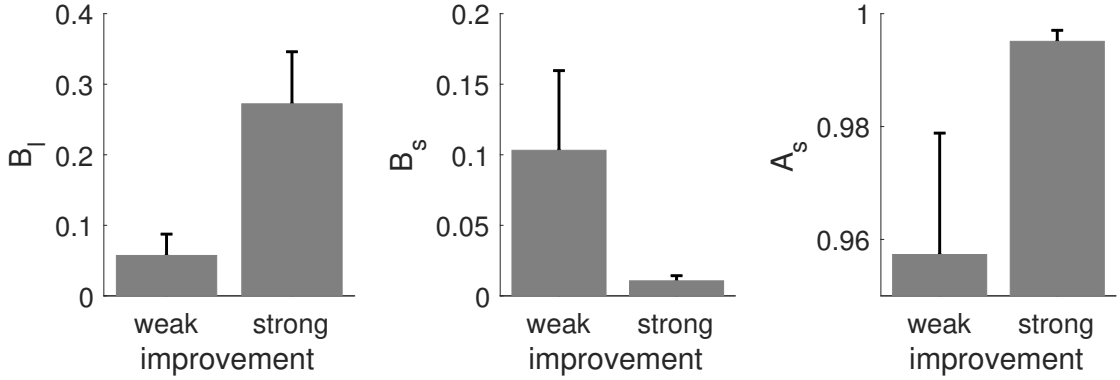

Figure 7.14 Some model parameters differ significantly in subjects with weak vs strong recovery: B_l (P = 0.03), B_s (P = 0.045), and A_s (P = 0.033).

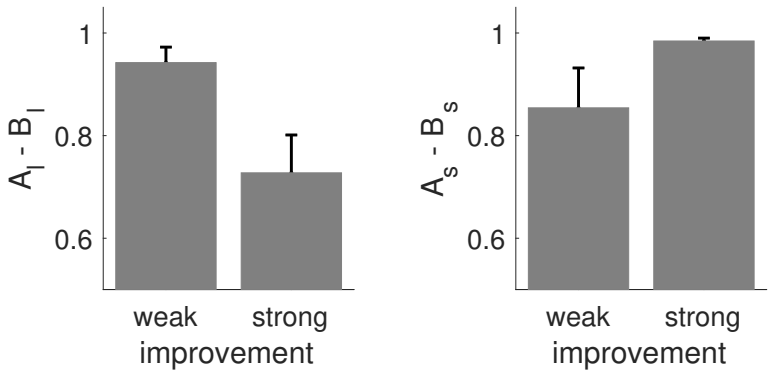

Figure 7.15 The average values of time constant of both linearity $A_l - B_l$ (P = 0.03) and smoothness $A_s - B_s$ (P = 0.041).

These results suggest that the recovery dynamics during training provides additional information with respect to diagnostic data (disease duration and initial impairment) which improves the prediction of the recovery outcome

7.4 Discussion

Robot assisted-rehabilitation facilitates the recovery of motor functions thanks to high intensity and repetitive exercises. It can allow to explore all the directions but focuses more on directions mainly impaired. I developed and tested a model of recovery which suggests how to adapt the rehabilitation protocol to the individual directional patterns of impairment. This model of recovery explicitly focuses on spatial generalization, i.e. the ability of exercises on a specific direction to promote recovery in those directions mostly impaired.

7.4.1 Model fitting captures the evolution of training performance

The model correctly reproduces the observed time series of performance within and across rehabilitation sessions. As previous studies suggest (Colombo et al., 2007; Krebs et al., 1998), some movement features such as smoothness and linearity improved more quickly than parameters that relate to the fine-tuning of movement, like velocity. First, subjects explore the work-space and try to reach the target with their residual abilities, then they try to optimize the movement to make it more efficient. The recovery model agrees with these previous studies, in fact it predicts that velocity recovers more slowly, but exhibits a greater spatial generalization in comparison to smoothness and linearity, see Figures 7.10, 7.12. This suggests that smoothness and linearity may depend on compensatory processes - e.g.

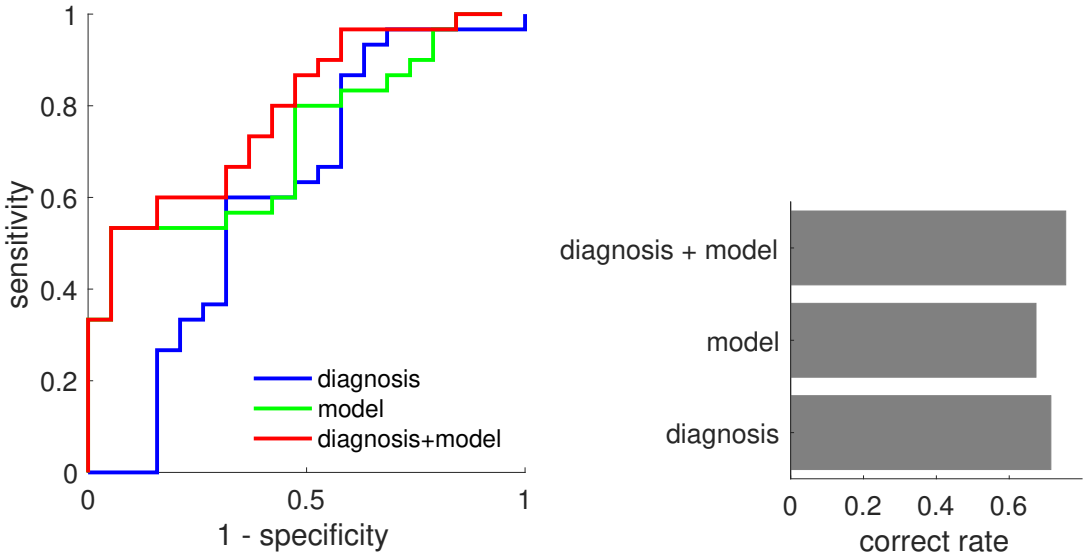

Figure 7.16 Naïve Bayes classifier to compare the model outcome prediction with diagnosis data (disease duration and impairment) and with the interaction between model predictions and diagnosis data. Classifier performances are compared with ROC curves and the related correct rate.

visual correction - which are more movement-specific and are less related to the actual ('true') recovery. Model fitting captures the evolution of performance, but the average fitting performance is more variable and lower than that observed in similar models of sensorimotor adaptation (see Donchin et al. (2003)), as shown in Figure 7.6. This may be due to a variety of factors. First, neuromotor recovery is fundamentally different from sensorimotor adaptation. In sensorimotor adaptation the development of an internal model of unfamiliar dynamics is a relatively fast process, largely based on implicit mechanisms. In contrast, the recovery process underlying robot-assisted rehabilitation is more like motor skill learning [36]–[38]. As such, the process of selection of future actions has an inherent exploratory component—an aspect that this model does not explicitly account for. Second, neuromotor recovery is likely to be influenced by factors that are not related to movement performance, e.g., attention and motivation. Again, these factors are not explicitly considered in the present model.

7.4.2 Models of recovery reveal different recovery mechanisms

Looking at the within-session dynamics (see Figures 7.13, 7.14), model suggests that 'strong' recovery is determined by the fast dynamics of trajectory curvature and the slow dynamics of trajectory smoothness. This means that subjects quickly learn to make straight

line movements (low retention of curvature) and maintain steady ability to make smooth movements (greater retention of smoothness), as shown in Figure 7.15.

Subjects exhibiting a stronger recovery tend to quickly regain movement smoothness whereas they are slower at recovering straighter paths. Greater smoothness is an indicator of predominantly feedforward control and less use of feedback (visual) corrections. The finding suggests that subjects use two strategies to improve motor performance during training: 1) some subjects focus on feedforward control. In these subjects, movements quickly become smoother, possibly at the expense of accuracy (hence a slower improvement in path linearity). 2) other subjects focus on feedback corrections. They more quickly improve path linearity, at the expense of smoothness. Our findings suggest that feedforward strategy results in stronger rehabilitation outcome and greater transfer to other tasks.

7.4.3 Models of recovery improve the prediction of the recovery outcome

Results displayed in Figure 7.16 suggest that model parameters provide better prediction of outcome with respect to impairment and disease duration alone. In particular they provide complementary information which cannot be derived from disease duration and impairment.

A model of recovery may contribute to personalization of therapy in a number of ways. First, as performance within a rehabilitation session predicts the recovery outcome and its retention, few exercise sessions may allow to predict individual subjects' recovery potential. Further, characterization of the directional patterns of impairment and spatial generalization of recovery may suggest personalized exercise schedules. Also, a recovery model may be incorporated into an adaptive controller of robot assistance and/or task difficulty aimed at optimizing recovery. This approach can easily adapt to different exercise scenarios (task, robot type). Finally, using data from different devices (e.g. hand, arm, gait), this method can be used to study interplay between different aspects of recovery.

Chapter 8

Computational rehabilitation of neglect: using state-space models to understand the recovery mechanisms [1]

8.1 Introduction

Unilateral spatial neglect (USN) is described as a 'failure to report, orient toward, or respond to stimuli in contralesional space, which cannot be attributed to primary motor or sensory dysfunction' (Heilman and Valenstein, 1979). This heterogeneous and common syndrome is most often observed after stroke.

Severe and enduring neglect is far more likely associated with right hemisphere damage – up to 2/3 of right hemisphere stroke patients have neglect symptoms acutely.

Many different deficits contribute to the syndrome, in variable proportions among different subjects, presumably depending on location and extent of brain damage. An inability to direct attention to the left hemispace is considered as one of the main symptoms. It is debatable whether neglect may result from an impaired representation of space (Karnath, 1997), which can be in multiple frames of reference (for example, retinotopic, head centred, trunk centred) or be specific to near or far space. Other investigators have argued that neglect may also reflect a directional motor impairment, with patients experiencing difficulty in initiating or programming contralesional eye or limb movements (Bisiach et al., 1990).

[1] *Parts of the content of this chapter has been published as Sedda, G., Ottonello, M., Fiabane, E., Pistarini, C., Sedda, A., and Sanguineti, V. (2017). Computational rehabilitation of neglect: Using state-space models to understand the recovery mechanisms. In 2017 International Conference on Rehabilitation Robotics (ICORR), pages 187–192. IEEE.*

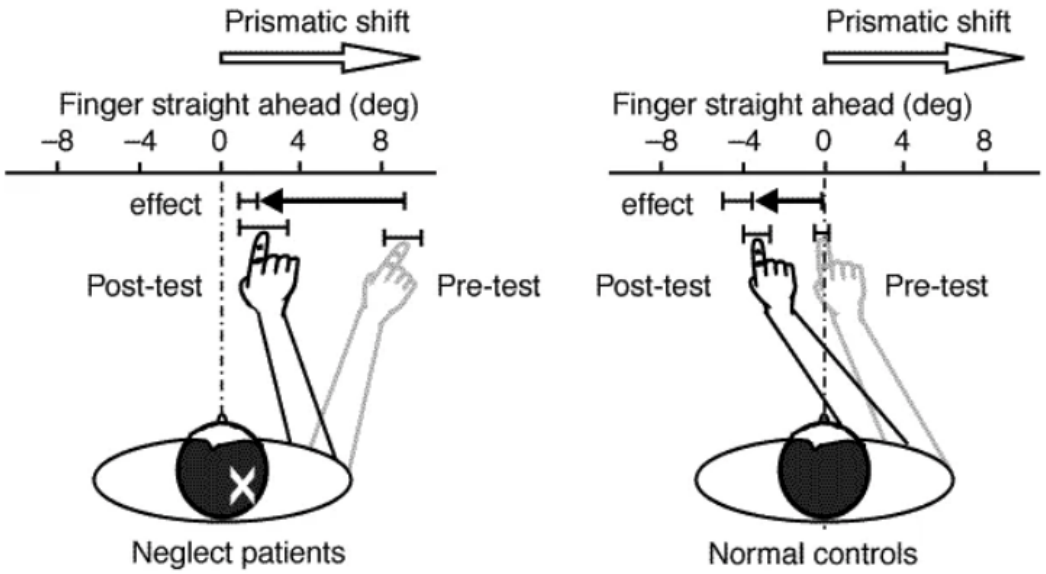

Figure 8.1 Two groups of blindfolded participants (neglect patients vs normal control) were required to point straight ahead while their head was kept aligned with their body's sagittal axis. Ten pointing trials were run in the pre-test (without prismatic goggles, 10 deg of deviation) and in the post-test (immediately upon removal of prisms; white arrow). Results show that the midline demonstrations made by the neglect group were initially shifted to the right, whereas control subjects pointed to their actual straight ahead. Patients were thus more affected by the adaptation than controls (black arrows), and the magnitude of this effect was less variable in the patients (arrow extensions). From Rossetti et al. (1998).

Early attempts to treat neglect were based on 'top-down' approaches, relying on patients' awareness, and aimed at deliberately modifying their behaviour, for instance by encouraging patients to direct their gaze towards the contra-lesional space (Pizzamiglio et al., 1992). These paradigms were somehow successful in reducing neglect within the task used for training, but failed to generalise to tasks outside of the training environment. 'Bottom-up' strategies aim at producing an automatic change in behaviour, or recalibration of the recruited sensorimotor mechanisms. In some cases improvements in performance induced by 'bottom-up' approaches have been shown to generalise to tasks that were not used in training. This is the case of caloric and vestibular stimulation, contralesional limb activation, trunk rotation, vibration or electrical stimulation of neck muscles, and prism adaptation (Lisa et al., 2013).

Rossetti et al. (1998) examined the effects of adaptation to a prism-induced rightward horizontal displacement of the visual field in neglect patients; see Figure 8.1. Immediately after adaptation, neglect improved in all clinical tests, as shown in Figure 8.2. The improvement persisted well beyond the wash-out of the adaptation effect (Frassinetti et al., 2002).

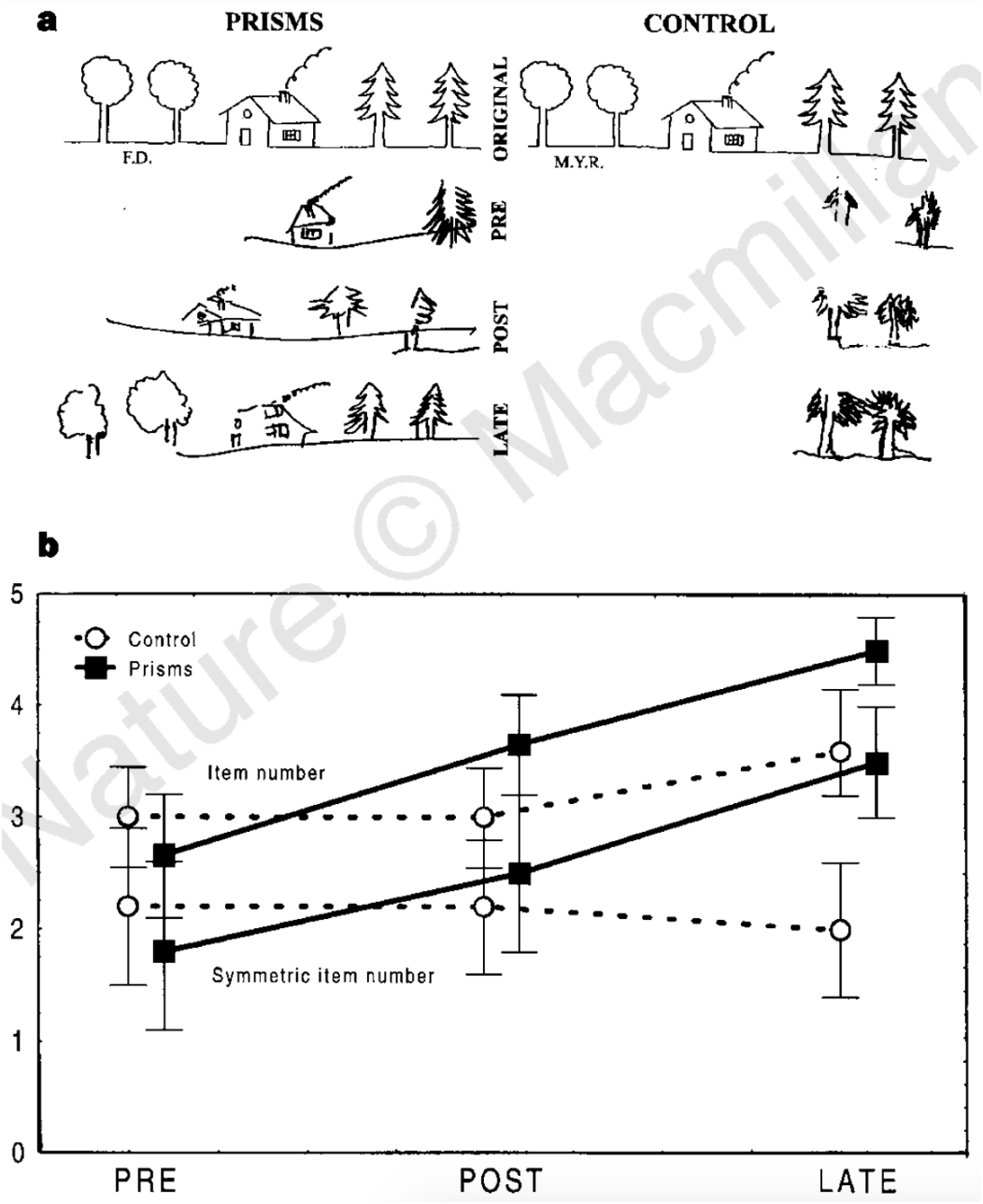

Figure 8.2 (a) Gainotti test, in which the patient is required to copy a drawing made of five items. A representative example of neglect from patient F.D. (left), who completely ignores three items in the drawing made before prism exposure (pre-test). On prism removal (post test) one item is added, and after 2 h (late test) all items are drawn. On the contrary, control patient M.Y.R (right) was exposed to neutral goggles and did not improve. (b) The average number of items drawn (reflecting space-based hemineglect) and the average of numbers drawn symmetrically (reflecting object-based hemineglect) in the two groups (prisms and control). The two scores are improved in the same way in the 'prisms' group. From Rossetti et al. (1998).

The mechanisms of action of prism adaptation are not yet clearly understood, but the effect does not seem to be a mere consequence of the leftward motor bias developed by the right arm during prism adaptation. Rather, prism adaptation is believed to affect higher level spatial representations (Frassinetti et al., 2002; Rossetti et al., 1998). Strategies based on virtual reality (VR) have been developed for USN assessment and rehabilitation (Pedroli et al., 2015). VR approaches may provide ecological and realistic types of interaction, involving the participation in functional activities that are otherwise unsafe to perform in real life.

Current approaches generally focus on remapping of space, which is strongly connected to updating of the body schema representation and multisensory integration (Borghese et al., 2013). Recently, robots have received attention for rehabilitation of neglect (Choi et al., 2016). Robot-assisted limb activation exercise (movements of the left limb within the left hemispace) was observed to produce benefits to neglect that were similar to those obtained with conventional treatment.

Computational models have been successfully applied to the study of motor learning and adaptation (Cheng and Sabes, 2006), providing important insights with respect how brain controls movement and reacts to the environment or task variables changes. Only recently these approaches have been applied to the rehabilitation field. Casadio and Sanguineti (2012) used a linear dynamical model to describe the trial-by-trial evolution of the motor performance of chronic stroke survivors who underwent a rehabilitation protocol based on a robot-assisted arm extension task. These early attempts may potentially lead to a deeper understanding of the mechanisms underlying neuromotor recovery (Reinkensmeyer et al., 2016; Ueyama, 2017).

In the case of neglect, Leigh et al. (2015) proposed a computational model which involved a realistic description of the lesions in the cortical parietal areas. Their main assumption was that prism adaptation primarily influences dorsal stream structures that mediate visual guidance of actions and is typically spared in neglect (Mort et al., 2003). The model reproduced a few symptoms of neglect, like line bisection behaviour and the beneficial effect of prism adaptation. However, model predictions are qualitative predictions and cannot be used to explain individual behaviours.

Here I apply the dynamical systems framework to model the trial-by-trial dynamics of training-induced recovery from neglect. I describe the model and show its predictions in the context of prism adaptation. I also apply the model to the study of the recovery dynamics in the context of a newly designed training protocol, based on reaching movements within an adaptive environment enriched with distractors and audio-visual cues (see Sedda et al. (2017, 2018b)).

8.2 Materials and Methods

8.2.1 Computational Model

Spatial attention and neglect

Visual spatial attention is the ability to direct attention to a specific location in space. Objects at this location will be processed faster and more accurately than events at other locations. Persons with neglect are often impaired in reporting spatial targets in the left hemispace and driving their own hand toward that target, in a way which cannot be explained by impaired movement alone. Leigh et al. (2015) assumed that visual target and hand position are encoded in the parietal cortex by a population of neurons, each with a 'preferred' target or hand position and a bell-shaped tuning curve. The left hemisphere only encodes contralateral (right) target positions, whereas the right hemisphere encodes for targets in both hemispaces (Heilman and Van Den Abell, 1980). These authors suggest that such a representational asymmetry may explain why neglect symptoms are more severe when damages are located in the right hemisphere. In my simulation I used 4800 neurons, 2400 for the right hemisphere and 2400 for the left hemisphere; see a representation in Figure 8.3. Each neuron was assumed to encode a preferred location respectively in the right hemispace (left hemisphere neurons), and in both hemispace (right hemisphere neurons). Assuming a uniform distribution of the preferred positions of these neurons, I simulated a lesion by destroying 90% of the neurons in the right hemisphere. A consequence of the lesion would be a less reliable representation of target and/or hand positions located in the left hemispace, as shown in Figure 8.4 (left).

In my model, I denote $x_T(t)$ and $x(t)$ as, respectively, target position and hand position in a person-centered coordinate frame at the end of the t-th movement trial. I also define $y_T(t)$ and $y(t)$ as the visually perceived target and hand position in retinotopic coordinates. I also assume that these visual stimuli are represented in the parietal cortex as $z_T(t)$ and $z(t)$, respectively. I model the right-hemisphere lesion as a multiplicative term $b(t)$, which leads to a distorted representation of stimuli located in the left visual hemispace:

$$z_T(t) = \begin{cases} y_T(t), & \text{if } y_T(t) >= 0, \\ \frac{b(t)}{H} y_T(t), & \text{if } y_T(t) < 0. \end{cases} \tag{8.1}$$

where H denotes the boundary of the visual hemispace. I assume the same value on both the right and the left side (Redding and Wallace, 2006). The targets are located within either the right ($y_T(t) > 0$) or left hemispace ($y_T(t) < 0$). When $b(t) = H$ there is no neglect, whereas

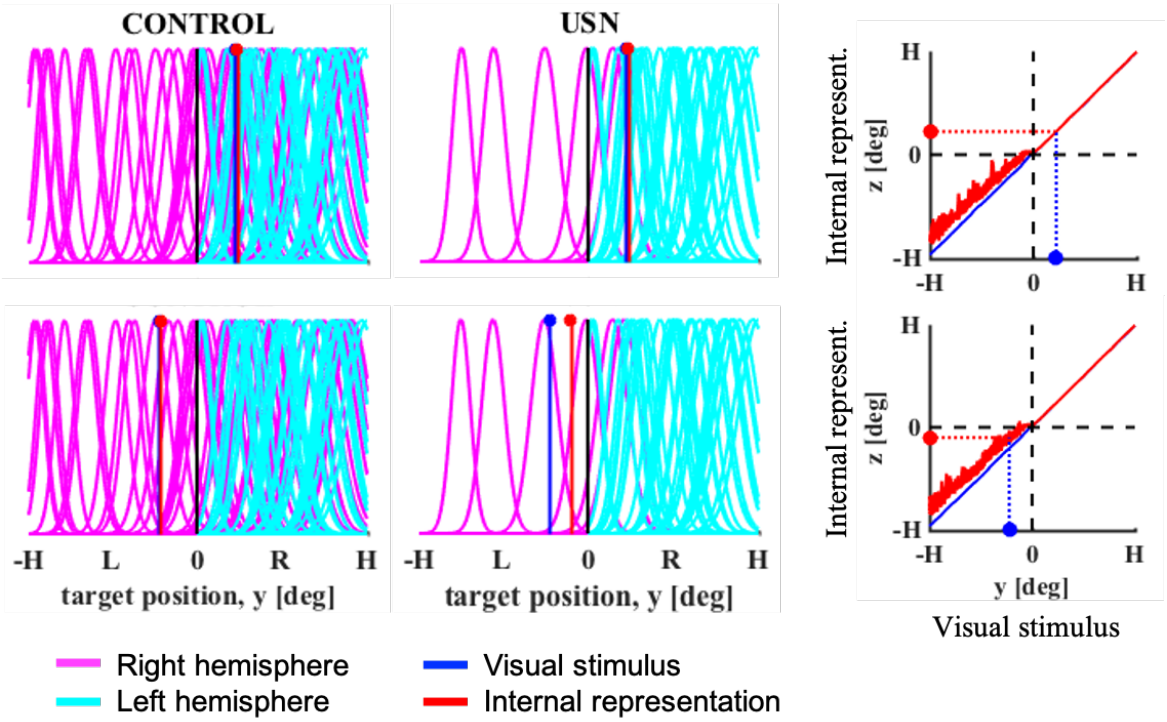

Figure 8.3 Model of right hemisphere lesion in the parietal cortex (USN). The 'CONTROL' case represents the parietal cortex without any lesion. Left: population of neurons (n=4800), each with a preferred location in space and a bell-shaped tuning curve, with a uniform distribution of preferred locations and curve selectivities: 2400 neurons in the left hemisphere (encoding the right hemispace), and 2400 in the right (encoding both hemispaces). Lesion was simulated destroying 90% of neurons in right hemisphere (USN). Right: simulated effect of lesions in the right parietal cortex (Leigh et al., 2015). Neglect is modelled as a distorted neural representation ($z_T(t)$) of visual targets ($y_T(t)$). Panels on the top show the internal representation of a visual stimulus processed in the left hemisphere (correct representation in both CONTROL and USN case), whereas panels on the bottom display the internal representation of a visual stimulus processed in the right hemisphere (distorted representation only in the USN case).

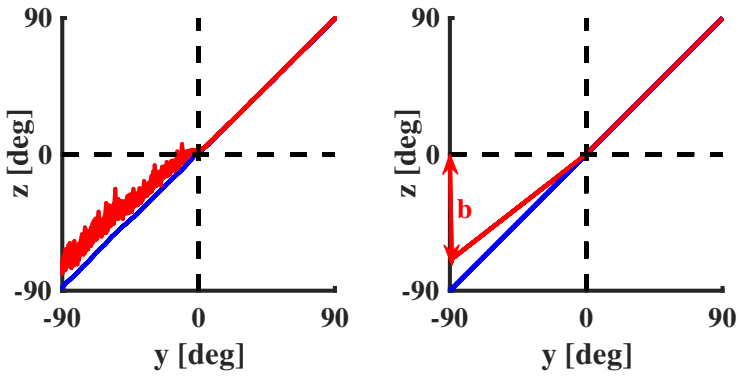

Figure 8.4 Neglect is modelled as a distorted neural representation ($z_T(t)$) of visual targets ($y_T(t)$). Left: simulated effect of lesions in the right parietal cortex (Leigh et al., 2015). Right: proposed macroscopic model. The quantity $b(t)$ is a measure of neglect.

$b(t) = 0$ corresponds to the complete lack of representation of the left visual hemispace; see Figure 8.4 (right). Eq. 8.1 reproduces, at a macroscopic level, the neural model proposed by Leigh et al. (2015). The model predicts that neglect causes a distortion of the mapping between a visual target located in the left hemispace and its internal representation, whose effect increases linearly with target position, as shown in Figure 8.4. When reaching for a visual target, hand movements are planned in terms of the internal representation of the visual target, so that:

$$x(t) = z_T(t) \tag{8.2}$$

Eqs. 8.1 and 8.2 predict that neglect only affects movements in the left hemispace. In this case, there will be a mismatch between hand movements and target position, $y_T(t)$.

The model also captures the notion that internally planned movements – like, for instance, line bisection or straight-ahead movements – are biased toward the right because the 'center' of the internal representation is shifted toward the right.

Neglect recovery

The mechanisms of training-induced recovery from neglect are little understood. I can only speculate that a possible driving force toward a reorganisation of the residual representation of the left hemispace is the mismatch between visual target and hand position at the end of the movement. Such a mismatch only occurs in the left hemispace, which suggests that movements of the hand in the left hemispace ($x(t) < 0$) are a necessary ingredient of neglect recovery. This leaves room to a large variety of possible recovery mechanisms, and the

available evidence is compatible with multiple mechanisms. As a starting point for further analysis, I tentatively assume that another condition for recovery to take place is that the visual targets are not too far left, i.e. $y_T(t) > -b(t)$. I hypothesise that inducing movements of the hand in areas of the workspace that are subject to neglect triggers a change in the internal representation of visually perceived targets. I make the simplifying assumption that the magnitude of adaptation is proportional to the amount of neglect, i.e. $H - b(t)$. The effect can be described by the following equations:

$$b(t+1) = A_n \cdot b(t) + B_n \cdot \big[H - b(t)\big] \cdot u_z(t) \tag{8.3}$$

The function $u(t)$ captures the conditions which trigger a neglect improvement:

$$u_z(t) = \begin{cases} 1, & \text{if } x(t) < 0 \text{ and } y_T(t) > -b(t), \\ 0, & \text{otherwise} \end{cases} \tag{8.4}$$

Parameters $0 < A_n < 1$ and $B_n > 0$ denote, respectively, the retention rate – how much neglect at the next trial is affected by neglect at the current trial – and the recovery rate – the amount of recovery occurring when $u_z(t) = 1$. If the conditions are not satisfied, i.e. $u_z(t) = 0$, neglect will decay, i.e. will get worse.

Prism Adaptation

Wearing prisms causes a mismatch between the hand position, $x(t)$ and its visual estimate, $y(t)$:

$$y(t) = x(t) + r(t) \tag{8.5}$$

where $r(t)$ is the visual shift due to the prisms. A similar mismatch is caused at the level of the visual targets:

$$y_T(t) = x_T(t) + r(t) \tag{8.6}$$

As in Eq. 8.2, hand movements are planned in terms of the visual representations of the target, $z_T(t)$. However, similar to visuomotor rotation experiments (Shadmehr et al., 2010) I assume that when planning a movement, subjects gradually develop an internal model $u(t)$ of the visual perturbation. This internal model is incorporated into the motor command, so that hand position is now specified as:

$$x(t) = z_T(t) - u(t) \tag{8.7}$$

Exercise with prisms induces an adaptation process, aimed at developing an 'internal model' of the prism perturbation, i.e. the amount of correction $u(t)$ with respect to the visual target that is necessary to minimise the error. It has been suggested (Shadmehr et al., 2010) that the development of an internal model of the visual perturbation is driven by the mismatch between the target position and the displayed hand position. This also corresponds to the prediction error, i.e. the difference between the actual and the predicted perturbation:

$$e(t) = y(t) - y_T(t) = r(t) - u(t) \tag{8.8}$$

This error is zero if the correction term, $u(t)$, equals the shift $r(t)$. Therefore, the correction term can be interpreted as a predictor of the shift magnitude, and $e(t)$ is a measure of the mismatch between the prism perturbation and its predictor or 'internal model'. However, what is available is not the visual error but rather the mismatch between the internal representations of $y(t)$ and $z_T(t)$:

$$e_z(t) = y(t) - z_T(t) \tag{8.9}$$

If there is no neglect, $e_z(t) = e(t)$. I assume that prism adaptation is driven by the prediction error, $e_z(t)$, according to the following equation:

$$u(t+1) = A_u u(t) + B_u e_z(t) \tag{8.10}$$

where $0 < A_u < 1$ and $B_u > 0$ are, respectively, a retention rate – reflecting the build-up of the predictor from trial to trial – and a rate of adaptation – reflecting how much the predictor is modified by the observed prediction error. On the very first prism trial, there is no prediction ($u(t) = 0$) and the subjects simply aim their hand at the visual target, $z_T(t)$. This leads to a visual error, which is exploited to correct the next prediction. From trial to trial, the prediction of the perturbation improves and the error decreases. In terms of hand movements, if $r(t)$ is directed toward the right, from trial to trial the movements of the hand are gradually shifted toward the left. This shift triggers the recalibration mechanism described by Eqs. 8.3 - 8.4, thus resulting in a reduction of the neglect symptoms. As the latter is more persistent than the effect of prism adaptation (Frassinetti et al., 2002; Rossetti et al., 1998), I expect that the neglect retention rate, A_n, is greater than the retention rate for prism adaptation, A_u. In conclusion, training with prisms leads to a recovery from the neglect symptoms. For protocol details, see (Rossetti et al., 1998).

8.2.2 Experiments

I compared the model predictions with experimental results from an ongoing rehabilitation trial, consisting of a reaching task within a virtual environment. The motivations underlying this approach are summarised in (Borghese et al., 2013).

Experimental apparatus

The experimental apparatus included a video projector, displaying a virtual reality environment on a 2 m $\times$ 2 m screen, as shown in Figure 8.5. Subjects sat in front of the screen, at a 2.5 m distance. A markerless motion capture sensor (Microsoft Kinect), placed below the screen, recorded the subjects' hand movements at a 20 Hz sampling rate. The screen continuously displays the subjects' mirror image – extracted from the depth image provided by the Kinect sensor – within a virtual scene (a tree with apples). Two speakers placed at each side of the screen provide spatialized sounds.

Task and exercise protocol

At the beginning of each trial, subjects sit in front of the screen with their hands on their knees (starting position). A target (apple) appears on the screen at random locations, evenly distributed in both hemispaces. Subjects are instructed to reach the target using their right hand as fast and accurate as possible. At the end of each movement a numeric score is provided, reflecting the movement time. If the target is not reached within a 20 s timeout, the score is considered to be zero. After each trial, subjects must return to the starting position. The virtual environment automatically adapts to subject performance through the introduction of a variable number of distractors (rotten apples) that subjects must avoid in order to complete the trial. Targets appear one at a time, while distractors appear all together. As training proceeds, subject go through three subsequent 'stages', during which subjects are initially given audiovisual cues (target flashing and spatialized beep sound), then visual only, and finally no cues. The treatment protocol consisted of 30 min training sessions, five days a week, for three consecutive weeks.

Subjects

The study involved a total of four subjects with subacute right hemisphere stroke, see Table 8.1 for demographic and clinical information, hospitalised at ICS Maugeri SpA SB - Istituto di Genova Nervi. All patients signed a consent form to participate in the study. Inclusion

Figure 8.5 Participants sit in front of the screen and reach one target (apple) at a time, which appears on the screen at random locations, evenly distributed in both hemispaces. At the end of each movement a numeric score is provided, reflecting the movement time. If the target is not reached within a 20 s timeout, the score is equal to zero. The virtual environment automatically adapts to subject performance through the introduction of a variable number of distractors (rotten apples) that subjects must avoid in order to complete the trial. As training proceeds, subject go through three subsequent 'stages', starting from audiovisual cues (target flashing and spatialized beep sound), then visual only, and finally no cues.

Table 8.1 Subjects data and model fitting. BIT: Behavioural Inattention Test; BI: Barthel Index; RT: Reading Test; CBS: Catherine Bergego Scale. A_n: retention rate; B_n: recovery rate; VAF: variance accounted for.

	Demographic data					Neuropsychological evaluation				Model fitting		
ID	sex	age	side	type	disease duration (weeks)	BIT (0-146)	BI (0-100)	RT (0-6)	CBS (0-30)	A_n	B_n $\times 10^{-5}$	VAF (%)
S1	F	88	R	ischemic	2	63	7	4	20	0.998	0.0003	89
S2	F	67	R	hemorrhagic	4	104	12	3	9	0.998	683	97
S3	M	52	R	hemorrhagic	3	63	19	4	19	0.998	924	96
S4	F	78	R	hemorrhagic	2	87	75	3	24	0.999	77.1	97

criteria were: unilateral neglect following a cerebro-vascular accident; dominant right hand assessed by the Edinburgh Inventory test; no previous history of psychiatric disorders or cognitive impairments (Mini-Mental State Examination); no drug or alcohol abuse. Exclusion criteria were aphasia, attention deficits and frontal syndrome, generalized hemianopia. Before the start of the treatment protocol, all subjects underwent a neuropsychological evaluation involving the following paper tests and clinical scales: Behavioural Inattention Test (BIT), Barthel Index (BI), Reading Test (RT), and Catherine Bergego Scale (CBS). The same tests were performed after completion of the treatment protocol.

8.2.3 Model Identification

For each subject, I took the recorded time series of the horizontal target location and hand position, expressed in degrees with respect to the body midline — one sample for each individual movement. Eqs. 8.3, 8.4 define a non-linear discrete-time state-space dynamical model in which the quantity b(t) is the state variable. Model parameters (A_n and B_n) were identified using a prediction error method. Parameter H was kept fixed and set to $H = 90$ deg. All calculations were carried out with MATLAB's System Identification Toolbox.

I treated the data from different sessions as separate experiments, but assumed that the model parameters do not change in the course of the whole recovery process. In addition to model parameters, the identification procedure gives estimates of the time course of the internal state ($b(t)$) during each session. As a measure of fitting performance, I calculated the correlation coefficient R between the observed and predicted performance. Its square, R^2, expressed in percent, can be interpreted as the fraction of variance accounted for (VAF) by the model.

8.3 Results

8.3.1 Simulations

I first used the model to simulate a prism adaptation task. Simulations are based on reaching movements toward two targets, located at the extreme left and the extreme right of the visual space. The simulated prism produced a 10° shift toward either the right or the left. The experiment was repeated with a healthy subject (for which I assumed an initial value $b(0) = 90^\circ$) and a neglect subject (for which I set an initial value $b(0) = 80^\circ$). The simulation results are summarised in Figure 8.6, 8.7.

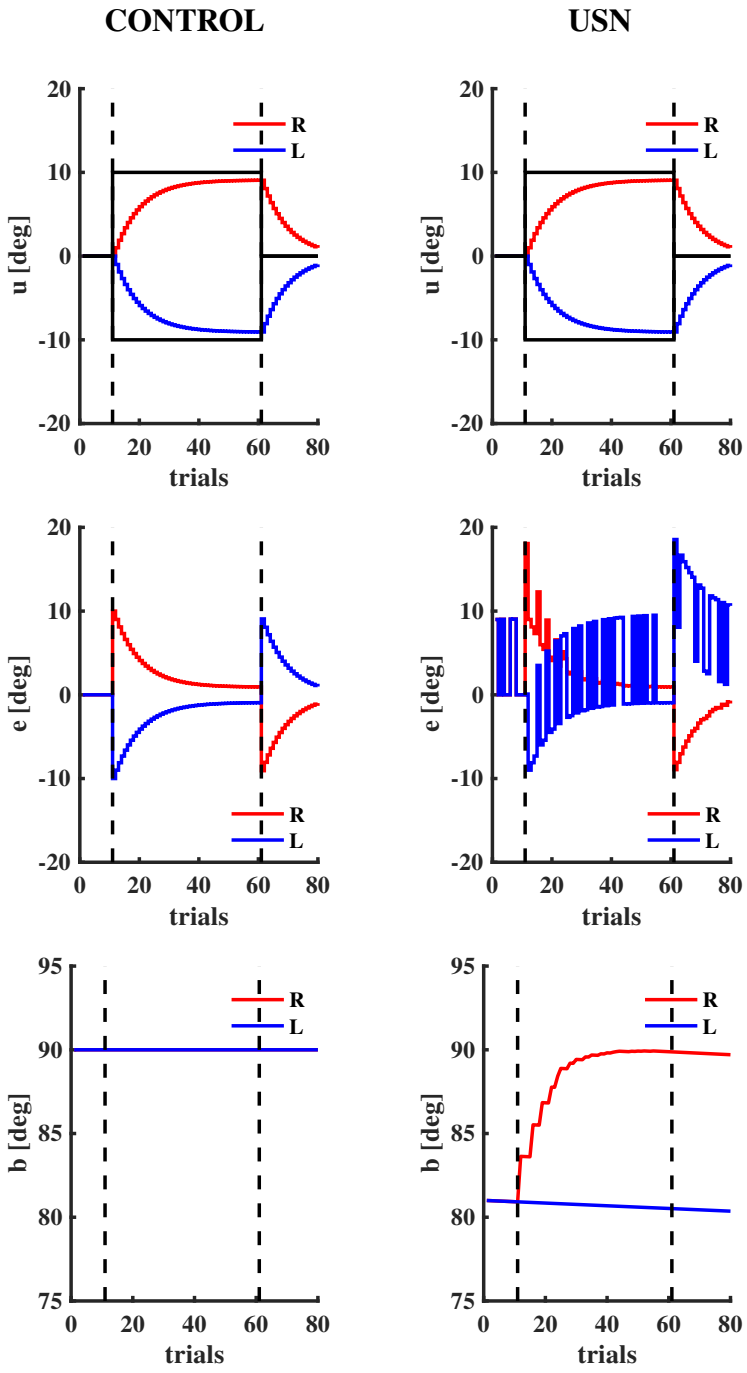

Figure 8.6 Simulation results: prism adaptation in healthy (left) and neglect (right) subject. From top to bottom, the traces display the prism shifts (black) and the evolution of the internal models, the prediction errors and the measure of neglect, for both right (red) and left prism (blue).

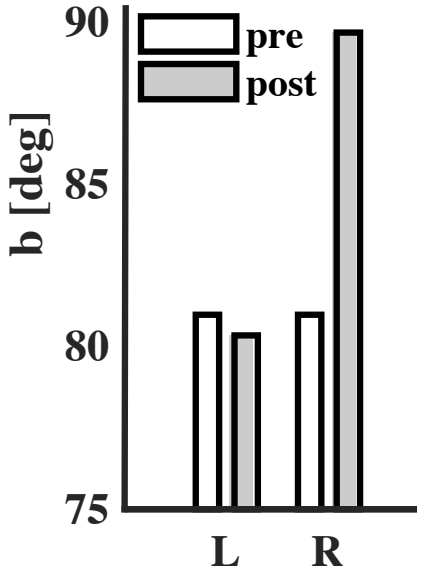

Figure 8.7 Simulation results: the bar plot summarizes the change in neglect.

After application of the prism, in order to reach the target the subject must move in the opposite direction with respect to the deviation induced by the prism. Healthy subjects adapt gradually to the prism, with a similar trend with both prism types. In both cases, the reaching error gradually reduces as the subject learns to compensate for the perturbation. When the prism is removed, the subject continues to move in the opposite direction with respect to the perturbation (aftereffect), which gradually washes out. USN subjects are equally capable of adapting to both left and right prisms. However, the two prisms have very different effect on neglect. Adaptation to the right prism results in a gradual increase of $b(t)$. In contrast, adaptation to the left prism results in a small decrease, corresponding to a worsening of the neglect symptoms. These results are in agreement with the experimental findings: adaptation to a right prism improves the neglect symptoms (Rossetti et al., 1998), whereas adaptation to a left prism has no effect (Luauté et al., 2012) or is even detrimental.

8.3.2 Model-based analysis of experimental results

The neglect recovery model was also used to interpret the temporal evolution of performance in a rehabilitation trial. Figure 8.8 summarizes, for a typical subject, the observed performance (black traces) and the model predictions (red traces). I also displayed, for the first and last training session, the relation between target location and final hand position and the corresponding neglect model according to Eq. 8.1. This plot suggests that the distortion in the target representation in the left hemisphere is gradually reduced as training proceeds. The

subject exhibits some variability in movements, especially in the early sessions. The overall model fitting performance is summarised in Table 8.1.

The estimated parameter values suggest that different subjects have different recovery rates. This may reflect the between-subjects differences in size and location of the cortical lesions. In contrast, the retention rate likely reflects basic features of cortical plasticity. The retention rate values are highly uniform across subjects, corresponding to a time constant of $\tau = -1/\log A_n = 500$ trials. The retention rate likely reflects basic features of cortical plasticity. This is about ten times the time constant estimated in adaptation experiments (visuomotor rotation and/or force fields) or in robot-assisted rehabilitation trials (Casadio and Sanguineti, 2012) and is consistent with the observation (Rossetti et al., 1998) that neglect recovery lasts much longer than the effect of prism adaptation. Notably, subject S1 exhibits a lower VAF value than other subjects. This may be due to presence of other symptoms, which the model does not explicitly account for.

8.4 Discussion and Conclusions

Different from approaches that explicitly focus on neural representations and the way they are affected by cortical lesions – e.g. (Leigh et al., 2015), my proposed model is formulated in terms of general principles and observable quantities. As such the model not only makes qualitative predictions, but can be used to interpret the trial-by-trial evolution of the neglect symptoms in individual subjects.

8.4.1 The model reproduces empirical observations in prism adaptation experiments

One major compensatory effect of short-term prism exposure is a mismatch between motor commands and visual targets. After adaptation, straight-ahead finger movements are shifted in a direction opposite to the optical deviation, indicating that internal visual and motor representations have been realigned. My computational framework predicts that right prism adaptation is beneficial to neglect (Rossetti et al., 1998). In particular, I propose that neglect recovery is facilitated by the leftward 'endogenous' movements induced by adaptation. This is not the only possible explanation of the empirical observations; in fact, alternative models are possible. The proposed modelling framework could be used to compare alternative theories and to contrast them with empirical findings.

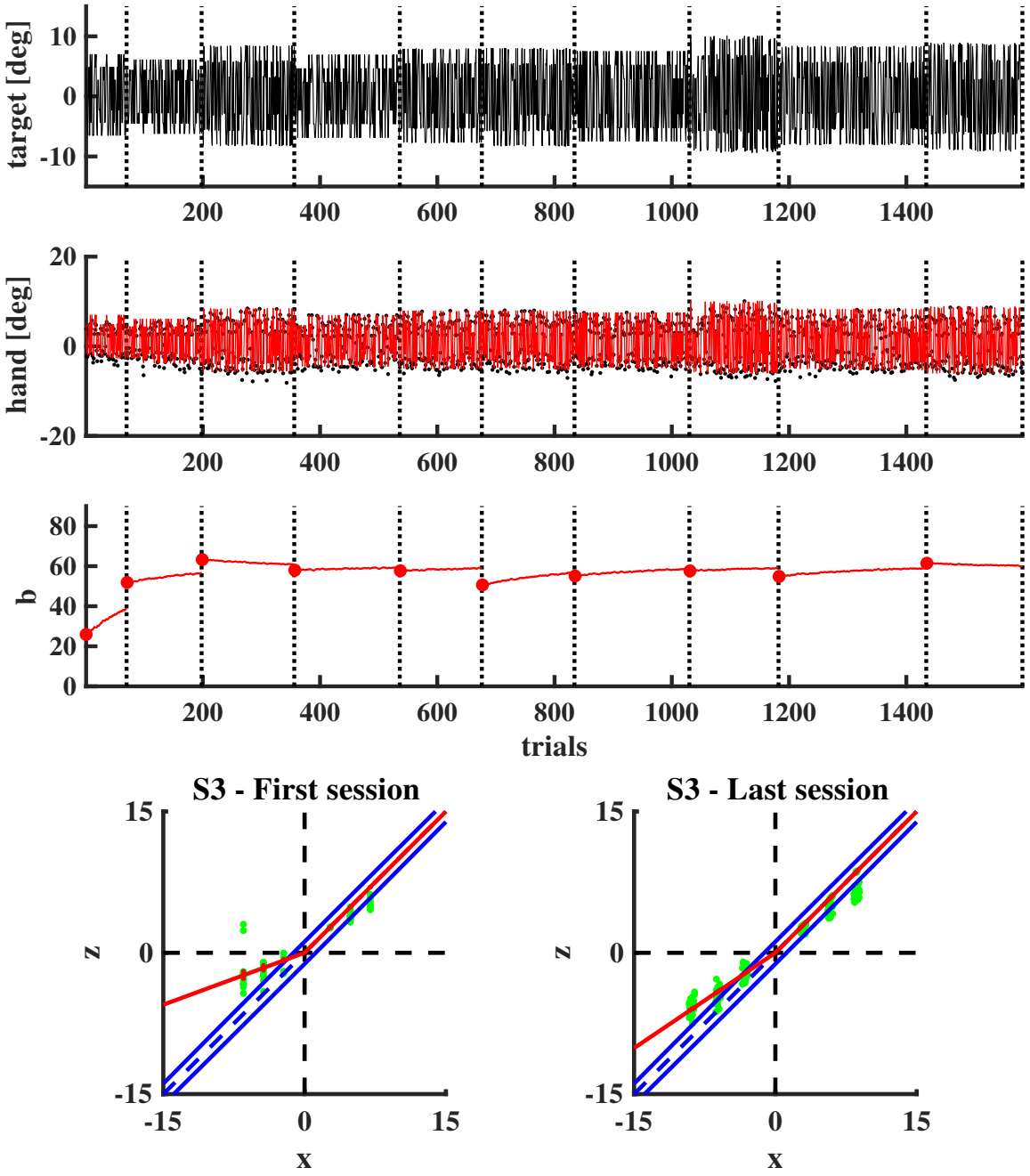

Figure 8.8 Model fitting. Time series: target positions ($y_T(t)$), hand movements ($x(t) = z_T(t)$) and neglect ($b(t)$). On the bottom: distorted internal representation of visual stimuli, on first and last training session. In all panels black traces denote experimental data, red traces denote model predictions. Blue lines indicate the size of the visual targets, green dots indicate final hand positions in experimental data (one point per trial on that session). All measures are expressed in degrees.

8.4.2 The model facilitates interpretation of rehabilitation training and may suggest optimal forms of treatment

One major feature of the model is that it can be used to interpret the performance time series and to detect implicit information in the performance time series of individual subjects. In fact, the application of a similar model to robot-assisted stroke rehabilitation trials has suggested that the estimated model parameters could be used, in individual subjects, to quantify the ongoing effect of treatment and to predict its outcome (Casadio and Sanguineti, 2012). Furthermore, a parametric description of the dynamics of the recovery process could be directly used to derive customized treatment solutions that can maximize the recovery outcome (Ueyama, 2017).

Chapter 9

General conclusions

The main contribution of the present thesis is to quantitatively explore how continuous experience of the perceptual consequences caused by self-generated movements can induce sensorimotor learning, and can be applied for neuromotor recovery.

Specifically, I demonstrated that, adopting properly designed visual stimuli with adequately impoverished and fragmented information, it is possible to systematically investigate, both experimentally and computationally, the role of interaction in combining cues and contextual information and eventually solving visual perceptual ambiguity. I showed that only active interaction with an ambiguous visual stimulus alters the subsequent visual and somatosensory perception of stimulus' motion. The change in perceptual threshold is strongly correlated with the change in movement direction measured during the active training, consistent with the idea that the perceptual change is tied to motor training. In addition, I proposed a quantitative Bayesian model suggesting that movement training affects visual perceptual judgement by improving the accuracy of the internal representation of the complex stimulus.

Visual and somatosensory perception may be based upon an empirical strategy which serves to resolve perceptual uncertainty. Perceptual decisions regarding motion direction provide, in turn, sensory evidence that drives behaviour. Our results suggest that visual and proprioceptive functions over time can be adapted with training, which is provided by interaction with the stimulus. The presented results can open novel perspective in different domains and research fields, such as modeling the complex relationships between movement and visual perceptual learning, and understanding how early vision oriented frequency channels are involved in the perceptual learning of coherent sensorimotor dependencies.

Moreover, I applied the idea that self-generated movements can induce neuromotor recovery in stroke patients. I developed and tested a model of recovery which suggests how to adapt the rehabilitation protocol to the individual directional patterns of impairment. This

model of recovery explicitly focuses on spatial generalization, i.e. the ability of exercises on a specific direction to promote recovery in those directions mostly impaired. Furthermore, I used the dynamical systems framework to model the trial-by-trial dynamics of training-induced recovery from unilateral spatial neglect, which is far more likely associated with right hemisphere damage in stroke survivors. In addition, I applied the model to the study of the recovery dynamics in the context of a newly designed training protocol, based on reaching movements within a VR-based adaptive environment.

Computational models may greatly contribute to a deeper understanding of the functional and physiological mechanisms underlying recovery, which would likely have a strong impact on neuromotor rehabilitation. As a future development, adaptively estimated computational models of recovery may contribute to personalization of therapy in a number of ways. First, the model is that it can be used to interpret the performance time series and to detect implicit information in the performance time series of individual subjects. Second, as performance within a rehabilitation session predicts the recovery outcome and its retention, few exercise sessions may allow to predict individual subjects' recovery potential. Further, characterization of the directional patterns of impairment and spatial generalization of recovery may suggest personalized exercise schedules. Also, a recovery model may be incorporated into an adaptive controller of robot assistance and/or task difficulty aimed at optimizing patient-specific interaction strategies of recovery with the robot. This approach can easily adapt to different exercise scenarios (task, robot type). Finally, using data from different devices (e.g. hand, arm, gait), this method can be used to study interplay between different aspects of recovery.

In a broader perspective, the scientific results and applications from this thesis suggest a paradigm shift towards movement-perception investigation, which includes continuous interacting conditions with visual ans somatosensory stimulations. Finally, the proposed research could also guide the design of training protocols in a combined sensory-motor therapeutic approach for recovering visual and proprioceptive disorders.

References

Adelson, E. H. and Bergen, J. R. (1991). The plenoptic function and the elements of early vision. computational models of visual processing. *Int. J. Comput. Vis*, 20.

Adelson, E. H. and Movshon, J. A. (1982). Phenomenal coherence of moving visual patterns. *Nature*, 300(5892):523.

Albright, T., Rodman, H., and Gross, C. (1986). Type ii mt neurons show pattern-motion direction selectivity. In *Neuroscience Abstr*, volume 12, page 1369.

Albright, T. D. (1984). Direction and orientation selectivity of neurons in visual area mt of the macaque. *J Neurophysiol*, 52(6):1106–30.

Albright, T. D. and Desimone, R. (1987). Local precision of visuotopic organization in the middle temporal area (mt) of the macaque. *Exp Brain Res*, 65(3):582–92.

Albright, T. D. and Stoner, G. R. (1995). Visual motion perception. *Proc Natl Acad Sci U S A*, 92(7):2433–40.

Andrew, D., Haavik, H., Dancey, E., Yielder, P., and Murphy, B. (2015). Somatosensory evoked potentials show plastic changes following a novel motor training task with the thumb. *Clinical neurophysiology*, 126(3):575–580.

Appelle, S. (1972). Perception and discrimination as a function of stimulus orientation: the "oblique effect" in man and animals. *Psychol Bull*, 78(4):266–78.

Avanzino, L., Bassolino, M., Pozzo, T., and Bove, M. (2011). Use-Dependent Hemispheric Balance. *Journal of Neuroscience*, 31(9):3423–3428.

Aytekin, M., Victor, J. D., and Rucci, M. (2014). The visual input to the retina during natural head-free fixation. *Journal of Neuroscience*, 34(38):12701–12715.

Bach-y Rita, P. (1972). *Brain mechanisms in sensory substitution*. Academic Press Inc.

Bach-y Rita, P., Collins, C. C., Saunders, F. A., White, B., and Scadden, L. (1969). Vision substitution by tactile image projection. *Nature*, 221(5184):963–964.

Bach-y Rita, P. and Kercel, S. W. (2003). Sensory substitution and the human–machine interface. *Trends in cognitive sciences*, 7(12):541–546.

Bagesteiro, L. B. and Sainburg, R. L. (2002). Handedness: dominant arm advantages in control of limb dynamics. *J Neurophysiol*, 88(5):2408–21.

Balasubramanian, S., Colombo, R., Sterpi, I., Sanguineti, V., and Burdet, E. (2012). Robotic assessment of upper limb motor function after stroke. *American journal of physical medicine & rehabilitation / Association of Academic Physiatrists*, 91(11 Suppl 3):S255–269.

Beck, J., Prazdny, K., and Ivry, R. (1984). The perception of transparency with achromatic colors. *Perception & psychophysics*, 35(5):407–422.

Beckett, P. A. (1980). Development of the third component in prism adaptation: effects of active and passive movement. *Journal of Experimental Psychology: Human Perception and Performance*, 6(3):433.

Beets, I. A. M., Rösler, F., and Fiehler, K. (2010a). Nonvisual motor learning improves visual motion perception: evidence from violating the two-thirds power law. *J Neurophysiol*, 104(3):1612–24.

Beets, I. A. M., 't Hart, B. M., Rösler, F., Henriques, D. Y. P., Einhäuser, W., and Fiehler, K. (2010b). Online action-to-perception transfer: only percept-dependent action affects perception. *Vision Res*, 50(24):2633–41.

Bejjanki, V. R., Clayards, M., Knill, D. C., and Aslin, R. N. (2011). Cue integration in categorical tasks: Insights from audio-visual speech perception. *PloS one*, 6(5).

Bergen, J. R. and Wilson, H. R. (1985). Prediction of flicker sensitivities from temporal three-pulse data. *Vision research*, 25(4):577–582.

Bertelson, P. and De Gelder, B. (2004). The psychology of multimodal perception. *Cross-modal space and crossmodal attention*, pages 141–177.

Bisiach, E., Geminiani, G., Berti, A., and Rusconi, M. L. (1990). Perceptual and premotor factors of unilateral neglect. *Neurology*, 40(8):1278–81.

Bock, O. (1987). Coordination of arm and eye movements in tracking of sinusoidally moving targets. *Behavioural brain research*, 24(2):93–100.

Bock, O. (2013). Basic principles of sensorimotor adaptation to different distortions with different effectors and movement types: a review and synthesis of behavioral findings. *Frontiers in human neuroscience*, 7:81.

Bohannon, R. W. and Smith, M. B. (1987). Interrater reliability of a modified Ashworth scale of muscle spasticity. *Physical therapy*, 67(2):206–207.

Borghese, N. A., Bottini, G., and Sedda, A. (2013). Videogame based neglect rehabilitation: a role for spatial remapping and multisensory integration? *Front Hum Neurosci*, 7:116.

Bowns, L. (1996). Evidence for a feature tracking explanation of why type ii plaids move in the vector sum direction at short durations. *Vision Res*, 36(22):3685–94.

Bradley, D. C. and Goyal, M. S. (2008). Velocity computation in the primate visual system. *Nat Rev Neurosci*, 9(9):686–95.

Brainard, D. H. (1997). The psychophysics toolbox. *Spat Vis*, 10(4):433–6.

Brass, M., Bekkering, H., and Prinz, W. (2001). Movement observation affects movement execution in a simple response task. *Acta psychologica*, 106(1-2):3–22.

Briscoe, R. and Grush, R. (2020). Action-based theories of perception. In Zalta, E. N., editor, *The Stanford Encyclopedia of Philosophy*. Metaphysics Research Lab, Stanford University, summer 2020 edition.

Brown, L. E., Wilson, E. T., Goodale, M. A., and Gribble, P. L. (2007). Motor force field learning influences visual processing of target motion. *Journal of Neuroscience*, 27(37):9975–9983.

Burke, D. and Wenderoth, P. (1993). The effect of interactions between one-dimensional component gratings on two-dimensional motion perception. *Vision Res*, 33(3):343–50.

Calvo-Merino, B., Glaser, D. E., Grèzes, J., Passingham, R. E., and Haggard, P. (2005). Action observation and acquired motor skills: an fmri study with expert dancers. *Cerebral cortex*, 15(8):1243–1249.

Cameirão, M. S., Badia, S. B. I., Oller, E. D., and Verschure, P. F. M. J. (2010). Neurorehabilitation using the virtual reality based Rehabilitation Gaming System: Methodology, design, psychometrics, usability and validation. *Journal of NeuroEngineering and Rehabilitation*, 7(1).

Casadio, M. and Sanguineti, V. (2012). Learning, retention, and slacking: a model of the dynamics of recovery in robot therapy. *IEEE Trans Neural Syst Rehabil Eng*, 20(3):286–96.

Casadio, M., Sanguineti, V., Morasso, P., and Solaro, C. (2008). Abnormal sensorimotor control, but intact force field adaptation, in multiple sclerosis subjects with no clinical disability. *Multiple Sclerosis Journal*, 14(3):330–342.

Casadio, M., Sanguineti, V., Morasso, P. G., and Arrichiello, V. (2006). Braccio di Ferro: a new haptic workstation for neuromotor rehabilitation. *Technology and health care : official journal of the European Society for Engineering and Medicine*, 14(3):123–42.

Casadio, M., Tamagnone, I., Summa, S., and Sanguineti, V. (2013). Neuromotor recovery from stroke: computational models at central, functional, and muscle synergy level. *Frontiers in computational neuroscience*, 7:97.

Chalupa, L. M. and Werner, J. S. (2004). *The visual neurosciences, Vols. 1 & 2*. MIT press.

Champion, R. A., Hammett, S. T., and Thompson, P. G. (2007). Perceived direction of plaid motion is not predicted by component speeds. *Vision Res*, 47(3):375–83.

Chen, J., Valsecchi, M., and Gegenfurtner, K. R. (2016). Lrp predicts smooth pursuit eye movement onset during the ocular tracking of self-generated movements. *Journal of neurophysiology*, 116(1):18–29.

Cheng, S. and Sabes, P. N. (2006). Modeling sensorimotor learning with linear dynamical systems. *Neural Comput*, 18(4):760–93.

Choi, Y. S., Lee, K. W., Lee, J. H., Kim, S. B., Park, G. T., and Lee, S. J. (2016). The effect of an upper limb rehabilitation robot on hemispatial neglect in stroke patients. *Ann Rehabil Med*, 40(4):611–9.

Cirstea, M. C. and Levin, M. F. (2000). Compensatory strategies for reaching in stroke. *Brain*, 123(5):940–953.

Colavita, F. B. (1974). Insular-temporal lesions and vibrotactile temporal pattern discrimination in cats. *Physiol Behav*, 12(2):215–8.

Colombo, R., Pisano, F., Delconte, C., Mazzone, A., Grioni, G., Castagna, M., Bazzini, G., Imarisio, C., Maggioni, G., and Pistarini, C. (2017). Comparison of exercise training effect with different robotic devices for upper limb rehabilitation: a retrospective study. *European journal of physical and rehabilitation medicine*, 53(2):240–248.

Colombo, R., Pisano, F., Mazzone, A., Delconte, C., Micera, S., Carrozza, M. C., Dario, P., and Minuco, G. (2007). Design strategies to improve patient motivation during robot-aided rehabilitation. *Journal of NeuroEngineering and Rehabilitation*, 4.

Colombo, R., Pisano, F., Micera, S., Mazzone, A., Delconte, C., Carrozza, M. C., Dario, P., and Minuco, G. (2005). Robotic techniques for upper limb evaluation and rehabilitation of stroke patients. *IEEE Transactions on Neural Systems and Rehabilitation Engineering*, 13(3):311–324.

Colombo, R., Pisano, F., Micera, S., Mazzone, A., Delconte, C., Carrozza, M. C., Dario, P., and Minuco, G. (2008). Assessing mechanisms of recovery during robot-aided neurorehabilitation of the upper limb. *Neurorehabilitation and Neural Repair*, 22(1):50–63.

Colombo, R., Sterpi, I., Mazzone, A., Delconte, C., Minuco, G., and Pisano, F. (2009). Measuring changes of movement dynamics during robot-aided neurorehabilitation of stroke patients. *IEEE Transactions on Neural Systems and Rehabilitation Engineering*, 18(1):75–85.

Colombo, R., Sterpi, I., Mazzone, A., Delconte, C., and Pisano, F. (2012). Taking a Lesson From Patients' Recovery Strategies to Optimize Training During Robot-Aided Rehabilitation. *IEEE Transactions on Neural Systems and Rehabilitation Engineering*, 20(3):276–285.

Colombo, R., Sterpi, I., Mazzone, A., Delconte, C., and Pisano, F. (2013). Robot-aided neurorehabilitation in sub-acute and chronic stroke: does spontaneous recovery have a limited impact on outcome? *NeuroRehabilitation*, 33(4):621–629.

Craighero, L., Fadiga, L., Umiltà, C. A., and Rizzolatti, G. (1996). Evidence for visuomotor priming effect. *Neuroreport*, 8(1):347–9.

Cressman, E. K. and Henriques, D. Y. (2009). Sensory recalibration of hand position following visuomotor adaptation. *Journal of neurophysiology*, 102(6):3505–3518.

Cropper, S. J., Mullen, K. T., and Badcock, D. R. (1996). Motion coherence across different chromatic axes. *Vision Res*, 36(16):2475–88.

Cuppone, A. V., Semprini, M., and Konczak, J. (2018). Consolidation of human somatosensory memory during motor learning. *Behavioural brain research*, 347:184–192.

Decety, J. and Ingvar, D. H. (1990). Brain structures participating in mental simulation of motor behavior: A neuropsychological interpretation. *Acta psychologica*, 73(1):13–34.

Di Pellegrino, G., Fadiga, L., Fogassi, L., Gallese, V., and Rizzolatti, G. (1992). Understanding motor events: a neurophysiological study. *Experimental brain research*, 91(1):176–180.

DiCarlo, J. J., Zoccolan, D., and Rust, N. C. (2012). How does the brain solve visual object recognition? *Neuron*, 73(3):415–434.

Dipietro, L., Krebs, H. I., Fasoli, S. E., Volpe, B. T., and Hogan, N. (2009). Submovement changes characterize generalization of motor recovery after stroke. *Cortex; a Journal Devoted to the Study of the Nervous System and Behavior*, 45(3):318–324.

Domalain, M., Vigouroux, L., Danion, F., Sevrez, V., and Berton, E. (2008). Effect of object width on precision grip force and finger posture. *Ergonomics*, 51(9):1441–1453.

Donchin, O., Francis, J. T., and Shadmehr, R. (2003). Quantifying generalization from trial-by-trial behavior of adaptive systems that learn with basis functions: theory and experiments in human motor control. *J Neurosci*, 23(27):9032–45.

Emken, J. L., Benitez, R., Sideris, A., Bobrow, J. E., and Reinkensmeyer, D. J. (2007). Motor Adaptation as a Greedy Optimization of Error and Effort. *Journal of Neurophysiology*, 97(6):3997–4006.

Engel, A., Burke, M., Fiehler, K., Bien, S., and Rösler, F. (2008). What activates the human mirror neuron system during observation of artificial movements: Bottom-up visual features or top-down intentions? *Neuropsychologia*, 46(7):2033–2042.

Fennema, C. L. and Thompson, W. B. (1979). Velocity determination in scenes containing several moving objects. *Computer graphics and image processing*, 9(4):301–315.

Ferrera, V. P. and Wilson, H. R. (1987). Direction specific masking and the analysis of motion in two dimensions. *Vision Res*, 27(10):1783–96.

Ferrera, V. P. and Wilson, H. R. (1990). Perceived direction of moving two-dimensional patterns. *Vision Res*, 30(2):273–87.

Ferrera, V. P. and Wilson, H. R. (1991). Perceived speed of moving two-dimensional patterns. *Vision Research*, 31(5):877–893.

Findlay, J. and Gilchrist, I. (2003). Active vision: The psychology of looking and seeing. new york, ny, us: Oxford university press.

Frassinetti, F., Angeli, V., Meneghello, F., Avanzi, S., and Làdavas, E. (2002). Long-lasting amelioration of visuospatial neglect by prism adaptation. *Brain*, 125(Pt 3):608–23.

Freeman, T. C. A., Champion, R. A., and Warren, P. A. (2010). A bayesian model of perceived head-centered velocity during smooth pursuit eye movement. *Curr Biol*, 20(8):757–62.

French, B., Thomas, L. H., Coupe, J., McMahon, N. E., Connell, L., Harrison, J., Sutton, C. J., Tishkovskaya, S., and Watkins, C. L. (2016). Repetitive task training for improving functional ability after stroke. *The Cochrane Database of Systematic Reviews*, 11:CD006073.

Fugl-Meyer, A. R. (1980). Post-stroke hemiplegia assessment of physical properties. *Scandinavian Journal of Rehabilitation Medicine. Supplement*, 7:85–93.

Furmanski, C. S. and Engel, S. A. (2000). An oblique effect in human primary visual cortex. *Nature neuroscience*, 3(6):535–536.

Gallese, V. and Goldman, A. (1998). Mirror neurons and the simulation theory of mind-reading. *Trends in cognitive sciences*, 2(12):493–501.

Gandolfo, F., Mussa-Ivaldi, F. A., and Bizzi, E. (1996). Motor learning by field approximation. *Proceedings of the National Academy of Sciences of the United States of America*, 93(9):3843–3846.

Gattass, R. and Gross, C. G. (1981). Visual topography of striate projection zone (mt) in posterior superior temporal sulcus of the macaque. *J Neurophysiol*, 46(3):621–38.

Georgopoulos, a. P., Kalaska, J. F., Caminiti, R., and Massey, J. T. (1982). On the relations between the direction of two-dimensional arm movements and cell discharge in primate motor cortex. *J.Neurosci.*, 2(11)(11):1527–1537.

Ghahramani, Z. and Hinton, G. E. (1996). Parameter estimation for linear dynamical systems. Technical report, Technical Report CRG-TR-96-2, University of Totronto, Dept. of Computer Science.

Gibson, J. (1977). The concept of affordances. *Perceiving, acting, and knowing*, 1.

Gibson, J. J. (1979). *The Ecological Approach to Visual Perception*. Houghton Mifflin.

Gibson, J. J. (2002). A theory of direct visual perception. *Vision and Mind: selected readings in the philosophy of perception*, pages 77–90.

Haith, A., Jackson, C. P., Miall, R. C., and Vijayakumar, S. (2009). Unifying the sensory and motor components of sensorimotor adaptation. In *Advances in Neural Information Processing Systems*, pages 593–600.

Han, C. E., Arbib, M. A., and Schweighofer, N. (2008). Stroke rehabilitation reaches a threshold. *PLoS computational biology*, 4(8):e1000133.

Harris, C. S. (1963). Adaptation to displaced vision: visual, motor, or proprioceptive change? *Science*, 140(3568):812–813.

Hecht, H., Vogt, S., and Prinz, W. (2001). Motor learning enhances perceptual judgment: A case for action-perception transfer. *Psychological research*, 65(1):3–14.

Hedges, J. H., Stocker, A. A., and Simoncelli, E. P. (2011). Optimal inference explains the perceptual coherence of visual motion stimuli. *Journal of vision*, 11(6):14–14.

Heilman, K. M. and Valenstein, E. (1979). Mechanisms underlying hemispatial neglect. *Ann Neurol*, 5(2):166–70.

Heilman, K. M. and Van Den Abell, T. (1980). Right hemisphere dominance for attention: the mechanism underlying hemispheric asymmetries of inattention (neglect). *Neurology*, 30(3):327–30.

Heinemann, A. W., Linacre, J. M., Wright, B. D., Hamilton, B. B., and Granger, C. (1993). Relationships between impairment and physical disability as measured by the functional independence measure. *Archives of Physical Medicine and Rehabilitation*, 74(6):566–573.

Held, R. and Hein, A. (1963). Movement-produced stimulation in the development of visually guided behavior. *Journal of comparative and physiological psychology*, 56(5):872.

Henriques, D. Y. and Cressman, E. K. (2012). Visuomotor adaptation and proprioceptive recalibration. *Journal of motor behavior*, 44(6):435–444.

Heuer, H. (1989). A multiple-representations' approach to mental practice of motor skills1. In *Normalities and abnormalities in human movement*, volume 29, pages 36–57. Karger Publishers.

Hidaka, Y., Han, C. E., Wolf, S. L., Winstein, C. J., and Schweighofer, N. (2012). Use it and improve it or lose it: interactions between arm function and use in humans post-stroke. *PLoS computational biology*, 8(2):e1002343.

Hommel, B., Müsseler, J., Aschersleben, G., and Prinz, W. (2001). The theory of event coding (tec): A framework for perception and action planning. *Behavioral and brain sciences*, 24(5):849–878.

Howard, I. S. and Franklin, D. W. (2016). Adaptive tuning functions arise from visual observation of past movement. *Scientific Reports*, 6.

Hsieh, Y.-w., Wu, C.-y., Lin, K.-c., Yao, G., Wu, K.-y., and Chang, Y.-j. (2012). Dose–Response Relationship of Robot-Assisted Stroke Motor Rehabilitation The Impact of Initial Motor Status. *Stroke*, 43(10):2729–2734.

Huang, F. C. and Patton, J. L. (2016). Movement distributions of stroke survivors exhibit distinct patterns that evolve with training. *Journal of neuroengineering and rehabilitation*, 13(1):23.

Huang, V. S. and Krakauer, J. W. (2009). Robotic neurorehabilitation: a computational motor learning perspective. *Journal of neuroengineering and rehabilitation*, 6(1):5.

Hubel, D. H. and Wiesel, T. N. (1968). Receptive fields and functional architecture of monkey striate cortex. *J Physiol*, 195(1):215–43.

Hupé, J.-M. and Rubin, N. (2003). The dynamics of bi-stable alternation in ambiguous motion displays: a fresh look at plaids. *Vision Research*, 43(5):531 – 548.

Hupé, J.-M. and Rubin, N. (2004). The oblique plaid effect. *Vision Research*, 44(5):489 – 500.

Hürlimann, F., Kiper, D. C., and Carandini, M. (2002). Testing the bayesian model of perceived speed. *Vision Res*, 42(19):2253–7.

Ishimura, G. (1995). Visuomotor factors for action capture. In *Investigative Ophthalmology & Visual Science*, volume 36, pages S357–S357. LIPPINCOTT-RAVEN PUBL 227 EAST WASHINGTON SQUARE, PHILADELPHIA, PA 19106.

Ishimura, G. and Shimojo, S. (1994). Voluntary action captures visual-motion. In *Investigative Ophthalmology & Visual Science*, volume 35, pages 1275–1275. LIPPINCOTT-RAVEN PUBL 227 EAST WASHINGTON SQ, PHILADELPHIA, PA 19106.

Izawa, J. and Shadmehr, R. (2011). Learning from sensory and reward prediction errors during motor adaptation. *PLoS computational biology*, 7(3).

Jarrassé, N., Charalambous, T., and Burdet, E. (2012). A framework to describe, analyze and generate interactive motor behaviors. *PloS One*, 7(11):e49945.

Jeannerod, M. (1994). The representing brain: Neural correlates of motor intention and imagery. *Behavioral and Brain sciences*, 17(2):187–202.

Jeannerod, M., Arbib, M., Rizzolatti, G., and Sakata, H. (1995). Grasping objects: the cortical mechanisms. *Trends Neurosci*, 18:314–32.

Jeannerod, M. and Jeannerod, M. (1997). *The cognitive neuroscience of action*, volume 1997. Blackwell Oxford.

Kaas, J. H. (1991). Plasticity of sensory and motor maps in adult mammals. *Annual review of neuroscience*, 14(1):137–167.

Kamper, D. G., McKenna-Cole, A. N., Kahn, L. E., and Reinkensmeyer, D. J. (2002). Alterations in reaching after stroke and their relation to movement direction and impairment severity. *Archives of Physical Medicine and Rehabilitation*, 83(5):702–707.

Karnath, H. O. (1997). Spatial orientation and the representation of space with parietal lobe lesions. *Philos Trans R Soc Lond B Biol Sci*, 352(1360):1411–9.

Keetels, M. and Stekelenburg, J. J. (2014). Motor-induced visual motion: hand movements driving visual motion perception. *Exp Brain Res*, 232(9):2865–77.

Kim, I. K. and Spelke, E. S. (1992). Infants' sensitivity to effects of gravity on visible object motion. *Journal of Experimental Psychology: Human Perception and Performance*, 18(2):385.

Kim, J. and Wilson, H. R. (1993). Dependence of plaid motion coherence on component grating directions. *Vision Research*, 33(17):2479 – 2489.

Kleiner, M., Brainard, D., and Pelli, D. (2007). What is new in psychophysics toolbox. *Perception*, 36.

Kontsevich, L. L. and Tyler, C. W. (1999). Bayesian adaptive estimation of psychometric slope and threshold. *Vision Res*, 39(16):2729–37.

Kooi, F. L., De Valois, K. K., Switkes, E., and Grosof, D. H. (1992). Higher-order factors influencing the perception of sliding and coherence of a plaid. *Perception*, 21(5):583–98.

Krakauer, J. W. (2006). Motor learning: its relevance to stroke recovery and neurorehabilitation. *Current Opinion in Neurology*, 19(1):84–90.

Krakauer, J. W. and Mazzoni, P. (2011). Human sensorimotor learning: adaptation, skill, and beyond. *Current opinion in neurobiology*, 21(4):636–644.

Krebs, H. I., Hogan, N., Aisen, M. L., and Volpe, B. T. (1998). Robot-aided neurorehabilitation. *IEEE Trans Rehabil Eng*, 6(1):75–87.

Kwakkel, G., Kollen, B., and Twisk, J. (2006). Impact of time on improvement of outcome after stroke. *Stroke; a Journal of Cerebral Circulation*, 37(9):2348–2353.

Kwakkel, G. and Kollen, B. J. (2013). Predicting activities after stroke: what is clinically relevant? *International Journal of Stroke: Official Journal of the International Stroke Society*, 8(1):25–32.

Lacquaniti, F., Terzuolo, C., and Viviani, P. (1983). The law relating the kinematic and figural aspects of drawing movements. *Acta psychologica*, 54(1-3):115–130.

Lametti, D., Nasir, S., and Ostry, D. (2012). Sensory preference in speech production revealed by simultaneous alteration of auditory and somatosensory feedback. *Journal of Neuroscience*, 32(27):9351–9358.

Langhorne, P., Bernhardt, J., and Kwakkel, G. (2011). Stroke rehabilitation. *Lancet*, 377(9778):1693–1702.

Latimer, K. W., Yates, J. L., Meister, M. L. R., Huk, A. C., and Pillow, J. W. (2015). Single-trial spike trains in parietal cortex reveal discrete steps during decision-making. *Science*, 349(6244):184–187.

Law, C. and Gold, J. (2008). Neural correlates of perceptual learning in a sensory-motor, but not a sensory, cortical area. *Nat Neurosci*, 11:505–513.

Leigh, S., Danckert, J., and Eliasmith, C. (2015). Modelling the differential effects of prisms on perception and action in neglect. *Exp Brain Res*, 233(3):751–66.

Levin, M. F. (1996). Should stereotypic movement synergies in hemiparetic patients be considered adaptive? *Behavioral and Brain Sciences*, 19(1):79–80.

Lisa, L. P., Jughters, A., and Kerckhofs, E. (2013). The effectiveness of different treatment modalities for the rehabilitation of unilateral neglect in stroke patients: a systematic review. *NeuroRehabilitation*, 33(4):611–20.

Ljung, L. (1998). *System Identification: Theory for the User*. Pearson Education.

Luauté, J., Jacquin-Courtois, S., O'Shea, J., Christophe, L., Rode, G., Boisson, D., and Rossetti, Y. (2012). Left-deviating prism adaptation in left neglect patient: reflexions on a negative result. *Neural Plast*, 2012:718604.

MacLeod, D. (1978). Visual sensitivity. *Annual review of psychology*, 29(1):613–645.

Macleod, D. I., Williams, D. R., and Makous, W. (1992). A visual nonlinearity fed by single cones. *Vision research*, 32(2):347–363.

Macpherson, F. (2015). The space of sensory modalities. *Perception and Its Modalities*, page 432.

Maiello, G., Kwon, M., and Bex, P. J. (2018). Three-dimensional binocular eye–hand coordination in normal vision and with simulated visual impairment. *Experimental brain research*, 236(3):691–709.

Mansfield, R. J. (1974). Neural basis of orientation perception in primate vision. *Science*, 186(4169):1133–5.

Marr, D. and Ullman, S. (1981). Directional selectivity and its use in early visual processing. *Proc R Soc Lond B Biol Sci*, 211(1183):151–80.

Maruya, K., Yang, E., and Blake, R. (2007). Voluntary action influences visual competition. *Psychological Science*, 18(12):1090–1098.

Massie, C. L., Du, Y., Conroy, S. S., Krebs, H. I., Wittenberg, G. F., Bever, C. T., and Whitall, J. (2016). A clinically relevant method of analyzing continuous change in robotic upper extremity chronic stroke rehabilitation. *Neurorehabilitation and neural repair*, 30(8):703–712.

Mattar, A. A., Darainy, M., and Ostry, D. J. (2012). Motor learning and its sensory effects: time course of perceptual change and its presence with gradual introduction of load. *Journal of neurophysiology*, 109(3):782–791.

McCullagh, P., Weiss, M. R., and Ross, D. (1989). Modeling considerations in motor skill acquisition and performance: an integrated approach. *Exerc Sport Sci Rev*, 17:475–513.

McDougle, S. D., Bond, K. M., and Taylor, J. A. (2015). Explicit and implicit processes constitute the fast and slow processes of sensorimotor learning. *Journal of Neuroscience*, 35(26):9568–9579.

Mehrholz, J., Pohl, M., Platz, T., Kugler, J., and Elsner, B. (2015). Electromechanical and robot-assisted arm training for improving activities of daily living, arm function, and arm muscle strength after stroke. *The Cochrane Database of Systematic Reviews*.

Metelli, F. (1974). The perception of transparency. *Scientific American*, 230(4):90–99.

Miikkulainen, R., Bednar, J. A., Choe, Y., and Sirosh, J. (2006). *Computational maps in the visual cortex*. Springer Science & Business Media.

Mingolla, E., Todd, J. T., and Norman, J. F. (1992). The perception of globally coherent motion. *Vision Research*, 32(6):1015–1031.

Mirdamadi, J. L. and Block, H. J. (2020). Somatosensory changes associated with motor skill learning. *Journal of Neurophysiology*, 123(3):1052–1062.

Mitsumatsu, H. (2009). Voluntary action affects perception of bistable motion display. *Perception*, 38(10):1522–35.

Mort, D. J., Malhotra, P., Mannan, S. K., Rorden, C., Pambakian, A., Kennard, C., and Husain, M. (2003). The anatomy of visual neglect. *Brain*, 126(Pt 9):1986–97.

Movshon, J., Adelson, E., Gizzi, M., and Newsome, W. (1985). The analysis of visual moving patterns. *Pattern recognition mechanisms*, pages 117–151.

Müsseler, J. (1999). How independent from action control is perception?: An event-coding account for more equally-ranked crosstalks. In *Advances in psychology*, volume 129, pages 121–147. Elsevier.

Nakayama, K. (1985). Biological image motion processing: a review. *Vision research*, 25(5):625–660.

Nasir, S. M., Darainy, M., and Ostry, D. J. (2013). Sensorimotor adaptation changes the neural coding of somatosensory stimuli. *Journal of neurophysiology*, 109(8):2077–2085.

Nasir, S. M. and Ostry, D. J. (2009). Auditory plasticity and speech motor learning. *Proceedings of the National Academy of Sciences*, 106(48):20470–20475.

Necker, L. (1832). Observations on some remarkable phenomenon which occurs in viewing a figure of a crystal or geometrical solid. *London and Edinburgh Philosophical Magazine and Journal of Science*, 3:329–337.

Nijland, R. H. M., van Wegen, E. E. H., Harmeling-van der Wel, B. C., and Kwakkel, G. (2010). Presence of finger extension and shoulder abduction within 72 hours after stroke predicts functional recovery: early prediction of functional outcome after stroke: the EPOS cohort study. *Stroke*, 41(4):745–750.

Noë, A. (2004). Action in perception (representation and mind). *Cambridge: Cambridge*.

Noë, A. (2010). Vision without representation. *Perception, action, and consciousness: sensorimotor dynamics and two visual systems*, pages 245–256.

Noë, A. and O'Regan, J. K. (2002). On the brain-basis of visual consciousness: A sensorimotor account. *Vision and mind: Selected readings in the philosophy of perception*, pages 567–598.

Noest, A. and Van Den Berg, A. (1993). The role of early mechanisms in motion transparency and coherence. *Spatial Vision*, 7:125–125.

Nudo, R. J. (2006). Mechanisms for recovery of motor function following cortical damage. *Curr Opin Neurobiol*, 16(6):638–44.

O'Callaghan, C. (2008). Seeing what you hear: Cross-modal illusions and perception. *Philosophical Issues*, 18(1):316–338.

O'Regan, J. K. (2011). *Why red doesn't sound like a bell: Understanding the feel of consciousness*. Oxford University Press.

O'Regan, J. K. and Noë, A. (2001). A sensorimotor account of vision and visual consciousness. *Behavioral and brain sciences*, 24(5):939–973.

Ostry, D. J., Darainy, M., Mattar, A. A., Wong, J., and Gribble, P. L. (2010). Somatosensory plasticity and motor learning. *Journal of Neuroscience*, 30(15):5384–5393.

Ostry, D. J. and Gribble, P. L. (2016). Sensory plasticity in human motor learning. *Trends in neurosciences*, 39(2):114–123.

Pack, C. C. (2001). The aperture problem for visual motion and its solution in primate cortex. *Sci Prog*, 84(Pt 4):255–66.

Pack, C. C. and Born, R. T. (2001). Temporal dynamics of a neural solution to the aperture problem in visual area mt of macaque brain. *Nature*, 409(6823):1040–2.

Panarese, A., Colombo, R., Sterpi, I., Pisano, F., and Micera, S. (2012). Tracking Motor Improvement at the Subtask Level During Robot-Aided Neurorehabilitation of Stroke Patients. *Neurorehabilitation and Neural Repair*, 26(7):822–833.

Patton, J. L., Stoykov, M. E., Kovic, M., and Mussa-Ivaldi, F. A. (2006). Evaluation of robotic training forces that either enhance or reduce error in chronic hemiparetic stroke survivors. *Experimental Brain Research*, 168(3):368–383.

Pedroli, E., Serino, S., Cipresso, P., Pallavicini, F., and Riva, G. (2015). Assessment and rehabilitation of neglect using virtual reality: a systematic review. *Front Behav Neurosci*, 9:226.

Pizzamiglio, L., Antonucci, G., Judica, A., Montenero, P., Razzano, C., and Zoccolotti, P. (1992). Cognitive rehabilitation of the hemineglect disorder in chronic patients with unilateral right brain damage. *J Clin Exp Neuropsychol*, 14(6):901–23.

Pleger, B., Foerster, A.-F., Ragert, P., Dinse, H. R., Schwenkreis, P., Malin, J.-P., Nicolas, V., and Tegenthoff, M. (2003). Functional imaging of perceptual learning in human primary and secondary somatosensory cortex. *Neuron*, 40(3):643–653.

Plummer, D. J. and Ramachandran, V. S. (1993). Perception of transparency in stationary and moving images. *Spat Vis*, 7(2):113–23.

Port, N. L., Lee, D., Dassonville, P., and Georgopoulos, A. P. (1997). Manual interception of moving targets i. performance and movement initiation. *Experimental Brain Research*, 116(3):406–420.

Posner, M. I., Nissen, M. J., and Klein, R. M. (1976). Visual dominance: an information-processing account of its origins and significance. *Psychol Rev*, 83(2):157–71.

Prins, N. (2013). The psi-marginal adaptive method: How to give nuisance parameters the attention they deserve (no more, no less). *J Vis*, 13(7):3.

Prinz, W. (1997). Perception and action planning. *European journal of cognitive psychology*, 9(2):129–154.

Purves, D., Monson, B. B., Sundararajan, J., and Wojtach, W. T. (2014). How biological vision succeeds in the physical world. *Proceedings of the National Academy of Sciences*, 111(13):4750–4755.

Qian, N., Andersen, R. A., and Adelson, E. H. (1994). Transparent motion perception as detection of unbalanced motion signals. iii. modeling. *J Neurosci*, 14(12):7381–92.

Redding, G. M. and Wallace, B. (2006). Prism adaptation and unilateral neglect: review and analysis. *Neuropsychologia*, 44(1):1–20.

Reinkensmeyer, D. J., Akoner, O. M., Ferris, D. P., and Gordon, K. E. (2009). Slacking by the human motor system: computational models and implications for robotic orthoses. In *2009 Annual International Conference of the IEEE Engineering in Medicine and Biology Society*, pages 2129–2132. Ieee.

Reinkensmeyer, D. J., Burdet, E., Casadio, M., Krakauer, J. W., Kwakkel, G., Lang, C. E., Swinnen, S. P., Ward, N. S., and Schweighofer, N. (2016). Computational neurorehabilitation: modeling plasticity and learning to predict recovery. *J Neuroeng Rehabil*, 13(1):42.

Reinkensmeyer, D. J., Cole, A. M., Kahn, L. E., and Kamper, D. G. (2002). Directional control of reaching is preserved following mild/moderate stroke and stochastically constrained following severe stroke. *Experimental brain research*, 143(4):525–530.

Reinkensmeyer, D. J., Guigon, E., and Maier, M. A. (2012). A computational model of use-dependent motor recovery following a stroke: optimizing corticospinal activations via reinforcement learning can explain residual capacity and other strength recovery dynamics. *Neural Networks: The Official Journal of the International Neural Network Society*, 29-30:60–69.

Reinkensmeyer, D. J., Iobbi, M. G., Kahn, L. E., Kamper, D. G., and Takahashi, C. D. (2003). Modeling Reaching Impairment After Stroke Using a Population Vector Model of Movement Control That Incorporates Neural Firing-Rate Variability. *Neural Computation*, 15(11):2619–2642.

Reithler, J., van Mier, H. I., Peters, J. C., and Goebel, R. (2007). Nonvisual motor learning influences abstract action observation. *Curr Biol*, 17(14):1201–7.

Rizzolatti, G., Fadiga, L., Gallese, V., and Fogassi, L. (1996). Premotor cortex and the recognition of motor actions. *Cognitive brain research*, 3(2):131–141.

Robson, J. G. (1966). Spatial and temporal contrast-sensitivity functions of the visual system. *Josa*, 56(8):1141–1142.

Rodman, H. R. and Albright, T. D. (1989). Single-unit analysis of pattern-motion selective properties in the middle temporal visual area (mt). *Exp Brain Res*, 75(1):53–64.

Rohrer, B., Fasoli, S., Krebs, H. I., Hughes, R., Volpe, B., Frontera, W. R., Stein, J., and Hogan, N. (2002). Movement smoothness changes during stroke recovery. *The Journal of neuroscience : the official journal of the Society for Neuroscience*, 22(18):8297–304.

Rossetti, Y., Rode, G., Pisella, L., Farné, A., Li, L., Boisson, D., and Perenin, M. T. (1998). Prism adaptation to a rightward optical deviation rehabilitates left hemispatial neglect. *Nature*, 395(6698):166–9.

Sakata, H., Taira, M., Murata, A., and Mine, S. (1995). Neural mechanisms of visual guidance of hand action in the parietal cortex of the monkey. *Cerebral Cortex*, 5(5):429–438.

Scheidt, R. A., Dingwell, J. B., and Mussa-Ivaldi, F. A. (2001). Learning to move amid uncertainty. *Journal of neurophysiology*, 86(2):971–985.

Schmidt, R. A. (2003). Motor schema theory after 27 years: reflections and implications for a new theory. *Research Quarterly for Exercise and Sport*, 74(4):366–375.

Schütz-Bosbach, S. and Prinz, W. (2007a). Perceptual resonance: action-induced modulation of perception. *Trends Cogn Sci*, 11(8):349–55.

Schütz-Bosbach, S. and Prinz, W. (2007b). Prospective coding in event representation. *Cogn Process*, 8(2):93–102.

Schweighofer, N., Han, C. E., Wolf, S. L., Arbib, M. A., and Winstein, C. J. (2009). A functional threshold for long-term use of hand and arm function can be determined: predictions from a computational model and supporting data from the extremity constraint-induced therapy evaluation (excite) trial. *Physical therapy*, 89(12):1327–1336.

Sedda, G., Franzosi, R., Mazzone, A., Sanguineti, V., and Colombo, R. (2018a). Robot assisted exercise: Modelling the recovery process to personalise therapy. In *International Conference on NeuroRehabilitation*, pages 236–240. Springer.

Sedda, G., Ottonello, M., Fiabane, E., Pistarini, C., Sedda, A., and Sanguineti, V. (2017). Computational rehabilitation of neglect: Using state-space models to understand the recovery mechanisms. In *2017 International Conference on Rehabilitation Robotics (ICORR)*, pages 187–192. IEEE.

Sedda, G., Summa, S., and Sanguineti, V. (2018b). Computational models of the recovery process in robot-assisted training. In *Rehabilitation Robotics*, pages 117–135. Elsevier.

Seth, A. K. (2015). Presence, objecthood, and the phenomenology of predictive perception. *Cognitive neuroscience*, 6(2-3):111–117.

Shadmehr, R. and Mussa-Ivaldi, F. A. (1994). Adaptive representation of dynamics during learning of a motor task. *Journal of Neuroscience*, 14(5):3208–3224.

Shadmehr, R., Smith, M. A., and Krakauer, J. W. (2010). Error correction, sensory prediction, and adaptation in motor control. *Annu Rev Neurosci*, 33:89–108.

Shiffrar, M. and Freyd, J. J. (1993). Timing and apparent motion path choice with human body photographs. *Psychological Science*, 4(6):379–384.

Shimojo, S., Silverman, G. H., and Nakayama, K. (1989). Occlusion and the solution to the aperture problem for motion. *Vision Res*, 29(5):619–26.

Sinnett, S., Spence, C., and Soto-Faraco, S. (2007). Visual dominance and attention: the colavita effect revisited. *Percept Psychophys*, 69(5):673–86.

Smith, M. A. (2005). Intact Ability to Learn Internal Models of Arm Dynamics in Huntington's Disease But Not Cerebellar Degeneration. *Journal of Neurophysiology*, 93(5):2809–2821.

Smith, M. A., Ghazizadeh, A., and Shadmehr, R. (2006). Interacting adaptive processes with different timescales underlie short-term motor learning. *PLoS Biology*, 4(6):1035–1043.

Souman, J. L., Hooge, I. T. C., and Wertheim, A. H. (2006). Localization and motion perception during smooth pursuit eye movements. *Exp Brain Res*, 171(4):448–58.

Spence, C. and Driver, J. (2004). *Crossmodal space and crossmodal attention*. Oxford University Press.

Steinbach, M. J. and Held, R. (1968). Eye tracking of observer-generated target movements. *Science*, 161(3837):187–188.

Stinear, C. (2010). Prediction of recovery of motor function after stroke. *The Lancet. Neurology*, 9(12):1228–1232.

Stocker, A. A. and Simoncelli, E. P. (2006). Noise characteristics and prior expectations in human visual speed perception. *Nat Neurosci*, 9(4):578–85.

Stone, L. S. and Thompson, P. (1992). Human speed perception is contrast dependent. *Vision Res*, 32(8):1535–49.

Stone, L. S., Watson, A. B., and Mulligan, J. B. (1990). Effect of contrast on the perceived direction of a moving plaid. *Vision Res*, 30(7):1049–67.

Stoner, G. R. and Albright, T. D. (1992). Motion coherency rules are form-cue invariant. *Vision Research*, 32(3):465 – 475.

Stoner, G. R. and Albright, T. D. (1996). The interpretation of visual motion: evidence for surface segmentation mechanisms. *Vision Res*, 36(9):1291–310.

Stoner, G. R., Albright, T. D., and Ramachandran, V. S. (1990). Transparency and coherence in human motion perception. *Nature*, 344(6262):153–5.

Summa, S., Palmieri, G., Basteris, A., and Sanguineti, V. (2012). Concurrent adaptation to force fields and visual rotations. In *2012 4th IEEE RAS & EMBS International Conference on Biomedical Robotics and Biomechatronics (BioRob)*, pages 338–343. IEEE.

Sung, K., Wojtach, W. T., and Purves, D. (2009). An empirical explanation of aperture effects. *Proceedings of the National Academy of Sciences*, 106(1):298–303.

Sutton, R. S. and Barto, A. G. (2018). *Reinforcement learning: An introduction*. MIT press.

Taira, M., Mine, S., Georgopoulos, A., Murata, A., and Sakata, H. (1990). Parietal cortex neurons of the monkey related to the visual guidance of hand movement. *Experimental brain research*, 83(1):29–36.

Takahashi, C. D. and Reinkensmeyer, D. J. (2003). Hemiparetic stroke impairs anticipatory control of arm movement. *Experimental brain research*, 149(2):131–140.

Taylor, J. A. and Ivry, R. B. (2013). Implicit and explicit processes in motor learning. *Action science*, pages 63–87.

Taylor, J. A., Krakauer, J. W., and Ivry, R. B. (2014). Explicit and implicit contributions to learning in a sensorimotor adaptation task. *Journal of Neuroscience*, 34(8):3023–3032.

Thompson, P. (1982). Perceived rate of movement depends on contrast. *Vision Res*, 22(3):377–80.

Thompson, P., Brooks, K., and Hammett, S. T. (2006). Speed can go up as well as down at low contrast: implications for models of motion perception. *Vision Res*, 46(6-7):782–6.

Thoroughman, K. A. and Shadmehr, R. (2000). Learning of action through adaptive combination of motor primitives. *Nature*, 407(6805):742–7.

Timmermans, A. A. A., Spooren, A. I. F., Kingma, H., and Seelen, H. A. M. (2010). Influence of task-oriented training content on skilled arm-hand performance in stroke: a systematic review. *Neurorehabil Neural Repair*, 24(9):858–70.

Trueswell, J. C. and Hayhoe, M. M. (1993). Surface segmentation mechanisms and motion perception. *Vision Res*, 33(3):313–28.

Tucker, M. and Ellis, R. (1998). On the relations between seen objects and components of potential actions. *Journal of Experimental Psychology: Human perception and performance*, 24(3):830.

Ueyama, Y. (2017). System identification of neural mechanisms from trial-by-trial motor behaviour: modelling of learning, impairment and recovery. *Advanced Robotics*, 31(3):107–117.

Uno, Y., Kawato, M., and Suzuki, R. (1989). Formation and control of optimal trajectory in human multijoint arm movement. *Biological cybernetics*, 61(2):89–101.

Vahdat, S., Darainy, M., Milner, T. E., and Ostry, D. J. (2011). Functionally specific changes in resting-state sensorimotor networks after motor learning. *Journal of Neuroscience*, 31(47):16907–16915.

Vallortigara, G. and Bressan, P. (1991). Occlusion and the perception of coherent motion. *Vision Res*, 31(11):1967–78.

van Kordelaar, J., van Wegen, E. E. H., Nijland, R. H. M., Daffertshofer, A., and Kwakkel, G. (2013). Understanding adaptive motor control of the paretic upper limb early poststroke: the EXPLICIT-stroke program. *Neurorehabilitation and Neural Repair*, 27(9):854–863.

Varela, F. J., Thompson, E., and Rosch, E. (1991). The embodied mind: Cognitive science and human experience. *Cambridge: Massachusetts Institution of Technology*.

Veto, P., Schütz, I., and Einhäuser, W. (2018a). Continuous flash suppression: Manual action affects eye movements but not the reported percept. *J Vis*, 18(3):8.

Veto, P., Uhlig, M., Troje, N. F., and Einhäuser, W. (2018b). Cognition modulates action-to-perception transfer in ambiguous perception. *J Vis*, 18(8):5.

Victor, J. D. and Conte, M. M. (1992). Coherence and transparency of moving plaids composed of fourier and non-fourier gratings. *Percept Psychophys*, 52(4):403–14.

Viviani, P. and Stucchi, N. (1992). Biological movements look uniform: evidence of motor-perceptual interactions. *Journal of experimental psychology: Human perception and performance*, 18(3):603.

Vogt, S. (1995). On relations between perceiving, imagining and performing in the learning of cyclical movement sequences. *British journal of Psychology*, 86(2):191–216.

Vogt, S. (1996). Imagery and perception-action mediation in imitative actions. *Cognitive Brain Research*, 3(2):79–86.

Vogt, S. (2002). 11 visuomotor couplings in object-oriented and imitative actions. *The imitative mind: Development, evolution, and brain bases*, 6:206.

Volcic, R., Fantoni, C., Caudek, C., Assad, J. A., and Domini, F. (2013). Visuomotor adaptation changes stereoscopic depth perception and tactile discrimination. *Journal of Neuroscience*, 33(43):17081–17088.

Wallach, H. (1935). Über visuell wahrgenommene bewegungsrichtung. *Psychologische Forschung*, 20(1):325–380.

Weiss, Y., Simoncelli, E. P., and Adelson, E. H. (2002). Motion illusions as optimal percepts. *Nat Neurosci*, 5(6):598–604.

Welch, L. and Bowne, S. F. (1990). Coherence determines speed discrimination. *Perception*, 19(4):425–35.

Werner, K., Raab, M., and Fischer, M. H. (2019). Moving arms: the effects of sensorimotor information on the problem-solving process. *Thinking & Reasoning*, 25(2):171–191.

Wilson, H. R., Ferrera, V. P., and Yo, C. (1992). A psychophysically motivated model for two-dimensional motion perception. *Vis Neurosci*, 9(1):79–97.

Wohlschläger, A. (2000). Visual motion priming by invisible actions. *Vision Res*, 40(8):925–30.

Wolpert, D. M. and Miall, R. C. (1996). Forward models for physiological motor control. *Neural Netw*, 9(8):1265–1279.

Xerri, C. (2012). Plasticity of cortical maps: multiple triggers for adaptive reorganization following brain damage and spinal cord injury. *The Neuroscientist*, 18(2):133–148.

Yo, C. and Wilson, H. R. (1992a). Moving two-dimensional patterns can capture the perceived directions of lower or higher spatial frequency gratings. *Vision Res*, 32(7):1263–9.

Yo, C. and Wilson, H. R. (1992b). Perceived direction of moving two-dimensional patterns depends on duration, contrast and eccentricity. *Vision Res*, 32(1):135–47.

Zago, M., Bosco, G., Maffei, V., Iosa, M., Ivanenko, Y. P., and Lacquaniti, F. (2004). Internal models of target motion: expected dynamics overrides measured kinematics in timing manual interceptions. *Journal of neurophysiology*, 91(4):1620–1634.

Zeki, S. M. (1974). Functional organization of a visual area in the posterior bank of the superior temporal sulcus of the rhesus monkey. *J Physiol*, 236(3):549–73.

Zhang, R. and Tadin, D. (2019). Disentangling locus of perceptual learning in the visual hierarchy of motion processing. *Scientific Reports*, 9:1557.

Zwickel, J., Grosjean, M., and Prinz, W. (2007). Seeing while moving: measuring the online influence of action on perception. *Q J Exp Psychol (Hove)*, 60(8):1063–71.